

9. SITE 676¹

Shipboard Scientific Party²

HOLE 676A

Date occupied: 1115, 10 August 1986
Date departed: 0030, 14 August 1986
Time on hole: 3 days, 13 hr, 15 min
Position: 15°31.849'N, 58°42.198'W
Water depth (sea level, corrected m; echo-sounding): 5052.5
Water depth (rig floor, corrected m; echo-sounding): 5063
Bottom felt (rig floor, m; drill-pipe measurement): 5070.1
Distance between rig floor and sea level (m): 10.5
Total depth (rig floor, m): 5380.3
Penetration (m): 310.2
Number of cores (including cores with no recovery): 33
Total length of cored section (m): 310.2
Total core recovery (%): 84.5
Oldest sediment cored:
Depth sub-bottom (m): 310.2
Nature: siliceous mudstone
Age: early Miocene
Measured velocity (km/s): 1.6

¹ Mascle, A., Moore, J. C., et al., 1988. *Proc., Init. Repts. (Pt. A), ODP*, 110: College Station, TX (Ocean Drilling Program).

² Alain Mascle (Co-Chief Scientist), Institut Français du Pétrole, 1-4 Ave Bois-Preau, B.P. 311, 92506 Reuil Malmaison Cedex, France; J. Casey Moore (Co-Chief Scientist), Dept. of Earth Sciences, University of California at Santa Cruz, Santa Cruz, CA 95064; Elliott Taylor (Staff Scientist), Ocean Drilling Program, Texas A&M University, College Station, TX 77840; Francis Alvarez, Borehole Research Group, Lamont-Doherty Geological Observatory, Columbia University, Palisades, NY 10964; Patrick Andreieff, BRGM, BP 6009, 45060 Orléans Cedex-2, France; Ross Barnes, Rosario Geoscience Associates, 104 Harbor Lane, Anacortes, WA 98221; Christian Beck, Département des Sciences de la Terre, Université de Lille, 59655 Villeneuve d'Ascq Cedex, France; Jan Behrmann, Institut für Geowissenschaften und Lithosphärenforschung, Universität Giessen, Senckenbergstr. 3, D6300 Giessen, FRG; Gerard Blanc, Laboratoire de Géochimie et Métallurgie U. A. CNRS 196 U.P.M.C., 4 Place Jussieu, 75252 Paris Cedex 05, France; Kevin Brown, Dept. of Geological Sciences, Durham University, South Road, Durham, DH1 3LE, U.K. (current address: Dept. of Earth Sciences, University of California at Santa Cruz, Santa Cruz, CA 95064); Murlene Clark, Dept. of Geology, LSCB 341, University of South Alabama, Mobile, AL 36688; James Dolan, Earth Sciences Board, University of California at Santa Cruz, Santa Cruz, CA 95064; Andrew Fisher, Division of Marine Geology and Geophysics, University of Miami, 4600 Rickenbacker Causeway, Miami, FL 33149; Joris Gieskes, Ocean Research Division A-015, Scripps Institution of Oceanography, La Jolla, CA 92093; Mark Hounslow, Dept. of Geology, Sheffield University, Brook Hill, Sheffield, England S3 7HF; Patrick McLellan, Petro-Canada Resources, PO Box 2844, Calgary, Alberta Canada (current address: Applied Geotechnology Associates, 1-817 3rd Ave. NW, Calgary, Alberta T2N 0J5 Canada); Kate Moran, Atlantic Geoscience Centre, Bedford Institute of Oceanography, Box 1006, Dartmouth, Nova Scotia B2Y 4A2 Canada; Yujiro Ogawa, Dept. of Geology, Faculty of Science, Kyushu University 33, Hakozaki, Fukuoka 812, Japan; Toyosaburo Sakai, Dept. of Geology, Faculty of General Education, Utsunomiya University, 350 Mine-machi, Utsunomiya 321, Japan; Jane Schoonmaker, Hawaii Institute of Geophysics, 2525 Correa Road, Honolulu, HI 96822; Peter J. Vrolijk, Earth Sciences Board, University of California at Santa Cruz, Santa Cruz, CA 95064; Roy Wilkens, Earth Resources Laboratory, E34-404 Massachusetts Institute of Technology, Cambridge, MA 02139; Colin Williams, Borehole Research Group, Lamont-Doherty Geological Observatory, Columbia University, Palisades, NY 10964.

Principal results: Located only 250 m arcward of the deformation front, Site 676 was designed to explore the incipient stages of accretion. Here, lithologic Unit 1 (0–162 mbsf) consists of uppermost Miocene-to-Pleistocene calcareous mudstones and claystones, marls, and ash layers. At the probable level of the frontal thrust (25–55 mbsf), conspicuous folding occurs in Pleistocene sediments with some bedding dips as steep as 75°. A second discrete thrust fault with folded scaly fabric occurs at 155 mbsf, at the Miocene/Pliocene boundary. Unit 2 (168–263 mbsf) comprises middle and upper Miocene claystone and mudstone with ash beds. Calcareous nannofossils occur in the upper half of Unit 2. At 206 m a biostratigraphically defined thrust fault with 30 m of throw is associated with a scaly zone. The lower portion of Unit 2 includes traces of radiolarians that cannot be zoned. Seismic stratigraphic data suggest that this fault is very recent and probably propagating upward and forward from the décollement. Unit 3 (272–310 mbsf) is composed of lower Miocene claystone, siliceous mudstone and ash layers. At 270 to 280 mbsf this unit includes a zone of incipient horizontal shearing which may represent a seaward forerunner of the décollement.

Physical properties at Site 676 are very similar to those at the reference Site 672. The porosity profile is repeated at about 40 mbsf, indicative of frontal thrust fault. The magnetic susceptibility profiles are also repeated below 40 m. Anomalously high temperatures in this interval suggest lateral flow of relatively warm fluid through this fault zone.

High values of methane occur at four depths; three of these anomalies correlate well (within the limits of sampling) with the three main structural features of the hole. The methane anomaly at 33 mbsf is probably related to the fault near this level defined by physical properties and magnetic susceptibility data. The high methane content at 190 mbsf is adjacent to the thrust that gives rise to the repeated upper Miocene section. The high methane anomaly at 286 mbsf is adjacent to the incipient shear zone of the propagating décollement. A low pore-water chloride concentration is observed only at 250 mbsf and does not correlate with any structural feature.

BACKGROUND AND OBJECTIVES

The deformation front of an accretionary complex is defined as the limit between the horizontal cover of the oceanic plain and the first megascopic fold and thrust fault as depicted on seismic reflection profiles. This front typically forms a linear scarp on the seafloor and is clearly imaged on Seabeam bathymetric maps. When the wavelengths of the frontal folds are more than several kilometers, the linear arrangement of seaward verging anticlines is also quite striking on the Seabeam maps (Mascle et al., 1986). Continentward verging folds have been described along a few active margins (Oregon and North Colombian margins for instance, see Bally, 1983) but they remain quite uncommon. In a few cases, local bedding disturbances in the oceanic plain or trench cover, immediately adjacent to the deformation front, may image the development of new faults or folds and the seaward propagation of the accretionary complex (Fig. 1; Mascle and Biscarrat, 1979; Mascle, et al., 1986). An example of this incipient folding occurs 3 km south of the Leg 110 site transect, seen on seismic line A1D (Fig. 1, Moore and Biju-Duval, 1984).

At a few localities, mud diapirs, a common feature of thick accretionary complexes, occur in the oceanic domain in front of the prism (i.e., Timor and Oregon margins). One of the best-

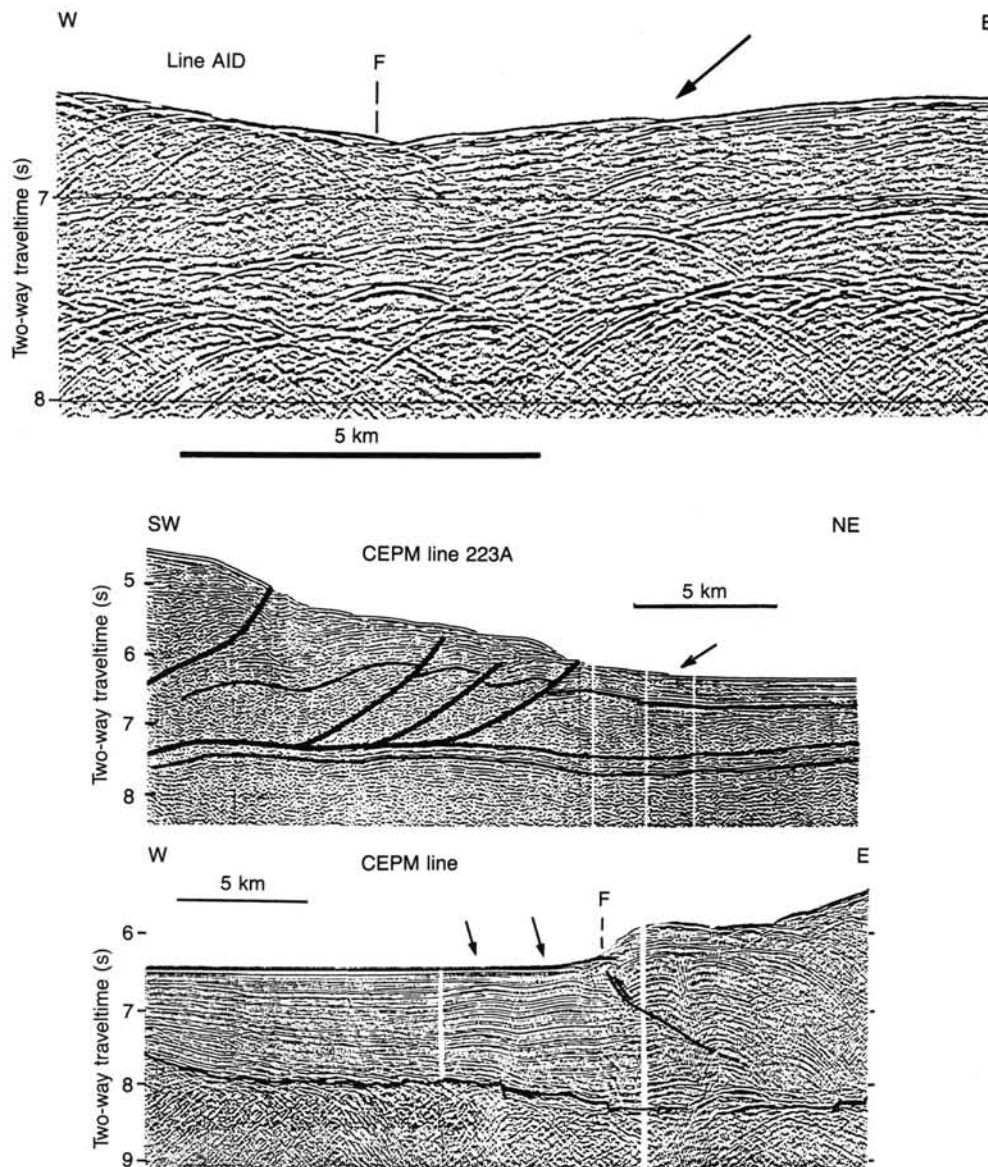


Figure 1. Examples of developing structures at the foot of the deformation front (F). Top: Leg 110 area; seismic line AID is located 3 km south and parallel to the Leg 110 site transect. Note the small slope anomaly on the seafloor (arrow). It is interpreted as the edge of a newly developed thrust package (Moore and Biju-Duval, 1984). Middle: North Venezuelan margin; thrust fault (arrow) and growing fold at the edge of the Curacao Ridge. Bottom: Sulu Sea, southeast Asia; gentle folds (arrows) in the trench infilling, close to the frontal thrust bounding the accreted series.

studied examples is about 120 km south of the Leg 110 site transect (Westbrook and Smith, 1983). A well-defined single mud volcano, located 8 km forward of the deformation front, apparently results from migration of overpressured pore water from the prism. Also, submersible observations at the Oregon margin (Kulm et al., 1986) and in the Japan Trench (Boulegue, et al., 1985) discovered benthic communities living on methane in expelled pore fluids.

Site 672 of this Leg was located 6 km east of the Barbados Ridge deformation front and was believed to be an oceanic reference site. However, an incipient shear zone was discovered in the lower Miocene section at a depth correlative with the décollement penetrated at Site 671. Furthermore, an anomalously high methane content in pore water close to this shear zone sug-

gests advection of fluid from the deformation front (see Site 672 summary).

Clearly, a variety of tectonic processes are strikingly active within 10 km arcward and seaward of the deformation front of the Barbados Ridge complex and elsewhere. Understanding these processes is of prime importance to explain the seaward propagation of the accretionary complex. Site 676 is located at the very edge of the accretionary complex (Figs. 2 and 3), only 250 m west of the deformation front and a few 10s of meters above the frontal thrust. This site is 3.5 and 1.5 km east of Sites 671 and 675, respectively, and 6.5 km west of Site 672. The main objectives of Site 676 were: a) to drill through the frontal thrust and penetrate the lower Miocene décollement horizon (estimated depth: 280–300 m), and b) to collect data on structural

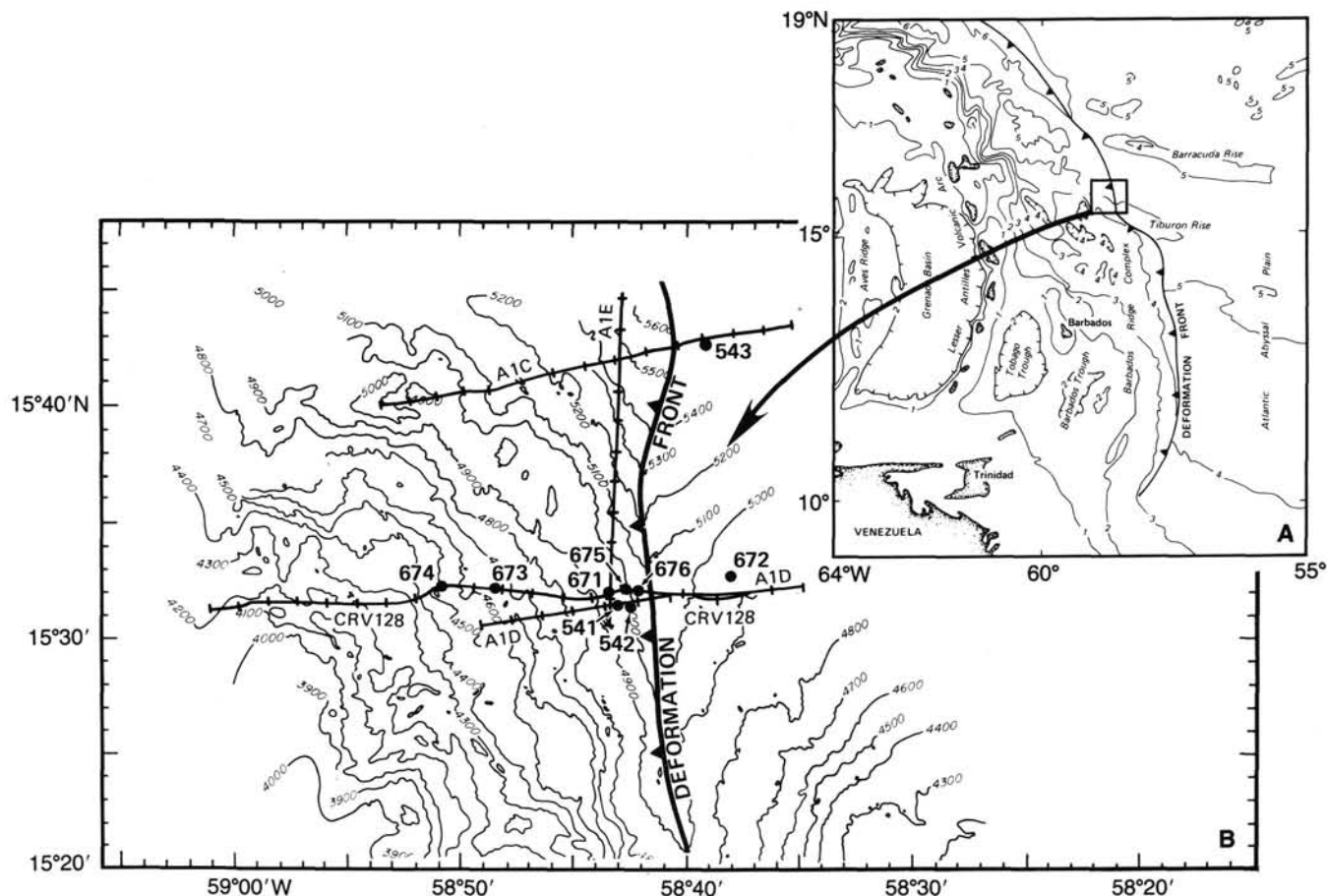


Figure 2. General (A) and detailed (B) location map of Site 676.

geology, physical properties, geochemistry, and *in-situ* temperatures to constrain the models of seaward propagation of the accretionary complex.

OPERATIONS

A single hole, Hole 676A, was drilled on the toe of the Barbados accretionary wedge to sample the frontal thrust zone. The goal was to drill through the décollement at 300 mbsf and identify evidence of fluid flow in the formation. The site, occupied at 1115, 10 August 1986, was located by offsetting from beacons at Sites 671 and 675. The location of Site 676 is 15° 31.849'N, 58°42.198'W.

The bottom hole assembly (BHA) consisted of six drill collars with a nonmagnetic collar above the core barrel. An 11-7/16-inch C-3 XCB bit and mechanical bit release with a float valve were used to drill the hole.

The bit was positioned 3 m above a PDR depth of 5052.5 m and the mudline was established, after one water core, at 5070.1 m of drill pipe (5059.6 m below sealevel). Eleven APC cores were taken with excellent recovery and with no crushed liners. APC coring was terminated when pullout forces reached 65,000 lbs. All APC cores were oriented except 110-676A-9H. The pore water and temperature tool was run after Cores 110-676A-4H, -8H and -11H. The HPC temperature shoe was run on Cores 110-676A-5H, -7H and -9H.

The XCB was used to core from 5171.3 to a total depth of 5380.3 m (310.2 mbsf) at which point the objective of coring to the décollement was achieved. Recovery in the XCB-cored interval was 75%, with one core lost owing to the flapper and core catcher dogs sticking open. Coring was stopped at the request

of the Co-chief scientists, who wished to use the remaining time for logging.

The hole was conditioned for logging by tripping the bit up to 5220 m of drill pipe and back to bottom. Bridging was encountered at 5326 m. The mechanical bit release spear was attached to the bottom of the XCB barrel, and the bit dropped on the first attempt. The pipe was rotated at high speed to ensure the bit was off the end of the pipe and the hole was displaced with 9.5-lb/gal salt water polymer gel mud. Backflow out of the top of the drill pipe was observed after the mud was displaced. The DIL-GR-SONIC-CAL Schlumberger logging tool was run down the pipe and into the hole; however, the tools stopped at a bridge 36 m below the end of the pipe. The 36-m interval was logged and the tools retrieved. Drill pipe was then tripped as the ship was made ready for steaming and departure for Barbados.

Operations at Site 676 retrieved a total of 262.1 m of sediment for a 84.5% recovery, and logged 36 m of open hole. Departure from Site 676 occurred at 0030, 14 August 1986, with a course set for Bridgetown, Barbados, after a total of 3.6 days at this location. Table 1 is the coring summary for Site 676.

STRUCTURAL GEOLOGY

The most important structural features encountered in Hole 676A are described as follows (Fig. 4): a) a zone of folding in association with small-scale reverse and thrust faulting from 25 mbsf to 52 mbsf, b) scaly fabrics and brittle reverse and thrust faulting from 199 to 223 mbsf, and c) intense dilatant veining and incipient subhorizontal shearing at 271 to 305 mbsf.

Bedding attitudes are subhorizontal throughout Hole 676A with the notable exception of Cores 110-676A-4H to -6H, where

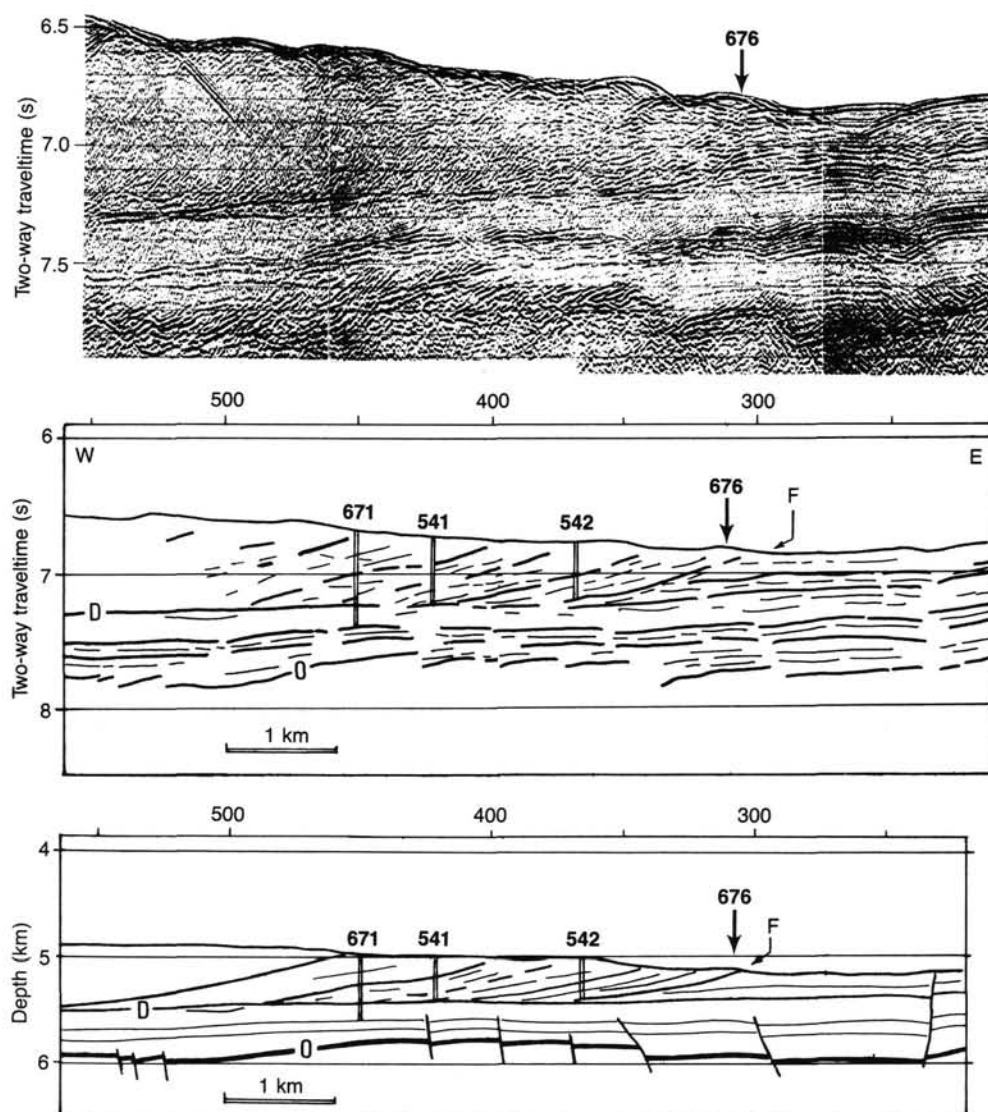


Figure 3. Location of Site 676 on seismic line CRV 128 (top), on a time section (middle), and on a depth section (bottom; no vertical exaggeration) of the same profile. D: Décollement; O: Top of the oceanic crust.

bedding dips are highly variable on a scale of an individual core. Lower hemisphere, equal-area plots of bedding orientation with respect to true north (Fig. 5) define tight folding around a horizontal axis with a 40-degree strike in Core 110-676A-4H. A close-up photograph (Fig. 6) documents the steep dip of an ash bed with a sharp lower contact in the lower part of Core 110-676A-4H. Change in dip direction is very rapid throughout the core. In the absence of crosscutting faults this feature is best interpreted as a downward tightening fold (Fig. 7). It has a steep but slightly irregular axial surface. The sense of bending of some beds in this core indicates that the fold must be an anticline. Core 110-676A-5H penetrated a pair of gentle folds (Figs. 5 and 7) with subhorizontal axes and steeply inclined axial surfaces. Owing to failure of the multishot camera this core could not be oriented with respect to north. Core 110-676A-6H also was found to contain open folds (Figs. 5 and 7). The trend of the horizontal fold axis in this core is approximately 150°, and the axial surfaces have a steep westerly dip. In the oriented cores below (110-676A-7H to -10H, Fig. 5) the bedding planes revert to a subhorizontal orientation.

Small-scale brittle faulting (Fig. 4) is concentrated in three discrete intervals. Cores 110-676A-5H to -10H contain 12 faults, four of which were positively identified as having thrust or reverse kinematics (Fig. 5). The faulting intensities in this interval are low, however, and are hardly higher than background if compared with the intensity of faulting in Hole 671B (this volume) further to the west. Cores 110-676A-11H to -16X mark a structurally quiet zone. Strong deformation is recorded in Core 110-676A-17X, with two distinct bands of scaly fabrics in mudstone. The dominant fabric dip is about 45°, and in the lower one of the two bands the fissility planes are refolded around subhorizontal axes (Fig. 8). The axial surface dips are significantly steeper than the enveloping surface of the folds. If interpreted as drag features, the sense of asymmetry of the folds indicates a late reverse movement along this zone of scaly fabrics. Cores 110-676A-18X to -21X show little deformation except for sets of shear fractures with predominantly steep dips. More intense small-scale reverse and thrust faulting is found in Cores 676A-22X to -24X, in association with discrete centimeter-to-meter-wide zones of subhorizontal scaly fabrics (Fig. 4). This zone of

Table 1. Coring summary, Site 676.

Core no. 110-676A-	Date August 1986	Time	Sub-bottom top (m)	Sub-bottom bottom (m)	Meters cored (m)	Meters recovered (m)	Percent recovery
1H	10	2110	0.0	6.2	6.2	6.20	100.0
2H	10	2235	6.2	15.7	9.5	9.69	102.0
3H	11	0000	15.7	25.2	9.5	9.88	104.0
4H	11	0140	25.2	34.7	9.5	9.82	103.0
5H	11	0615	34.7	44.2	9.5	9.78	103.0
6H	11	0810	44.2	53.7	9.5	9.80	103.0
7H	11	1005	53.7	63.2	9.5	9.88	104.0
8H	11	1200	63.2	72.7	9.5	9.67	102.0
9H	11	1500	72.7	82.2	9.5	9.71	102.0
10H	11	1705	82.2	91.7	9.5	9.21	96.9
11H	11	1800	91.7	101.2	9.5	9.65	101.0
12X	11	2152	101.2	110.7	9.5	5.67	59.7
13X	11	2350	110.7	120.2	9.5	9.36	98.5
14X	12	0155	120.2	129.7	9.5	0.90	9.5
15X	12	0410	129.7	139.2	9.5	4.33	45.6
16X	12	0630	139.2	148.7	9.5	6.73	70.8
17X	12	1035	148.7	158.2	9.5	9.54	100.0
18X	12	1217	158.2	167.7	9.5	9.55	100.0
19X	12	1410	167.7	177.2	9.5	6.80	71.6
20X	12	1615	177.2	186.7	9.5	9.34	98.3
21X	12	1808	186.7	196.2	9.5	5.61	59.0
22X	12	2215	196.2	205.7	9.5	9.19	96.7
23X	13	0020	205.7	215.2	9.5	9.57	101.0
24X	13	0210	215.2	224.7	9.5	8.81	92.7
25X	13	0401	224.7	234.2	9.5	2.52	26.5
26X	13	0545	234.2	243.7	9.5	3.78	39.8
27X	13	1020	243.7	253.2	9.5	9.49	99.9
28X	13	1200	253.2	262.7	9.5	9.60	101.0
29X	13	1405	262.7	272.2	9.5	0.00	0.0
30X	13	1610	272.2	281.7	9.5	9.49	99.9
31X	13	1750	281.7	291.2	9.5	9.29	97.8
32X	13	1955	291.2	300.7	9.5	9.63	101.0
33X	13	2200	300.7	310.2	9.5	9.60	101.0
					310.2	262.09	

deformation corresponds to a biostratigraphic inversion (see Biostratigraphy Section), and can accordingly be interpreted as a major thrust fault.

Very few structural features were recorded in Cores 110-676A-25X to -28X. From the lower part of Core 110-676A-28X to the bottom of the drill hole at 310 mbsf there is an abundance of dilatant veining (Fig. 4). The fillings are generally clay minerals. Most of the veins in this zone have steep dips (60° to 90°), indicating that they were formed in subhorizontal tension rather than compression. However, a second type of mud-filled veining is abundant in Core 110-676A-31X. These veins have slightly sigmoidal shapes (Fig. 9) and form en-echelon arrays similar to those found in Cores 110-672A-20X to -22X in Hole 672A. The enveloping surfaces of the vein arrays have dips between 10° and 14° , indicating incipient subhorizontal shearing in a regime of high fluid pressures at this stratigraphic level. In addition there is subordinate low-angle faulting. The bottom part of Core 110-676A-31X contains a small biostratigraphic inversion (see Biostratigraphy section). This inversion provides additional evidence for subhorizontal thrusting at this structural level.

In summary, the sediments intersected in Hole 676A host three distinct zones of deformation and displacement. The uppermost (25 mbsf to 52 mbsf) is a case of distributed deformation mainly represented by folding. Where faults occur, they take up only very minor displacements. The depth position corresponds to the position of the frontal thrust of the accretionary prism (see Seismic Stratigraphy section). The prevalence of folding may indicate that here the frontal thrust has not achieved significant displacement, but is represented by its "ductile head" in front of the upward propagating thrust tip line. The only evidence for discontinuous thrusting is the sharp downward de-

crease in horizontal east-west shortening calculated from the fold profiles between the bottom of Core 110-676A-4H and the top of Core 110-676A-5H. Note that owing to the excellent recovery a major thrust surface is unlikely to remain undetected in the core, but there is, of course, the possibility that the surface is positioned exactly between Cores 110-676A-4H and -5H.

The description of the second zone at 199 mbsf to 223 mbsf is a better example of the type of deformation encountered in connection with thrust faults in other holes (see Site Reports 671 to 675, this volume). The biostratigraphic inversion at this depth proves that there has been displacement, but individual relative movements may be small and are distributed over an unusually wide section.

The third zone, at 271 mbsf to 305 mbsf, hosts the oceanward propagating basal décollement of the Lesser Antilles accretionary prism. The lithological and stratigraphic level corresponds to the décollement position in Holes 671B and 675A (see Site Reports, this volume), and the inventory of structures is identical to that found in the relevant stratigraphic interval in Hole 672A several kilometers oceanward. The combined structural information of Holes 672A and 676A provides compelling evidence that there is incipient subhorizontal shearing in the sedimentary cover of the Atlantic oceanic crust well ahead of the deformation front.

LITHOSTRATIGRAPHY

Sediment Lithology: Description

The sediments recovered at Site 676 are divided into three units on the basis of visual core descriptions and smear-slide analyses (Table 2).

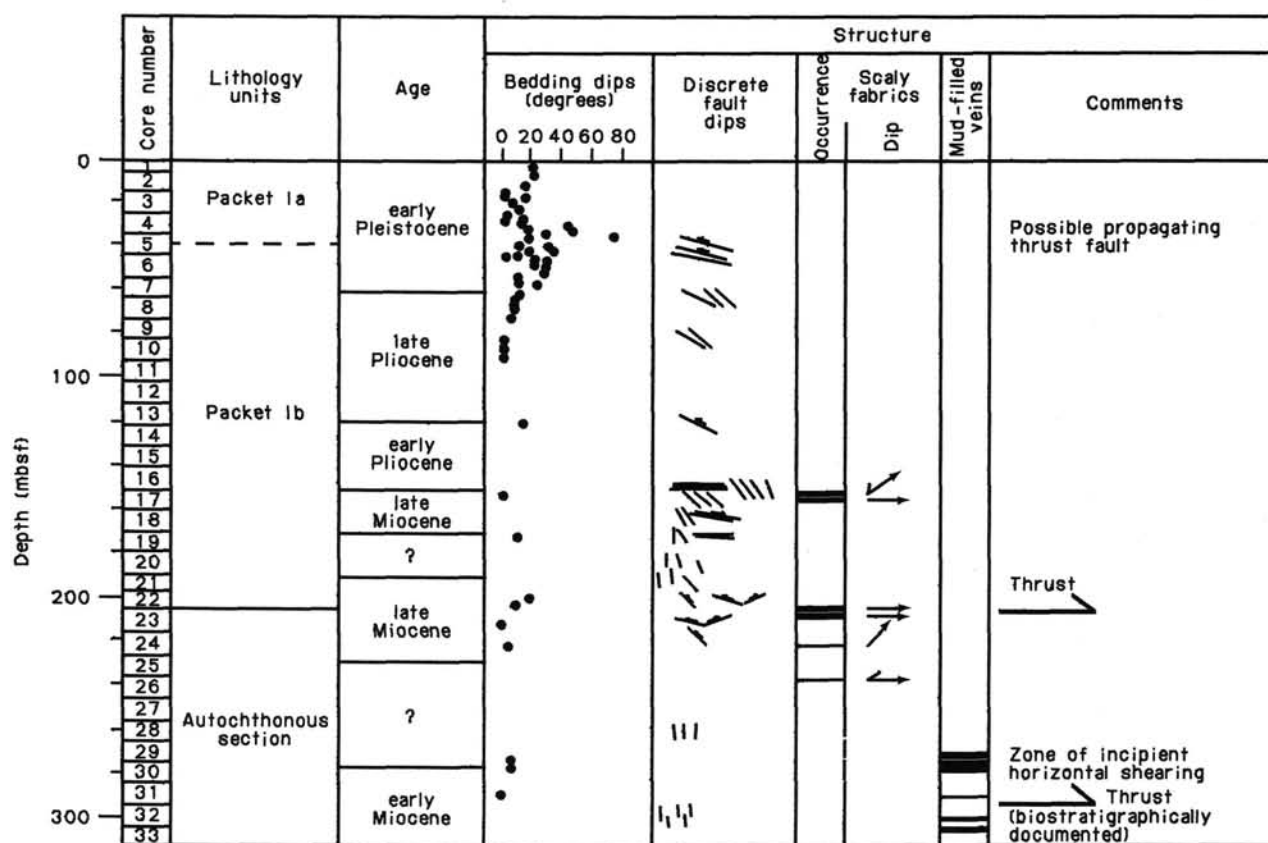


Figure 4. Log of the mesoscopic structures found in cores of Hole 676A. Dominant dip angles of the scaly fabrics are indicated by arrows, the range of dips is indicated by ticks. The two upper zones of deformation (25 to 52 mbsf and 199 to 223 mbsf) probably represent propagating thrust faults that will in the future define two thrust packets. For discussion, see text.

Unit 1

This unit consists of 162.2 m of Pleistocene to upper Miocene calcareous muds/mudstones, calcareous clay/claystone, marls/marlstone, and volcanic ash. Unit 1 sediments are typically olive brown, olive gray and brown in color, except for the ash, which is generally dark gray. Moderate-to-intense bioturbation occurs throughout Unit 1, and most volcanic ash layers have been completely disrupted by burrowing. *Planolites* are common, and these burrows are locally reburrowed by *Chondrites*. In addition, several examples of *Teichichnus* and *Zoophycos* occur in this unit. Most sediments of Unit 1 are devoid of sedimentary structures, although one ash layer in Sample 110-676A-1H-1, 105–110 cm, has a sharp base and contains laminated and low-angle cross-bedded intervals (Fig. 10). In general, ash layers in Cores 110-676A-1H to -10H appear to have relatively sharper, less bioturbated bases than do ash layers lower in Hole 676A. At least one ash layer in Core 110-676A-2H exhibits slight positive grading. In addition, a 5-mm-thick graded siltstone consisting of volcanic glass, foraminifers, and radiolarian fragments occurs at Core 110-676A-17X-5, 79 cm. Sediments in Sections 110-676A-1H through -16X-1 typically contain 3% to 10% disseminated foraminifers, whereas sediments in the lower part of Core 110-676A-16X and Cores 110-676A-17X and 676A-18X are devoid of foraminifers. Coincident with the disappearance of foraminifers, carbonate content decreases markedly downhole in Cores 110-676A-17X and -18X and the calcareous sediments of Unit 1 grade down into the predominantly noncal-

careous sediments of Unit 2 at approximately 162.2 mbsf (Section 110-676A-18X-3 at 100 cm). See Figure 11.

Unit 2

The unit is 100.5 m thick (Sections 110-676A-18X-3, 100 cm, to -28X, CC) and is made up of two subunits: 2-A and 2-B. Subunit 2-A extends from 162.2 mbsf (Section 110-676A-18X-3, 100 cm) to 243.7 mbsf (Section 110-676A-26X, CC) and consists of homogeneous olive gray to olive green claystone and mudstone with intervals of slightly calcareous to calcareous claystone and mudstone. Cores 110-676A-19X and -20X are barren of microfossils, but nannofossils recovered from Cores 110-676A-21X to -24X indicate that most of this subunit is of late Miocene age. Subunit 2-B extends from 243.7 mbsf (Core 110-676A-27X-1) to 262.7 mbsf (Section 110-676A-28X, CC) and consists of olive green to olive gray claystone and mudstone containing local trace amounts of radiolarians. This subunit is of indeterminate age. The presence of siliceous biogenic detritus distinguishes subunit 2-B from subunit 2-A. Section 110-676A-27X-2 contains rare, 1-mm diameter, white spherules of clinoptilolite similar to those observed near the décollement in Hole 671B. Unit 2 sediments contain common volcanic ash, both as highly bioturbated layers and as a minor disseminated constituent of the sediment (Fig. 12). All of the sediments from Unit 2 are moderately to intensely bioturbated, exhibiting common *Planolites* and less common *Chondrites* and *Zoophycos* (Fig. 12). Locally this burrowing carries ash as much as 35 cm downcore

BEDDING AND FAULT PLANE ORIENTATIONS

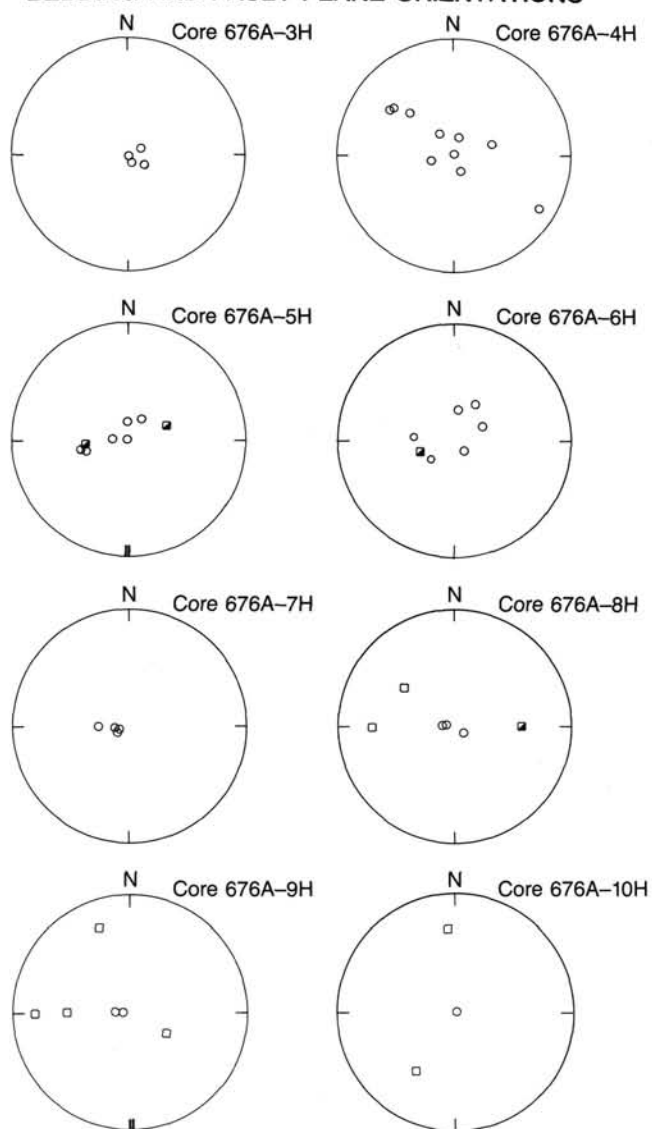


Figure 5. Lower hemisphere, equal-area projections of poles to bedding (open circles) and poles to fault planes (squares) in Cores 110-676A-5H and -9H are related to true north. Open squares denote faults whose kinematic character is not known, semifilled quadrangles indicate reversed thrust displacements.

(Sample 110-676A-20X-4, 110–145 cm), suggesting locally deep, exichnia-type bioturbation. Unit 2 is separated from Unit 3 by a 9.5-m interval of no recovery (Core 110-676A-29X).

Unit 3

This unit is 38 m thick (Core 110-676A-30X-1 to -33X, CC) and consists of lower Miocene olive brown to orange brown siliceous mudstone, slightly siliceous mudstone, claystone, and volcanic ash. These sediments typically contain between 2% and 26% radiolarians and sponge spicules. Local minor pinkish orange mottling occurs throughout this unit, which closely resembles portions of the décollement horizon cored at Site 671. Unit 3 sediments are all slightly to intensely bioturbated, with common *Planolites* and subordinate *Chondrites* and *Zoophycos*.

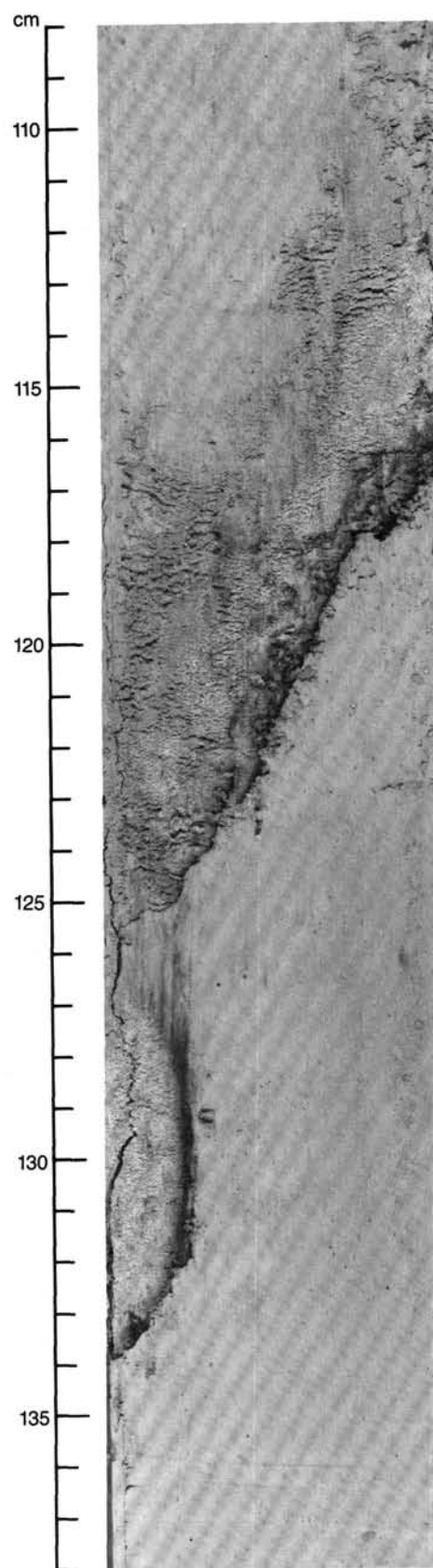


Figure 6. Close-up photograph of Sample 110-676A-4H-5, 108–138 cm, showing steeply dipping bed of volcanic ash with a sharply defined lower boundary in mud wall rock.

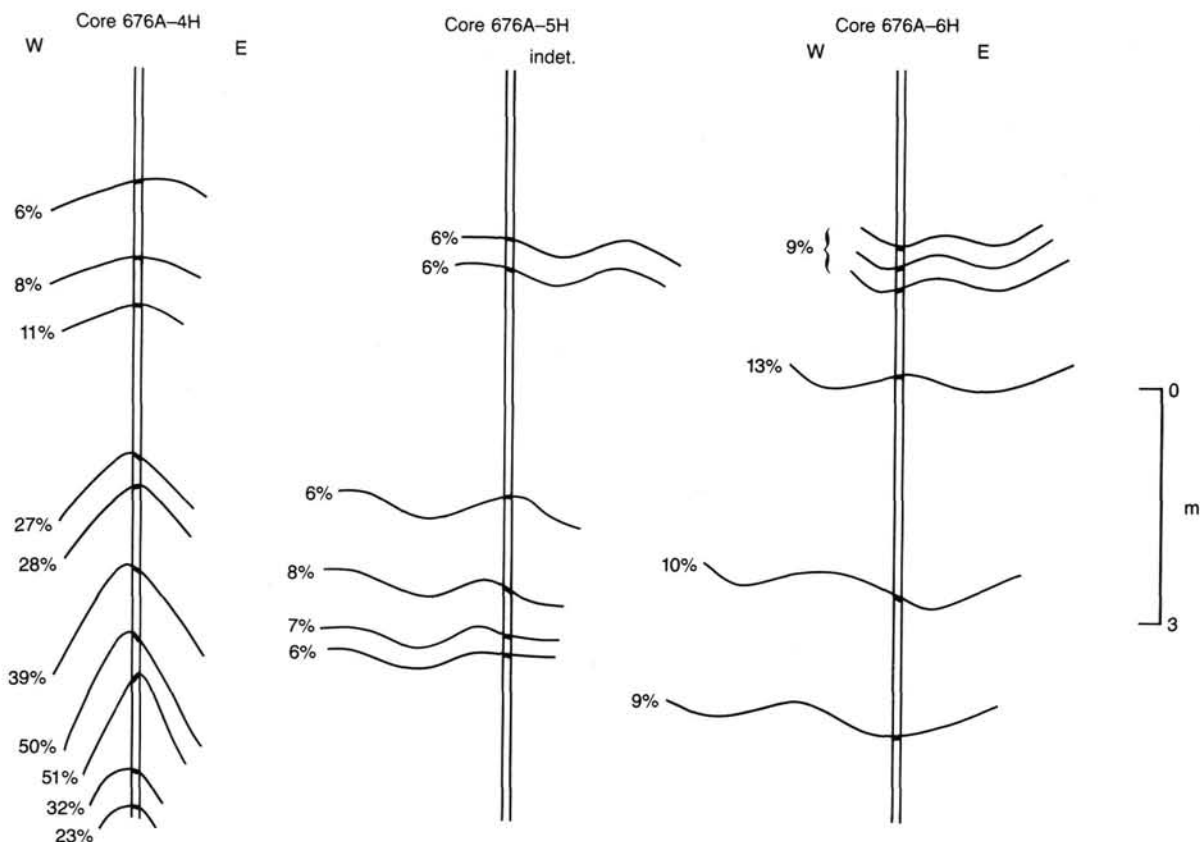


Figure 7. Interpretive sketches of fold geometries as a function of changing downhole bedding orientations in Cores 110-676A-4H to -6H. The numbers to the left of each core log indicate the horizontal shortening (E-W directed in the cases of Cores 110-676A-4H and -6H) suffered by the rocks during folding, assuming no layer elongation of shortening. For discussion see text.

Figure 13 shows the occurrence of volcanic ash in Hole 676A. In general, all three units contain significant ash, although there is a general downhole decrease in ash abundance. Figure 14 is a plot of sediment thickness vs. age for Site 676.

Depositional Environments and Processes

The homogeneous, bioturbated sediments recovered at Site 676 record predominantly hemipelagic-pelagic deposition on the Atlantic abyssal plain. However, the sharp-based, cross-bedded ash layer observed in Core 110-676A-1H indicates current-related reworking of at least some of the ash at this site. The ash layers in the Pleistocene-Pliocene section generally consist of relatively pure, undiluted ash, suggesting limited transport during current-related reworking. Although the nature of these currents remains unclear, they may have been local bottom currents. Whatever the case, the ash probably reached the Site 676 area as air-fall material from the Lesser Antilles Arc. The only other evidence of current-related deposition observed at Site 676 was the 5-mm-thick graded silt layer consisting of vitric ash, foraminifers, and broken radiolarians. The grading and composition of this thin layer suggest that it is probably a distal turbidite, possibly derived from the Tiburon Rise. The complete lack of other sedimentary structures in these sediments, including bedding, may be partially owing to complete disruption of the sediment by bioturbation.

The abundant calcareous microfossils preserved in Unit 1 indicate that these sediments were deposited above the CCD. In contrast, the general lack of biogenic carbonate in Unit 2 suggests deposition predominantly below the CCD. Local, slightly calcareous intervals in subunit 2-B indicate that it was deposited near the depth of the CCD, and was therefore quite sensitive to

slight relative changes in CCD depth. As in subunits 2-A and 2-C, the complete lack of calcareous microfossils in Unit 3 indicates deposition below the CCD.

In general, the sediments recovered at Site 676 correlate well with those cored at the reference Site 672. However, the upper Miocene section at Site 676 is somewhat thicker than that at Site 672 as a result of thrust repetition.

Bulk Mineralogy

The bulk mineralogy of 32 samples from Site 676 was determined by X-ray diffraction using the methods described in Chapter 1. A plot of cumulative percent of the four major phases, total clay minerals, quartz, plagioclase, and calcite, is given in Figure 11.

The most distinctive mineralogical trend with depth at Site 676 is the change from calcareous sediments to essentially calcite-free sediments at a depth of about 162 mbsf. This depth corresponds to the break between lithologic Units 1 and 2.

Lithologic Unit 1 sediments, in addition to being relatively calcite-rich, are characterized by variable plagioclase contents, reflecting the variable occurrence of ash layers (as high as 84% in an ash layer at 42 mbsf). Quartz content varies between 3% and 16%, and total clay mineral content shows a general increase downsection with a range of 10% (in the ash layer at 42 mbsf) to 70%.

Lithologic Unit 2 sediments are essentially calcite-free. Total clay mineral contents are higher than in Unit 1 sediments, varying from 77% to 92% (with one quartz-rich sample containing only 53% clay). Percent plagioclase varies between 2% and 15% and percent quartz between 5% and 12%, with one sample containing 33% quartz. There is no significant difference in bulk

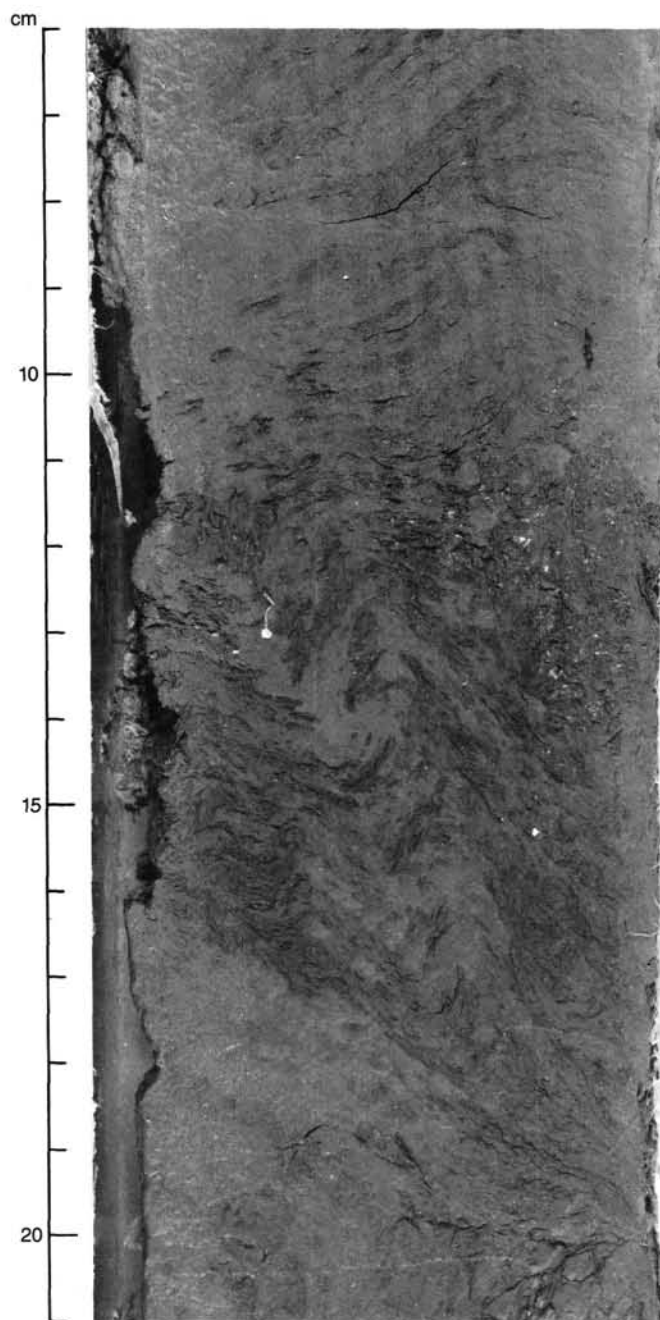


Figure 8. Photograph showing folded scaly fabrics in Section 110-676A-17X-4, 5–21 cm.

mineralogy between the sediments of lithologic Subunits 2-A and 2-B.

Lithologic Unit 3 (272–310 mbsf) is very similar to Unit 2 in terms of bulk mineralogy. The sediments of this unit tend to be slightly less clay-rich (percent total clay varies from 62% to 79%). An increase in quartz content to the range 10% to 20% balances the decrease in clay content. The percentage of plagioclase in Unit 3 sediments varies between 7% and 19%.

BIOSTRATIGRAPHY

Summary

Hole 676A was drilled at the toe of the Barbados accretionary wedge, 250 m west of the Atlantic abyssal plain. Coring re-

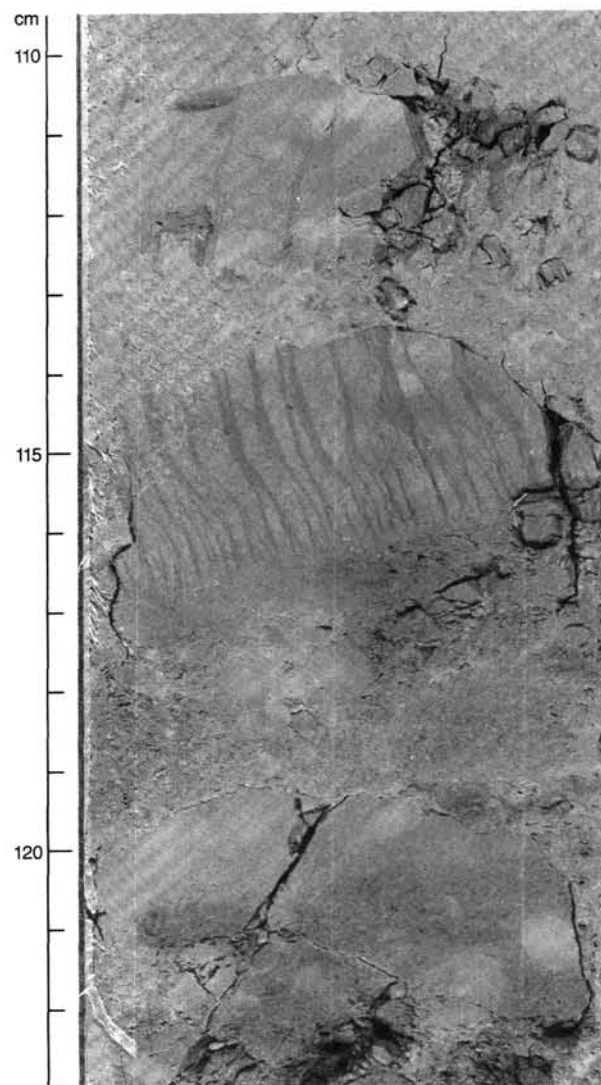


Figure 9. Photograph of slightly sigmoidally shaped set of en-echelon mud-veins in Section 110-676A-30X-3, 109–123 cm.

covered 310 m of sediment, which ranged from Pleistocene to early Miocene in age. Biostratigraphic resolution of these sediments is based on a combination of radiolarian, planktonic foraminifer, and calcareous nannofossil data (Fig. 15). The Pliocene-Pleistocene portion of the sequence is composed of hemipelagic sediments which contain abundant and well-preserved carbonate microfossils. The Miocene section is highly dissolved and becomes progressively depleted in carbonate, downhole. Lower Miocene radiolarian assemblages occur at the base of the section within the décollement zone.

The recovery of a complete Pliocene-Pleistocene biostratigraphic sequence is indicated by planktonic foraminifers and calcareous nannofossils. A missing section near the Pliocene/Miocene boundary is also suggested by the nannofossil biostratigraphy.

The Miocene section at Site 676 is slightly more complete than at Sites 671 and 672. Barren intervals occur in Cores 110-676A-19X, -20X, and -26X through -29X. Two reversals of sedimentary sequence are observed in the upper Miocene units between Samples 110-676A-22X-CC and -23X-7, 24–26 cm and in the lower Miocene units between Samples 110-676A-31X-6, 120–122 cm and -31X-CC. This biostratigraphic inversion is indicative of faulting associated with tectonic underthrusting.

Table 2. Summary of lithologic units, lithology, and depths to lithologic boundaries, Hole 676A.

Unit/ Subunit	Lithology	Core Range (core-section, cm level)	Depth (mbsf)	Age
110-676A-				
1	olive brown, olive gray, calcareous mud, marl, and minor clay and calcareous ooze; vitric or crystalline ash layers	1H-1 to 18X-3, 100	0-162.2	early Pleistocene to late Miocene
2-A	olive green to olive gray claystone and mudstone, locally slightly calcareous; disturbed and altered ash layers	18X-3, 100 to 26X, CC	162.2-243.7	late Miocene
2-B	olive green to olive gray claystone and mudstone, with traces of biogenic silica; highly dispersed and altered ashes	27X-1 to 28X, CC	243.7-262.7	Indeterminate
3	olive brown to orange brown siliceous (radiolarian) claystone and mudstone; highly dispersed and altered ashes	30X-1* to 33X, CC	272.2-310	early Miocene

* No recovery for Core 110-676A-29X.

Radiolarians are abundant in Sections 110-676A-30X-CC through -33X-CC and provide an early Miocene age assignment for the décollement zone.

Calcareous Nannofossils

Nannofossiliferous sediments at Site 676 range in age from upper Miocene to Pleistocene. Nannofossil assemblages are generally abundant and well preserved throughout the Pliocene-Pleistocene section; however, upper Miocene floras are more dissolved and only dissolution resistant species remain.

The early Pleistocene *Pseudoemiliania lacunosa*/small *gephyrocapsa* Zone of Gartner (1977) is slightly expanded at Site 676 owing to repetition of section. Samples 110-676A-1H-1, 66-68 cm through 3H-5, 84-86 cm and 4X-CC through 6X-2, 81-83 cm contain *P. lacunosa* without *Discoaster brouweri* and are included within this zonal designation. The *Helicosphaera sellii* Zone of Gartner (1977) is interjected into the section above, between Samples 110-676A-3X-6, 84-86 cm and -4X-6, 80-82 cm. The *H. sellii* Zone is also observed in Samples 110-674A-6X-3, 81-83 cm through 6X-CC. The early Pleistocene *Calcidiscus macintyreii* Zone occurs in Samples 110-674A-7X-1, 80-82 cm through 7X-6, 80-82 cm based on the presence of *C. macintyreii* without *D. brouweri*.

The Pliocene/Pleistocene boundary is marked in Sample 110-676A-7H-7, 60-62 cm by the presence of *D. brouweri* and *D. triradiatus*. The interval between Sections 110-676A-7H-7, 60-62 cm and -9H-1, 80-82 cm is placed within Subzone CN12d of Okada and Bukry (1980) based on the presence of *D. brouweri* without *D. pentaradiatus*.

Sample 110-676A-9H-2, 80-82 cm occurs in Subzone CN12c owing to the presence of *D. pentaradiatus* above the LAD of *D. surculus*. Subzone CN12b is encountered in Sample 110-676A-9H-4, 80-82 cm based on the first downhole occurrence of *Discoaster surculus*. Well-preserved specimens *D. pentaradiatus*, *D. brouweri*, *D. asymmetricus*, and *D. variabilis* are common in this interval. The addition of *D. tamalis* to the above assemblage within Sample 110-676A-10H-6, 16-18 cm indicates a zonal assignment of CN12a for sediments down through Sample 110-676A-13X-5, 80-82 cm. Rare specimens of *Sphenolithus abies*

place Samples 110-676A-12X-CC through -13X-5, 80-82 cm at the base of the late Pliocene.

Samples 110-676A-13X-6, 80-82 cm through -15X-CC are assigned to Zone CN11 of Okada and Bukry (1980) based on the presence of *Reticulofenestra pseudumbilica* without *A. tricorniculatus*.

A. tricorniculatus is common in Samples 110-676A-16X-1, 80-82 cm through 16X-CC. The LAD of this species defines the top of Subzone CN10c of Okada and Bukry (1980). Subzone CN10b was not observed and may indicate a gap in the sedimentary record. The Miocene/Pliocene boundary contained in Subzone CN10a represented by Sample 110-676A-17X-1, 100-102 cm. Subzone CN10a is recognized by the absence of *Amaurolithus tricorniculatus* and *Ceratolithus acutus*.

Samples 110-676A-17X-2, 100-102 cm through -18X-6, 30-32 cm are late Miocene in age and occur within Zone CN9b of Okada and Bukry (1980) owing to the coincidence of *Discoaster quinquaramus* and *Amaurolithus primus*. A barren interval exists in Cores 110-676A-19X and -20X that may have resulted from a late Miocene elevation of the carbonate compensation depth (CCD). Zone CN9a of Okada and Bukry (1980) occurs in Samples 110-676A-21X-1, 50-52 cm through -21X-3, 50-52 cm and is recognized by the presence of *Discoaster berggrenii* without *Amaurolithus primus*.

Samples 110-676A-21X-4, 50-52 cm through -22X-6, 80-82 cm are late Miocene in age and also have undergone moderate levels of dissolution. Placcoliths have been selectively removed from the assemblage and only discoasters remain. The assemblage is characteristic of the *Discoaster neohamatus* Zone CN8 of Okada and Bukry (1980) based on the absence of *D. berggrenii* and *D. hamatus*. Good specimens of *D. bollii* and six rayed specimens of *D. hamatus* define the *D. hamatus* Zone CN7 of Okada and Bukry (1980) in Section 110-676A-22X-CC.

Samples 110-676A-23X-7, 80-82 cm through -24X-5, 80-82 cm are assigned to Zone CN9a of Okada and Bukry (1980) owing to the common occurrence of *Discoaster berggrenii* without *Amaurolithus primus*. This interval is slightly younger than Zone CN7 encountered in Core 110-676A-22X. The apparent reversal of biostratigraphic sequence indicates that a thrust fault exists



Figure 10. Photograph of sharp-based, laminated vitric ash with low-angle cross-bedded interval from 106.5–107.5 cm. The cross-bedding suggests that this layer has been reworked by bottom currents. Apparent planar laminations in sediment below ash layer are artifacts related to core splitting.

between Samples 110-676A-22X-CC and -23X-7, 24–26 cm. A repetition of Zone CN8b occurs in Sections 110-676A-24X-CC and 25X-2 cm.

An intense episode of early-middle Miocene dissolution is evident between Sections 110-676A-25X-CC and -33X-CC. Section 110-676A-25X-CC contains a sparse assemblage of discoasters that could not be assigned to a specific biostratigraphic

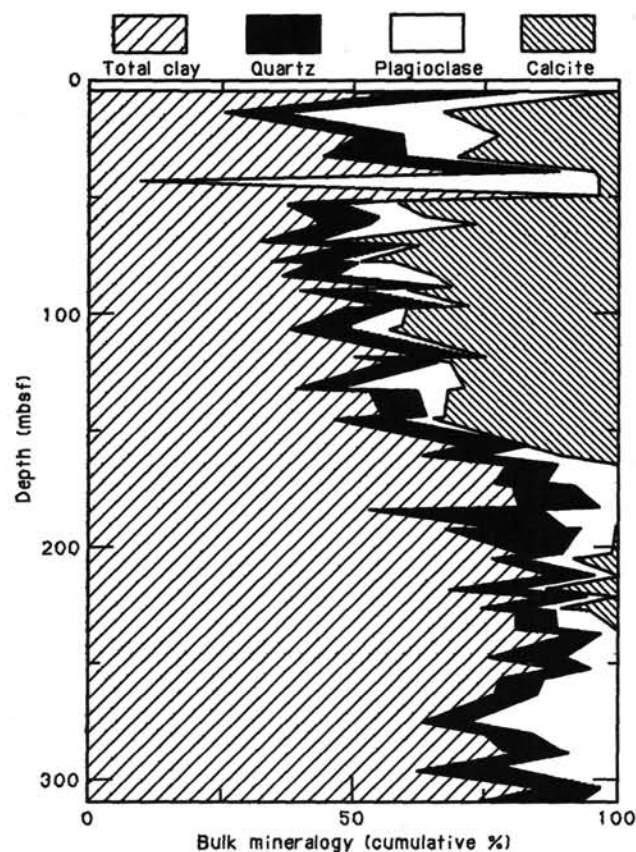


Figure 11. Bulk mineralogy of Site 676 sediments. Measurements are expressed as cumulative percentages of total clay minerals, quartz, plagioclase, and calcite.

zone. Sections 110-676A-26X-CC through -33X-CC are barren of nannofossils.

Planktonic Foraminifers

Sediments drilled at Site 676 provide a complete lower Pleistocene–Pliocene planktonic foraminiferal biostratigraphic succession. All the zones and subzones defined by Bolli and Premoli-Silva (1973) and Berggren (1977) have been identified.

The following planktonic foraminiferal events are noted from top to bottom:

1. First downhole occurrence of *Globorotalia hessi* in Section 110-676A-2H-CC;
2. Last downhole occurrence (= FAD) of *Globorotalia hessi* in Section 110-676A-6H-CC;
3. First downhole occurrence (= LAD) of *Globorotalia viola*, and last downhole occurrence of *G. truncatulinoides* in Section 110-676A-7H-CC;
4. First downhole occurrence of *Globorotalia miocenica* in Section 110-676A-9H-CC;
5. First downhole occurrences of *Globorotalia multicamerata* and *Globoquadrina altispira* in Section 110-676A-11H-CC;
6. First downhole occurrence of *Sphaeroidinellopsis* ssp. in Section 110-676A-12H-CC;
7. First downhole occurrences of *Pulleniatina primalis*, *Globorotalia plesiotumida*, and *Sphaeroidinellopsis hancocki*, and last downhole occurrence of *Sphaeroidinella immatura* in Section 110-676A-14X-CC; and
8. First downhole occurrence of *Globigerina nepenthes* in Section 110-676A-16X-CC.

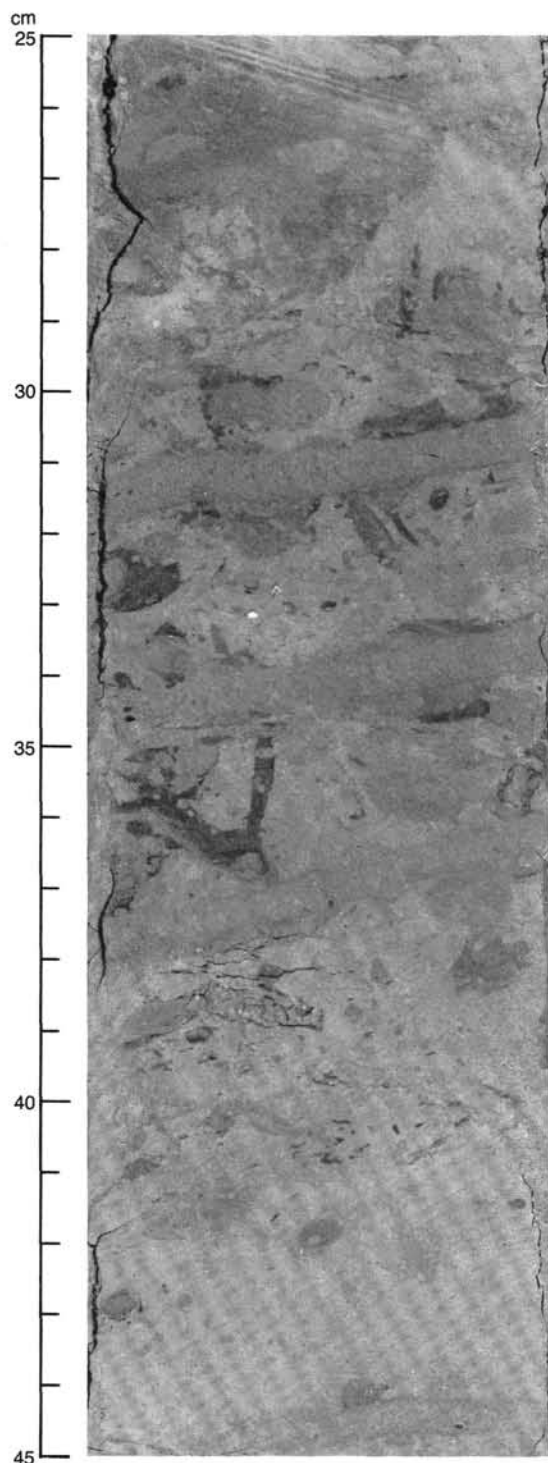


Figure 12. Photograph of typical highly bioturbated hemipelagic sediment from lithologic Unit 2. Note shallowly dipping *Zoophycos*, common *Planolites*, and local reburrowing by *Chondrites*. The darker burrow infilling contains a few percent disseminated ash.

Consequently, Cores 110-676A-2H through -6H belong to the lower Pleistocene, *Globorotalia hessi* subzone of the *G. truncatulinoides* Zone (Bolli and Premoli-Silva, 1973), owing to the presence of the subzonal marker and the absence of the younger key species *Globigerina calida*. No subzonal assignment was attempted in Section 110-676A-1H-CC, which contains only sparse and badly preserved Pleistocene foraminifers, including *G. truncatulinoides*. The above mentioned event (3) defines the earliest

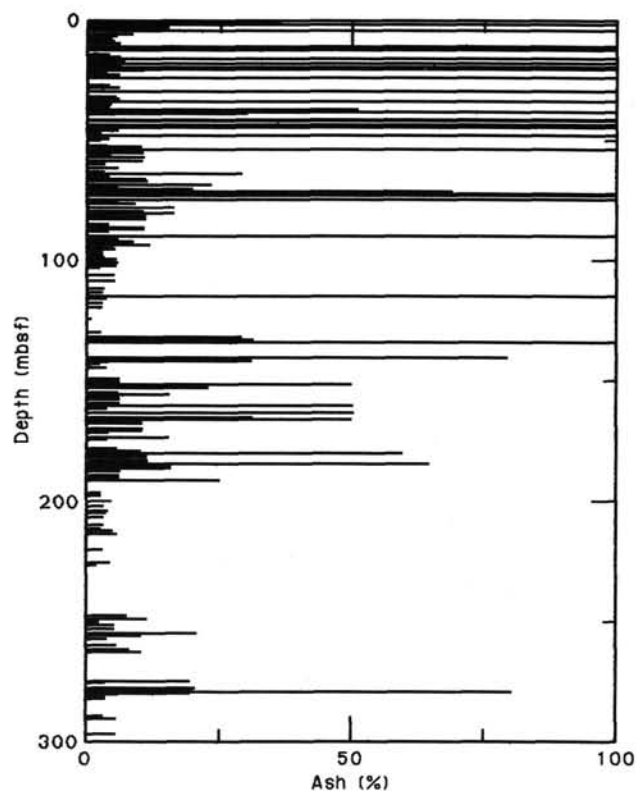


Figure 13. Plot of the occurrence of volcanic ash in Hole 676A. Length of horizontal lines denotes the concentration of ash at that interval.

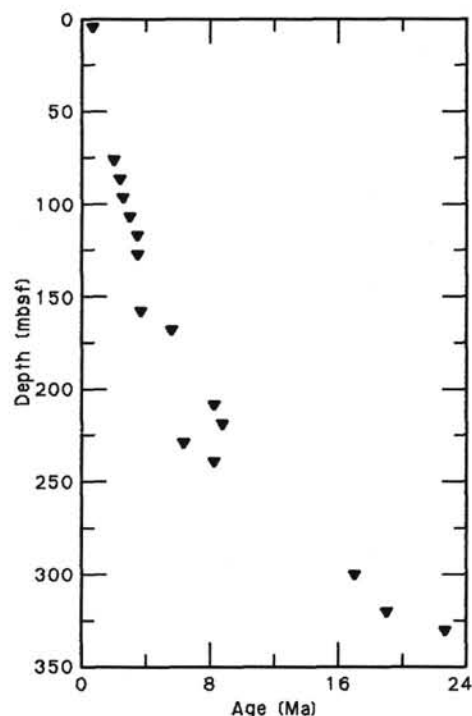


Figure 14. Graph of sediment thickness vs. sediment age for Hole 676A. Note that the upper Miocene interval may be slightly thickened owing to thrust repetition.

Pleistocene *Globorotalia viola* subzone of the *G. truncatulinoides* Zone, which is identified in Core 110-676A-7H. Typical specimens of the subzonal marker occur commonly in this section.

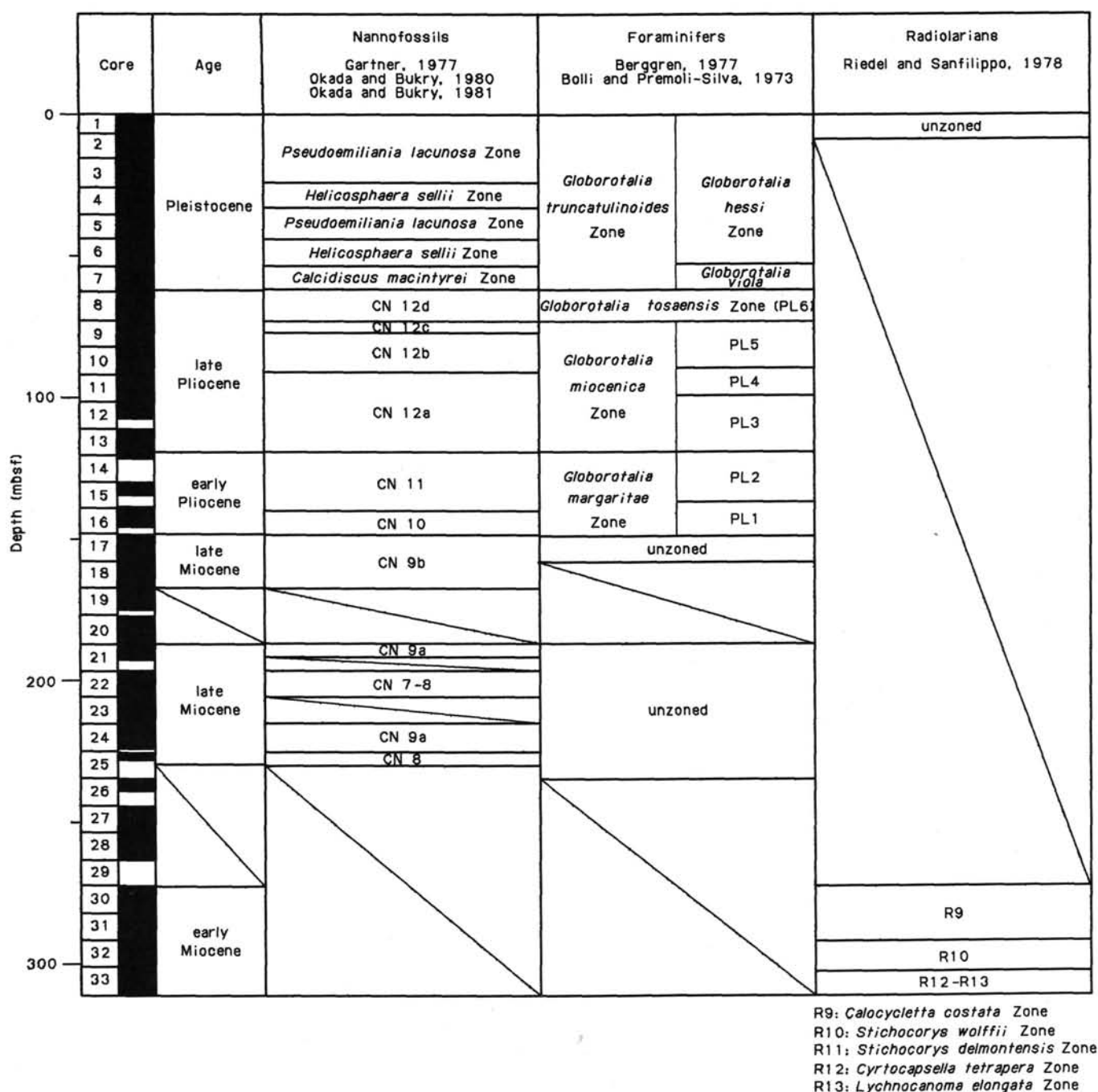


Figure 15. Site 676 biostratigraphic summary.

Core 110-676A-8H is bracketed by events (3) and (4) and thus falls within the latest Pliocene *Globorotalia tosaensis* Zone (Bolli and Premoli-Silva, *op. cit.*), equivalent to Zone PL 6 (Berggren, 1977). The nominate taxon and the subspecies *G. tosaensis tenuitheka* are present although rare.

Event (4) marks the top of the late Pliocene *Globorotalia miocenica* Zone. Cores 110-676A-9H and -10H belong to the upper part of this zone and are assigned to Zone PL 5 (Berggren, *op. cit.*); the first downhole occurrence of *Globigerinoides extremus* is noted within this interval in Section 110-676A-10H-CC, which confirms the reliability of the LAD of this taxon at about 2.8 Ma in the Caribbean. The middle part of the *G. miocenica* Zone corresponds to the short (0.1 m.y., according to Berggren *et al.*, 1984) Zone PL 4, defined by event (5), and is re-

covered in Core 110-676A-11H; the core-catcher sample yields a typical assemblage including abundant *Globorotalia multica-merata*, *Globigerina venezuelana*, *Globoquadrina altispira*, and *Sphaeroidinella dehiscens*, without *Sphaeroidinellopsis* ssp. The lower part of the *G. miocenica* Zone (PL 3) is recognized in Cores 110-676A-12X and -13X, between events (6) and (7).

As usual in sediments drilled during Leg 110, *Globorotalia margaritae* has not been identified. Thus, event (7) is used as an alternative to determine the top of the lower Pliocene. A bipar-tite subdivision of this interval is provided by event (8): Cores 110-676A-14X and -15X belong to the upper part of the *G. mar-garitae* Zone (PL 2) and Core 110-676A-16X to its lower part (PL 1). The last downhole occurrence of *Sphaeroidinella immatura* in Section 110-676A-14X-CC is in good agreement with its

regional first evolutionary appearance in the upper part of the *G. margaritae* Zone.

The Pliocene/Miocene boundary is put between Sections 110-676A-16X-CC and -17X-CC on the basis of the nannofossil data; indeed, the sparse and dissolved foraminifers which occur in Core 110-676A-17X do not allow any accurate biostratigraphic assignment.

Cores 110-676A-18X through -21X are barren of foraminifers. Cores 110-676A-22X through -25X yield very poor assemblages composed of the dissolution-resistant species *Globigerina nepenthes* and *Sphaeroidinellopsis cf. seminulina*. Although the core-catcher samples are not assigned to specific zones because of the absence of key species, they are regarded as late Miocene in age.

Cores 110-676A-26X through -33X are barren of foraminifers.

Radiolarians

Radiolarians occur in sediments below Core 110-676A-30X, and are absent above this horizon with the exception of Core 110-676A-1H. In Section 110-676A-1H-CC very few radiolarian species are present, and none of these are diagnostic.

Cores 110-676A-30X through -33X (the bottom of the Hole) (272.2–310.2 mbsf), contain abundant radiolarians. Ten assemblages are assigned to the lower Miocene. One assemblage repetition and one hiatus are detected at 290.4–291.2 mbsf and 300.5–300.9 mbsf, respectively. The upper sequence (272.2–290.4 mbsf) is assigned to *Calocyclus costata* Zone (Riedel and Sanfilippo, 1978) and *Stichocorys wolffii* Zone (Riedel and Sanfilippo, *op. cit.*). The middle (291.2–300.5 mbsf) is a repetition of the upper sequence and also assigned to *C. costata* Zone and *S. wolffii* Zone. In the lower sequence, the lower part of *Cyrtocapsella tetrapera* Zone (Riedel and Sanfilippo, *op. cit.*), *Lychnocanoma elongata* Zone (Riedel and Sanfilippo, *op. cit.*), and an indeterminate interval containing strongly dissolved radiolarians are found from top to bottom. The *Stichocorys delmontensis* Zone of Riedel and Sanfilippo (*op. cit.*) and the upper part of *C. tetrapera* Zone are missing between the middle and lower sequences.

Sections 110-676A-30X-1 through -31X-CC are assigned to the *C. costata* Zone because of the presence of *C. costata* and *Dorcadospyrus dentata* and the absence, or presence of few *Dorcadospyrus alata*. The last occurrence of *Carpocanistrum cingulata* is in Sample 110-676A-30X-6, 115–117 cm, and the evolutionary first appearance (Riedel and Sanfilippo, *op. cit.*) of *Liriospyris parkerae* is placed above Sample 110-676A-30X-1, 40–42 cm, probably being placed in the no-recovery core, 110-676A-29X. The preservation state of radiolarians in these samples is moderate to good.

Samples 110-676A-31X-3, 40–42 cm through -31X-6, 120–122 cm are assigned to *S. wolffii* Zone owing to the presence of *S. wolffii* and *C. cingulata* and the absence of *C. costata*. The first occurrence of *D. dentata* and that of *L. stauropora* are in the same horizon, Sample 110-676A-31X-4, 120–122 cm. Radiolarians are well preserved in these samples.

In Section 110-676A-31X-CC, *C. costata* occurs again. The occurrence of this species continues down to Sample 110-676A-32X-4, 30–32 cm. *C. cingulata* is included in all samples. This interval is assigned to the lower part of *C. costata* Zone. Samples 110-676A-32X-4, 70–72 cm through -32X-CC are assigned to *S. wolffii* Zone. The first occurrence of *D. dentata* and that of *L. stauropora* are in Sample 110-676A-32X-6, 30–32 cm.

Samples 676A-33X-1, 20–22 cm through -33X-3, 20–22 cm are assigned to the lower part of the *Cyrtocapsella tetrapera* Zone because of the presence of *Calocyclus serrata* as well as *Dorcadospyrus ateuchus*, *Cyrtocapsella cornuta*, and the absence of *C. tetrapera* and *Stichocorys delmontensis*. The radiolarian tests in these samples are slightly dissolved.

Samples 110-676A-33X-3, 80–82 cm through -33X-5, 11–13 cm are assigned to the *Lychnocanoma elongata* Zone (Riedel and Sanfilippo, *op. cit.*) owing to the presence of *L. elongata* and the absence of *C. tetrapera* and *C. cornuta*. The state of preservation in this interval is poor because of dissolution.

In Samples 110-676A-33X-5, 80–82 cm through -33X-CC, radiolarians are remarkably dissolved and only *D. ateuchus* is identified. Zonal assignment is not made.

PALEOMAGNETICS

Time constraints did not allow any samples for paleomagnetic analysis to be processed. The cores did provide the opportunity to examine the magnetic susceptibility correlations with the records from Sites 671 and 672, which are positioned west and east of this site, respectively. We hoped that susceptibility measurements would provide some control on the placement of the frontal thrust and the amount of throw.

The methods used to measure the whole core magnetic susceptibility are described in Chapter 1. Measurements were performed every 10 cm on all cores down to Core 110-676A-20X.

Results

All of the magnetic susceptibility measurements are shown in Figure 16 and indicate little overall difference in comparison to Sites 671 and 672. The two closely spaced high-susceptibility ash beds in Core 110-676A-15X (132 mbsf) correspond to the similar peaks in Core 110-671B-11X at 97 mbsf and in Core 110-671B-32X at 299 mbsf, and ash beds in Core 110-672A-11X at 97 mbsf. The excellent detail of these susceptibility records enables fine-scale between-site correlations which are better than those possible through biostratigraphy based on core-catcher samples alone, although any magnetic correlation is first constrained by the biostratigraphic data.

The correlations between Holes 671A, 672A, and 676A are indicated in Figure 17. There is a good correlation between Cores 1H from each site. In the Pleistocene section of Hole 671B, at least to Core 110-671B-4H, the magnetic susceptibility record is quite different to those of Holes 672A and 676A. This is expected since initial biostratigraphic data indicate zones missing in Holes 676A and 672A. Since Site 676 is approximately halfway between Sites 672 and 671, it might be expected that the susceptibility for Site 676 would have characteristics intermediate between these two sites. The correlation between Sites 672 and 676 is good down to the base of Core 110-676A-3H, where the susceptibility is quite different.

The exceptionally thick *P. lacunosa* zone in Hole 676A (this chapter, Biostratigraphy section) is suggestive of a repeated sequence. Indeed there is a very good correspondence between the middle of Core 110-676A-2H to bottom of Core 110-676A-3H and the bottom of Core 110-676A-4H to middle of Core 110-676A-6H (Fig. 18), which indicates that this part is the repeated section. The exact position of the frontal thrust is difficult to place because there is similarity between the top of Core 110-676A-4H and the base of Core 110-676A-6H, and between the top of Core 110-676A-4H and the base of Core 110-676A-1H. The similarity is greater between the former two and the likely position of the thrust is placed somewhere between the middle of Core 110-676A-4H and the bottom of Core 110-676A-4H, that is at about 29 to 32 mbsf. This position would agree approximately with the position of the discontinuity in the physical properties data, a zone of variable bedding dips and a change in the structural style. Placement of the thrust here would result in a stratal repetition of about 20 m. The repeated section below Core 110-676A-4H is slightly thicker than the section above this level, which is compatible with the steeper bedding dips recorded in this section. There may also be a thrust with a small throw in the middle of Core 110-676A-5H, since the record for this core

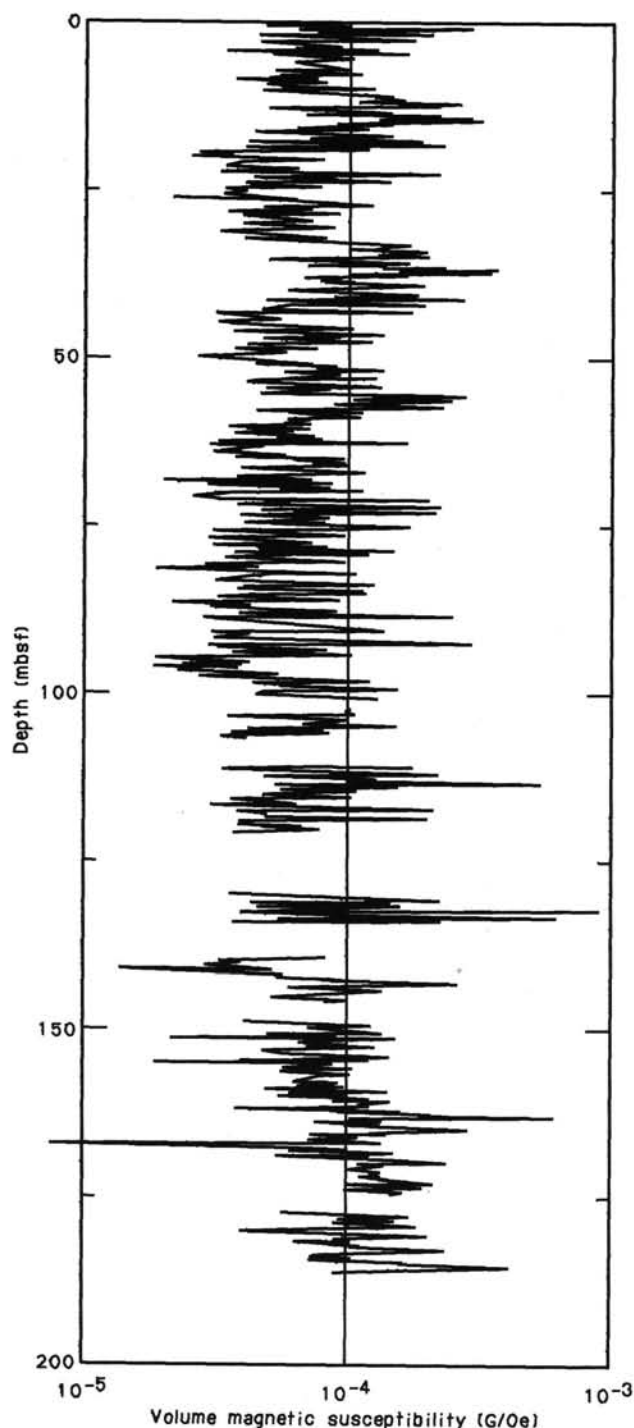


Figure 16. The volume magnetic susceptibility record for Site 676.

does not exactly match Cores 110-676A-2H to -3H, and 110-672A-2H to -3H (Fig. 18).

Tentative correlations are also made between the lower part of Holes 676A and 672A, which are compatible with the foraminifer data. At the top of Core 110-676A-10H, there is an interval that is not represented in Hole 672A and may be an expanded interval.

GEOCHEMISTRY

Site 676 was located near the toe of the Barbados accretionary complex along the Leg 110 transect, between Sites 671 and

672. Where possible we shall attempt comparisons with these sites.

Inorganic Geochemistry

The data are presented in Table 3 and in Figure 19.

Chloride

Figure 19 shows the profile of dissolved chloride and indicates the occurrence of a minimum at about 250 mbsf. The low chloride of the *in-situ* sample at 92 mbsf is curious because of the agreement of the other major constituents with the data above and below. We view this sample with suspicion, especially because only a small one was taken and because the entire sampling tube from filter head to copper coil was sampled. Perhaps a very small amount of distilled water was entrained which was present somewhere in the tubing, possibly as a result of the cleaning of the filter head prior to sampling. A 0.25-cm³ volume of water would cause a 5% dilution effect in the 5-cm³ sample. A steady decrease in the chloride concentration with depth to the area of the chloride minimum suggests that the observed minimum is real. Unfortunately the core just above the minimum was recovered empty, so that the curvature drawn in Figure 19 is somewhat tentative. Interestingly, no methane anomaly was observed in this zone, whereas a clear anomaly was observed near the fault zone at about 40 mbsf. In the latter case no chloride anomaly was evident.

Calcium and Magnesium

The calcium and magnesium concentration depth profiles are presented in Figure 19. A rapid increase in calcium and decrease in magnesium are the result of volcanic matter alteration in the upper part of the sediment column, with the magnesium being intermediary between that of Sites 671 and 672.

Below about 150 mbsf a slow increase in magnesium is apparent, presumably related to the increases observed at Sites 671 and 672 just above the décollement. We suggest that the radiolarian-rich section encountered at this site is much thicker than at the other two sites and that this is perhaps the reason for the lesser slope in the magnesium concentration profile.

Sodium and Potassium

The concentration depth profile of (Na + K) is presented in Figure 19. The profile shows a gradual decrease in Na + K below 110 mbsf, with a minimum in the chloride minimum zone. However, as is also shown by the (Na + K)/Cl plot, Figure 19, the decrease in Na + K exceeds that of chloride and indicates an influence of the large decreases observed below the décollement in Sites 671 and 672. Thus again the similarity in profiles is preserved.

Sulfate and Ammonia

The profiles of sulfate and ammonia (Fig. 19) show opposite behavior, as is to be expected from the underlying process of sulfate reduction and concomitant release of ammonia by the organic matter. The sulfate anomaly at 286 mbsf confirmed our suspicion that the low chloride at this level was indeed owing to a slight contamination with surface seawater (Cl = 520 mmol/L).

Silica

Dissolved silica is again relatively high in the uppermost part of the Pleistocene section (Fig. 19). In addition, a slight maximum occurs at 42 mbsf, possibly related in some uncertain manner to the fault described in the physical properties report at about this level. The radiolarian-rich décollement zone is again clearly characterized by high silica concentrations as a result of solubility control by biogenic opal-A.

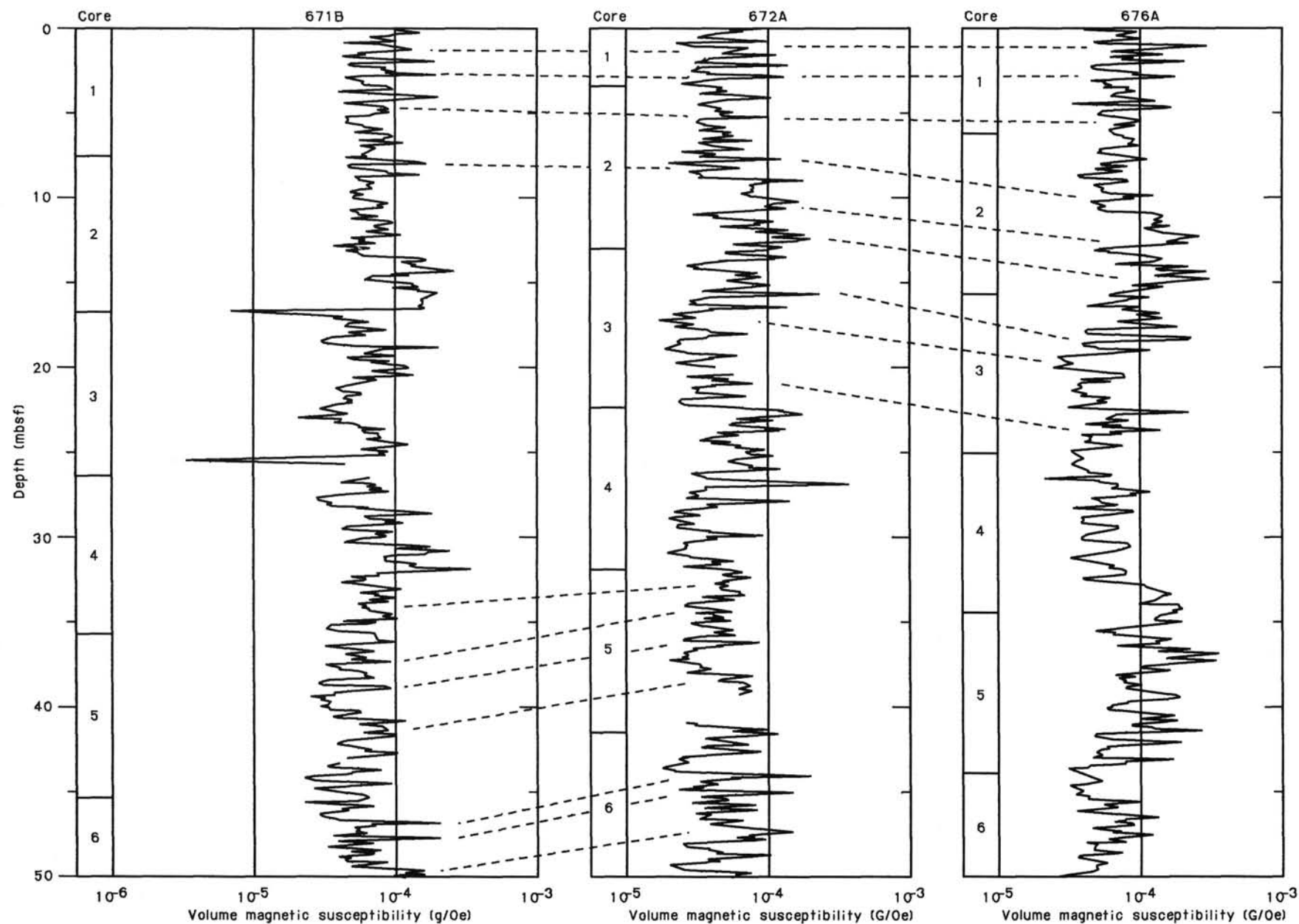


Figure 17. Correlations between magnetic susceptibility records of Holes 671A, 672A, and the upper part of Hole 676A.

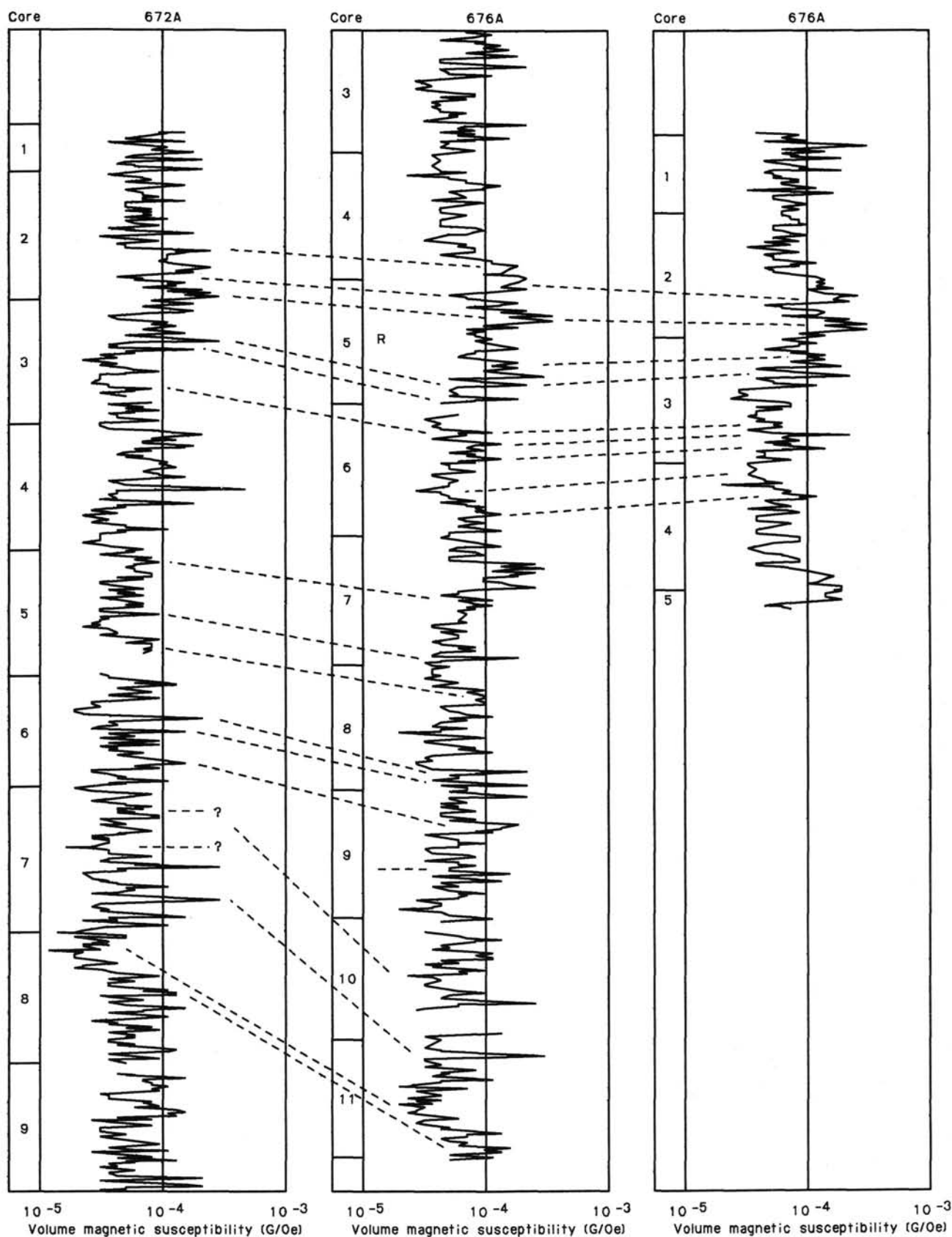


Figure 18. Detailed magnetic susceptibility correlations within Hole 676A and between Hole 672A and Hole 676A. The 'R' marked in Core 110-676A-5H indicates the possible position of a small thrust discussed in the text.

Table 3. Geochemistry data, Site 676.

Core 110-676A-	Sec.	Int. (cm)	Depth (mbsf)	PH	Alk. (mmol/L)	Salinity (‰)	Cl (mmol/L)	Ca (mmol/L)	Mg (mmol/L)	NH ₄ (μmol/L)	Si (μmol/L)	SO ₄ (mmol/L)	Na + K (mmol/L)	(Na + K)/Cl
1	3	145-150	5	7.88	4.71	34.2	558	12.0	49.8	25	—	25.5	490	0.88
2	5	145-150	13	7.55	3.26	34.0	561	14.7	46.7	89	525	26.0	494	0.88
3	5	145-150	22	7.41	3.55	34.1	563	16.0	43.3	116	284	24.0	496	0.88
4	5	145-150	33	7.43	3.00	33.9	560	17.7	41.4	148	345	22.3	489	0.874
I.S.*			36	—	—	34.4	562	17.5	45.9	90	260	24.6	486	0.865
5	5	145-150	42	—	—	34.0	561	18.6	39.9	178	529	21.1	488	0.87
7	5	145-150	61	7.74	1.90	33.7	558	19.9	37.7	188	271	21.4	488	0.874
8	5	145-150	70	7.76	1.41	33.5	563	20.4	35.9	209	284	19.8	491	0.873
I.S.*			73	—	—	—	559	21.5	—	100	184	21.5	—	—
10	5	145-150	89	7.75	1.47	33.5	559	22.1	34.7	207	227	20.5	488	0.875
I.S.*			92	—	—	—	530	24.1	34.4	121	142	20.0	455	0.858
12	2	145-150	105	7.78	2.17	33.8	560	24.2	33.6	253	206	20.7	488	0.871
15	2	145-150	133	7.38	1.42	33.8	558	26.9	31.7	265	239	20.3	483	0.865
17	5	145-150	155	7.67	1.34	33.8	554	28.9	30.5	263	248	18.3	473	0.853
19	5	145-150	170	7.95	3.49	33.5	549	30.0	30.5	289	182	19.0	467	0.85
21	5	145-150	190	7.85	1.57	32.2	547	31.0	30.9	298	203	18.0	460	0.841
23	4	145-150	210	—	—	33.5	544	31.3	32.5	269	208	18.1	454	0.835
25	1	145-150	228	—	—	33.5	543	31.0	32.3	313	208	18.2	454	0.836
27	5	145-150	250	—	—	32	519	31.6	32.6	314	233	16.4	425	0.819
28	6	145-150	260	—	—	32.2	536	32.9	32.6	330	224	16.9	440	0.821
30	5	145-150	275	7.71	2.39	33.5	547	32.7	33.1	385	1225	16.5	451	0.825
31	3	145-150	286	—	—	32.5	537	29.5	36.4	340	1050	18.3	443	0.825
32	3	145-150	295	—	—	33	546	32.2	33.5	346	1220	16.0	448	0.820
33	5	145-150	305	—	—	—	548	30.9	36.0	378	1163	15.0	445	0.812

*I.S. = *in-situ* sample.

Total Organic Content and Dissolved Methane

Methane

The highest methane concentrations at Site 676 (Table 4, Fig. 20) are correlated with three major thrust zones (see Structural Geology section). The high methane concentration of about 84 μmol/L found at 5 mbsf strongly indicates venting of fluids at the toe of the prism. Biological communities could be associated with these venting fluids. At 200 mbsf, the large methane amount is probably related to the eastward-propagating thrust described in Site 675. At 280 mbsf, the large methane amount is probably related to the eastward-propagating décollement described for Sites 671 and 675.

Total Organic Carbon

Similar to Sites 673, 674, and 675, the total organic carbon content in Site 676 is very low (<0.15%, Table 5). This organic matter value is too low to allow an exploitation of Rock-Eval parameters. In the sampled series from lower Pleistocene to lower Miocene, the organic matter is residual.

PHYSICAL PROPERTIES

Introduction

Site 676 is located very near the frontal thrust of the Barbados accretionary prism. This location was chosen to permit the examination of the sediments and physical processes occurring at the tip of the prism. Index properties, velocity, resistivity, and thermal conductivity data have been collected from 33 cores to a total depth of 310 mbsf.

Index Properties

Methods

The methods used to measure index properties at Site 676 are described in Chapter 1. Additional information may be found in the references cited in that chapter.

Results

The complete index properties dataset is located in Table 6. Figure 21 presents bulk density, porosity, grain density, water content (wet and dry calculations), velocity vs. depth below seafloor, and lithology. The following description of index proper-

ties will be presented in comparison to the lithostratigraphy and tectonic units which are described elsewhere in this chapter. No attempt was made to define unique index property units.

Lithostratigraphic Unit 1 consists predominantly of calcareous muds with occasional volcanic ash beds. Within the upper 35 mbsf there is a well-defined decrease in porosity from near 80% to 60% with a concomitant increase in bulk density from about 1.5 to 1.75 g/cm³. A very well-defined break at 35 mbsf marks a sharp increase in porosity back to seabed values, and a similar decline in the bulk density. This depth does not appear to correspond to a lithology change; however, it probably correlates to the zone of small-scale reverse and normal faulting as noted on the structural log. The most obvious feature that would give rise to such a pattern would be a thrust fault.

Below this level to a depth of about 140 mbsf there is a gradual decrease in porosity and water content, and increase in bulk density, with somewhat greater scatter noted between 35 and 80 mbsf. Between 140 and 170 mbsf there is a slight trend to increasing porosity and water content that does not match a similar change in lithology or structural fabric. Biostratigraphic evidence however, marks the top of this interval as the transition from Pliocene to late Miocene age sediments.

Lithostratigraphic Unit 2, from 162 to 244 mbsf, consists of barren upper Miocene, calcareous to noncalcareous, sometimes siliceous, mudstones and claystones. The porosity and water content measurements (Fig. 21), remain relatively constant through this interval, showing no obvious correlation with age, lithology, or structural fabric. Note, however, the enhanced variability in the bulk density throughout this interval. The scatter about a mean of 1.6 g/cm³ is likely a reflection of slight changes in grain density.

Lithostratigraphic Unit 3 consists of lower Miocene siliceous mudstones. A zone of dilatant veins and scaly fabric, which defines the propagating décollement zone, is present between 270 and 309 mbsf. However, a more distinct change occurs in index properties between 270 and 280 mbsf (Fig. 21). Bulk density takes a notable drop from near 1.60 to 1.50 g/cm³ throughout this interval and increases thereafter to near 1.70 g/cm³ at the bottom of the hole. Porosity and water contents display a concomitant decrease over the same interval. Some of the increase in bulk density may be explained by the increase in grain density through the same interval, which may be seen on Figure 21. Some of the lowest grain densities for Leg 110, less than 2.55 g/cm³, were observed in these siliceous sediments.

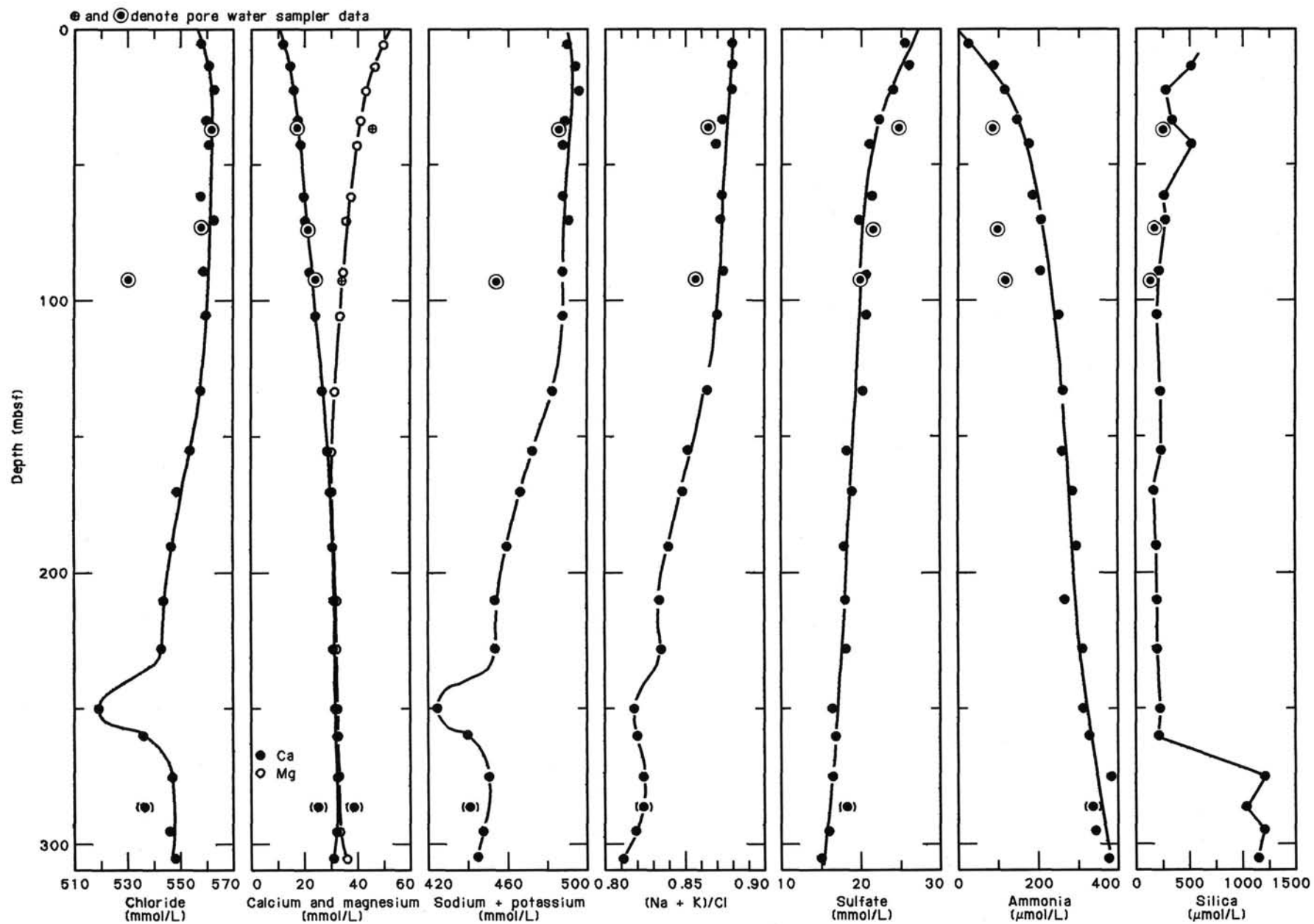
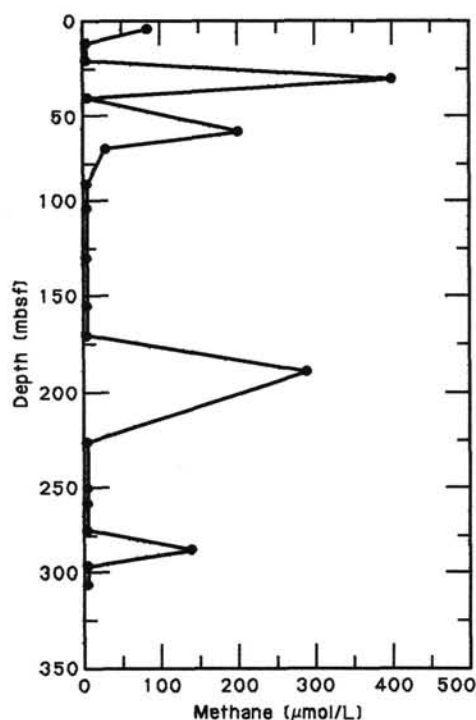


Figure 19. Profiles of chloride, calcium and magnesium, Na + K, (Na + K)/Cl, sulfate, ammonia, and silica, Site 676.

Table 4. Methane data, Site 676.

Core 110-676A-	Section	Depth (mbsf)	Methane ($\mu\text{mol/L}$)
1	3	5	84
2	5	13	—
3	5	22	—
4	5	33	409
5	5	42	—
7	5	61	206
8	5	70	26
10	5	89	—
12	2	105	—
15	2	133	—
17	5	155	—
19	3	170	—
21	3	190	293
25	1	228	—
27	5	250	—
28	6	260	—
30	5	275	—
31	3	286	141
32	3	295	—
33	5	305	—

— In these samples, the methane concentration is expected to be less than $3 \mu\text{mol/L}$.

**Figure 20. Methane profile, Site 676.**

Compressional Wave Velocity

Methods

The methods used at Site 676 to collect compressional wave velocity data are described in Chapter 1.

Results

Results of velocity measurements are listed in Table 7 and plotted vs. depth in Figure 21. The profile shows a rather general increase in velocity with depth, characteristic of a normally consolidating, unlithified sediment column. Figure 22 illustrates the relationship between velocity and porosity at Site 676. Virtually all of the data fall on the theoretical line describing the ve-

locity behavior of particles in a fluid matrix (Kuster and Toksöz, 1974). The range covered by the data from this site are very much like those of the upper sediments from the reference site (Site 672).

Discussion

It is unlikely that any seismic reflectors result from changes in the velocity profile, given the gradual nature of the change in velocity with depth. It is also unlikely that the sediments cored at Site 676 have undergone any significant amount of lithification. There is no indication in the velocity record of the deformation and disruption of strata evaluated in the core descriptions.

Thermal Conductivity

Methods

The method used to record thermal conductivity was that of the needle probe, described and referenced in Chapter 1.

Results

Thermal conductivity measurements at Site 676 are listed in Table 8 and plotted vs. depth in Figure 23. Thermal conductivity shows several breaks in downhole trends, related to the changes in water content seen in the index property profiles. Figure 25 illustrates that thermal conductivity is linearly related to water content at Site 676. Thus the maximum value of thermal conductivity occurs around 100 mbsf, where there is also a maximum in porosity. There is no indication in Figure 24 of a change to a solid matrix-dominated system, as has been seen at sites where the sediments have undergone diagenetic change.

Formation Factor

Methods

The method used to measure formation factor at Site 676 was the same as that used for all the other sites. A discussion of the method and references are contained in Chapter 1.

Results

Formation factor values at Site 676 are listed in Table 9 and plotted vs. depth in Figure 25. The formation factor appears to show an almost en echelon character with increasing depth. There are a series of increases and decreases occurring between 0 and 20, 20 and 40, 40 and 70 mbsf, and so on down the hole. A plot of formation factor vs. porosity (Fig. 26) suggests a general relationship between the two properties, with some amount of scatter which may be related to some of the reversals in the depth profile. The general trend of formation factor is an increase with depth to 100 mbsf.

Shear Strength

Methods

The methods used to measure undrained shear strength are the same as at the previous Leg 110 sites. Refer to Chapter 1 for a detailed discussion of the methods. Measurements were made to 161.2 mbsf. The measurements between 102.7 and 161.2 mbsf were made on XCB recovered samples.

Results

The miniature vane peak shear strength profile shows a consistent increase with depth below seafloor (Fig. 27). All measurements were made within lithologic Unit 1 (Table 10).

A linear least-squares approximation of the data results in the following relationship:

$$\text{Strength} = 34 + (0.82 \cdot \text{Depth})$$

where strength is in units of kPa and depth in units of meters.

Table 5. Rock-Eval data, Site 676.

Core 110-676A-	Sec.	Depth (mbsf)	Int. (cm)	T (°C)	S1	S2	S3	PI	S2/S3	PC	TOC	HI	OI
1	5	3	145-150	546	0.06	0.08	3.33	0.43	0.02	0.01	0.04	200	8325
2	5	13	145-150	578	0.03	0.09	2.54	0.25	0.03	0.01	0.05	180	5080
3	5	22	145-150	473	0.04	0.12	2.86	0.25	0.04	0.01	0.03	400	9533
4	5	33	145-150	433	0.05	0.09	3.09	0.36	0.02	0.01	0.03	300	10300
5	5	42	145-150	431	0.06	0.20	1.71	0.23	0.11	0.02	0.02	1000	8550
7	5	61	145-150	473	0.02	0.09	2.80	0.20	0.03	0.00	0.02	450	14000
8	5	70	145-150	416	0.04	0.06	2.60	0.40	0.02	0.00	0.02	300	13000
10	5	85	145-150	436	0.01	0.05	2.65	0.17	0.01	0.00	0.02	250	13250
12	2	105	145-150	441	0.10	0.11	4.07	0.50	0.02	0.01	0.04	275	10175
15	2	133	145-150	472	0.06	0.11	3.78	0.37	0.02	0.01	0.01	1100	37800
19	3	170	145-150	468	0.05	1.11	0.19	0.04	5.84	0.09	0.09	1233	211
21	3	190	145-150	480	0.03	1.38	0.62	0.02	2.22	0.11	0.11	1254	563
25	4	228	145-150	468	0.08	1.58	0.18	0.05	8.77	0.13	0.13	1215	138
27	5	250	145-150	481	0.06	1.28	0.18	0.04	7.11	0.11	0.11	1163	163
28	6	260	145-150	484	0.07	1.47	0.28	0.05	5.25	0.12	0.12	1225	233
30	5	275	145-150	473	0.08	0.97	0.26	0.08	3.73	0.08	0.08	1212	325
31	3	286	145-150	453	0.22	1.61	0.33	0.12	4.87	0.15	0.15	1073	220
32	3	295	145-150	449	0.18	1.34	0.30	0.12	4.46	0.12	0.12	1116	250
33	5	305	145-150	449	0.06	0.75	0.29	0.07	2.58	0.06	0.06	1250	483

S1 (mg hydrocarbon/g rock): the quantity of free hydrocarbons present in the rock and which are volatilized below 300°C.

S2 (mg hydrocarbon/g rock): the amount of hydrocarbon-type compounds produced by cracking of kerogen as the temperature increases to 550°C.

S3 (mg CO₂/g rock): quantity of CO₂ produced from pyrolysis of the organic matter in the rock.

S2/S3: A means of determining the type of organic matter in the rock.

— from 0.0 to 2.5: gas, type III

— from 2.5 to 5.0: oil/gas, type III

— from 5.0 to 10.0: oil, types I and II

Temperature (°C): maximum temperature at which maximum generation of hydrocarbon from kerogen occurs.

PI (Productivity index): $PI = S1/(S1 + S2)$.

PI characterizes the evolution level of the organic matter.

PC "Pyrolyzed carbon": $PC = k(S1 + S2)$ where $k = 0.083$ mg C/g rock.

PC corresponds to the maximum quantity of hydrocarbons capable of being produced from the source rock given sufficient burial and time.

TOC: Total Organic Carbon

HI "Hydrogen index": $HI = (100 \times S2)/TOC$

OI "Oxygen index": $OI = (100 \times S3)/TOC$

The residual shear strength, as described in Site Chapter 671 when used in a ratio with peak strength to obtain a measure of sediment sensitivity results in values of 1 to 3.

Within the upper zone of faults as described in the "Structural Geology" section, this chapter, high values of 103.8 kPa at 33.45 mbsf and 126.81 kPa at 42.95 mbsf were measured. In addition, measurements made on the full round section (lateral) are higher within this interval than the measurements made on the split core (vertical).

The total and hydrostatic stress conditions were calculated for Site 676 using the bulk density data summed with depth below seafloor. The stresses are very close to linear with depth (Fig. 28).

Discussion

The strength data are very consistent at Site 676. The only deviations from increase with depth below seafloor are the peak values measured within Cores 110-676A-4H and -5H. The linear approximation to the data is very similar to the reference Site 672 below 40 mbsf and Site 674 (intercept = 36 kPa and slope = 0.8). As discussed in the Site 674 chapter, the high intercept may be indicative of a loss of sediment within the upper 20 m of Hole 676A on the order of tens of meters.

SEISMIC STRATIGRAPHY

Site 676 is located on the lower slope of the deformation front, about 250 m west and 20–25 m above the adjacent oceanic plain. At this site we drilled through the youngest accreted sequences (0–34 mbsf), which slightly overthrust the sedimentary cover of the incoming oceanic crust (34–310 mbsf).

Three seismic sequences in the Atlantic sedimentary cover are clearly depicted on the upper section of line CRV 128 (Fig. 29). The two upper sequences were penetrated at Site 676 and their stratigraphic characteristics are consistent with those at Site 672, 6 km to the east. The upper seismic sequence (A) comprises weak to very weak reflectors and is of Pliocene to Pleistocene age. Seismic sequence B, downsection, is composed of relatively strong and discontinuous reflectors and is of Miocene age. The lower seismic sequence was not drilled at Site 676, but it is well correlated with sequences C of Site 672. Sequence C is almost transparent and is of late Eocene to Oligocene age. The deepest sequences, D of middle Eocene age and E of Senonian to early Eocene age at Site 672, are also present below sequence C at Site 676 as seen on Figure 3.

Frontal deformation in Pleistocene sediments (Cores 110-676A-4H and -5H) is not visible in the seismic record, but it forms a prominent scarp on the seafloor. The wavelengths of folds above the thrust fault at 34 mbsf are obviously too short for these structures to be imaged by seismic surveying tools, and, additionally, acoustic impedance contrasts are very low in the Pleistocene series. However, a few hundred meters west of Site 676 the frontal thrust is seen deeper in the section (arrow). Assuming an interval velocity of 1600 m/s, the apparent dip of this thrust is about 10° to the west. The repetition of a portion of the upper Miocene section at a depth of 205 m was quite unexpected from the initial interpretation of line CRV 128. A closer examination of the seismic record, however, revealed, at the appropriate depth, a weak westward dipping reflector (R) that can be interpreted as the trace of a deep thrust fault originating from the décollement (D). This fault represents a new upward-propagating frontal thrust as the décollement is itself propagating to the east.

Table 6. Index properties summary, Hole 676A.

Core 110-676A-	Sec.	Int. (cm)	Depth (mbsf)	% water (wet)	% water (dry)	Porosity (%)	Bulk density	Grain density
1	2	75	2.25	53	116	77.5	1.47	2.59
2	2	70	8.40	49	97	72.9	1.52	2.59
2	4	75	11.45	49	96	72.9	1.52	2.60
2	6	75	14.45	49	97	73.2	1.52	2.62
3	2	70	17.90	46	85	70.1	1.56	2.69
3	4	70	20.90	41	70	65.8	1.64	2.63
3	6	70	23.90	41	71	66.4	1.64	2.63
4	2	70	27.40	43	75	67.4	1.61	2.66
4	4	70	30.40	39	63	64.2	1.70	2.64
4	6	70	33.40	35	54	59.2	1.73	2.70
5	2	80	37.00	48	91	73.9	1.59	2.85
5	4	75	39.95	50	100	74.6	1.53	2.63
5	6	75	42.95	44	79	69.4	1.61	2.64
6	2	80	46.50	40	68	63.3	1.60	2.68
6	4	75	49.45	36	56	61.4	1.74	2.76
6	6	75	52.45	42	71	65.8	1.62	2.67
7	2	65	55.85	46	85	70.3	1.56	2.67
7	4	65	58.85	38	61	63.2	1.70	2.71
7	6	65	61.85	38	62	63.6	1.70	2.70
8	2	65	65.35	40	67	64.8	1.65	2.70
8	4	65	68.35	36	57	60.5	1.70	2.53
8	6	65	71.35	36	56	60.2	1.72	2.67
9	2	62	74.82	42	73	66.2	1.61	2.65
9	4	60	77.80	43	76	67.8	1.60	2.60
9	6	65	80.85	34	51	57.1	1.74	2.69
10	2	65	83.65	37	58	61.4	1.71	2.68
10	4	66	86.66	32	47	56.1	1.79	2.67
10	6	65	89.65	35	54	59.6	1.75	2.68
11	2	65	93.85	35	54	59.1	1.74	2.66
11	4	67	96.87	33	50	57.5	1.78	2.69
11	6	62	99.82	35	54	59.2	1.73	2.65
12	2	69	103.39	35	56	60.1	1.74	2.67
12	4	68	106.38	34	53	58.3	1.73	2.62
13	2	69	112.89	38	61	62.6	1.69	2.64
13	4	68	115.88	35	53	59.1	1.75	2.67
13	6	70	118.90	37	59	62.1	1.72	2.69
15	1	70	130.40	37	59	61.7	1.70	2.63
15	2	74	131.94	38	62	63.4	1.70	2.58
16	2	66	141.36	31	46	56.1	1.83	2.73
16	4	75	144.45	31	44	54.7	1.82	2.63
17	2	7	150.27	39	64	62.9	1.66	2.62
17	4	84	154.04	38	61	64.4	1.74	2.81
17	6	10	156.30	35	53	59.8	1.77	2.72
18	2	70	160.40	40	66	64.8	1.67	2.62
18	4	80	163.50	38	60	62.4	1.70	2.74
18	6	69	166.39	43	76	68.4	1.63	2.62
19	2	70	169.90	47	89	71.8	1.56	2.68
19	4	80	173.00	42	73	67.0	1.63	2.65
20	2	70	179.40	46	85	70.0	1.56	2.61
20	4	78	181.48	39	65	65.1	1.69	2.68
20	6	132	186.02	40	67	66.3	1.69	2.67
21	2	60	188.80	42	72	66.1	1.61	2.65
21	4	29	191.49	41	70	65.5	1.63	2.61
22	2	95	198.65	40	68	65.9	1.67	2.62
22	6	50	204.20	47	89	71.5	1.55	2.55
23	3	107	209.77	46	87	70.6	1.56	2.61
23	5	69	212.39	43	77	68.0	1.60	2.56
24	2	74	217.44	34	52	59.1	1.77	2.73
24	4	74	220.44	36	56	58.6	1.69	2.67
24	6	73	223.43	41	69	68.3	1.71	2.80
25	1	111	225.81	40	65	64.3	1.67	2.60
26	1	35	234.55	42	73	67.4	1.63	2.62
27	2	67	245.87	40	67	65.0	1.66	2.65
27	4	54	248.74	46	84	70.2	1.57	2.66
27	6	64	251.84	43	76	68.8	1.63	2.80
27	6	64	251.84	43	76	68.8	1.63	2.80
28	2	60	255.30	48	91	72.0	1.54	2.64
28	4	79	258.49	48	92	71.9	1.54	2.65
28	6	45	261.15	43	75	67.3	1.61	2.75
30	2	68	274.38	51	103	73.7	1.49	2.49
30	4	110	277.80	51	104	73.8	1.48	2.56
30	5	54	278.74	47	89	69.8	1.51	2.56
30	6	77	280.47	46	84	70.5	1.58	2.66
31	2	70	283.90	40	66	64.1	1.65	2.57
31	4	135	287.55	38	62	61.5	1.65	2.56
31	6	70	289.90	41	70	65.0	1.62	2.57
32	2	81	293.51	43	75	66.5	1.58	2.64
32	4	77	296.47	40	66	64.6	1.67	2.62
32	6	77	299.47	41	68	64.7	1.64	2.59
33	2	90	303.10	39	64	63.2	1.66	2.67
33	4	77	305.97	36	56	60.7	1.74	2.68
33	6	85	309.05	36	57	60.0	1.70	2.64

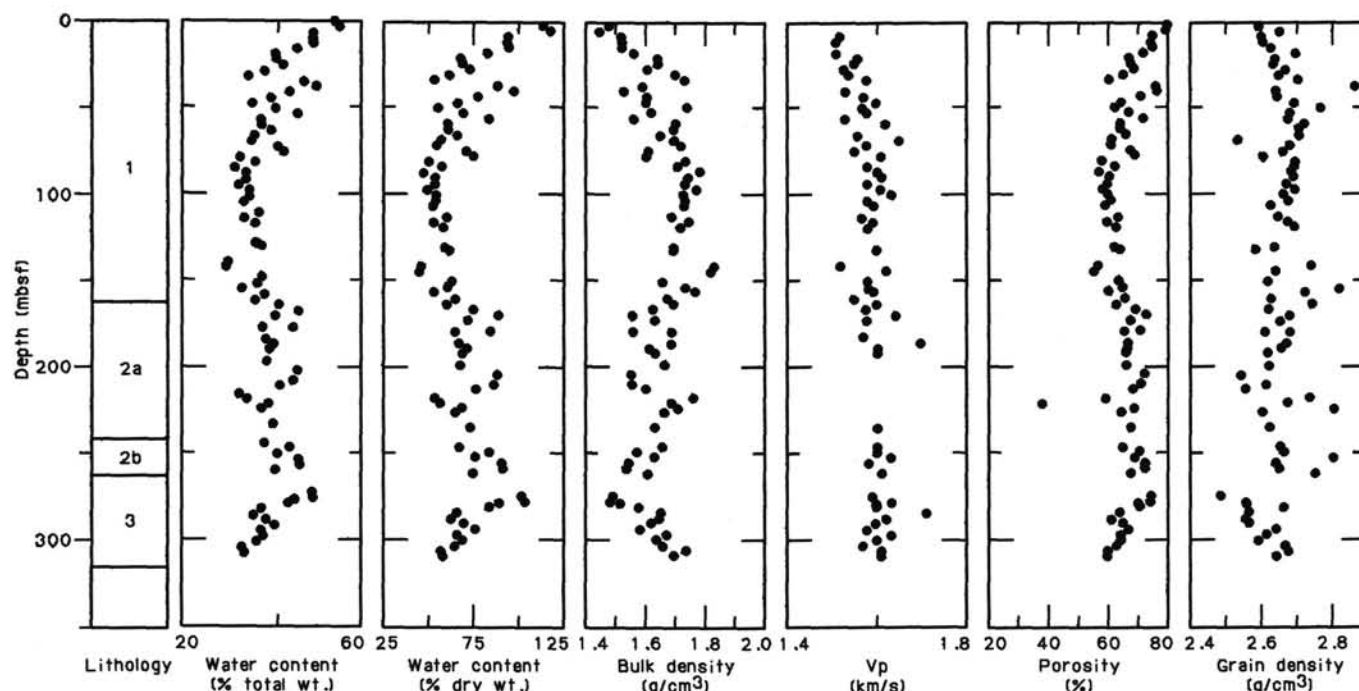


Figure 21. Index properties and compressional wave velocity vs. depth at Site 676.

HEAT FLOW

Introduction

Site 676 was positioned with the intent of drilling first through the propagating frontal thrust of the offscraped sediments and then down through the décollement into the underthrust sequence. Site 676 is the easternmost site drilled into the complex itself on Leg 110. Thus Hole 676A was drilled through some of the structurally youngest sediments of the complex.

Methods and Results

Experimental methods and tools are discussed in Chapter 1. The APC tool recorded temperatures at 15-s intervals, while the T-probe measured temperatures every 60 s. Tool properties are summarized in Table 11 and temperature measurements are summarized in Table 12.

The APC tool was deployed three times in Hole 676A to depths of 25.6, 44.6, and 63.6 mbsf. Before shooting the core into the sediment on the first deployment, the shoe was held at mudline for 10 min to measure bottom-water temperature. The record from this run (Fig. 30) indicates a bottom-water temperature of 2.18°C ($\pm 0.05^{\circ}\text{C}$). This temperature is slightly lower than bottom water measured at other sites on Leg 110, but was confirmed by later deployments of the APC tool and the T-probe at Site 676.

The record from the first APC tool run with Core 110-676A-3H at 25.6 mbsf (Fig. 30) indicates that the shoe moved while in the sediment, causing frictional heating of the probe. It is not unusual for the bit assembly to move a small amount in these fairly unconsolidated upper sediments. The final temperature extrapolated from the first portion of the record from this run is 6.95°C ($\pm 0.10^{\circ}\text{C}$). The second APC tool deployment with Core 110-676A-5H at 44.6 mbsf resulted in a superior record (Fig. 31) and a final temperature of 8.30°C ($\pm 0.05^{\circ}\text{C}$). The third and final APC tool deployment was with Core 110-676A-

7H at 63.6 mbsf and produced the best record of the group (Fig. 32) with a final sediment temperature of 8.00°C ($\pm 0.05^{\circ}\text{C}$).

The T-probe was deployed six times in Hole 676A, with five successful runs. The first run, to a depth of 35.7 mbsf after Core 110-676A-4H, was unsuccessful as the probe moved continuously while in the sediment (Fig. 33A). The next run, after Core 110-676A-8H at 73.4 mbsf (Fig. 33B), yielded an extrapolated temperature of 9.05°C ($\pm 0.05^{\circ}\text{C}$). Later runs after Cores 110-676A-11H, -16X, -21X, and -26X, were also successful (see Figs. 33C, 34A, 34B, and 34C, respectively). The final temperatures from these runs are 11.50°C ($\pm 0.05^{\circ}\text{C}$) at 101.6 mbsf, 13.95°C ($\pm 0.05^{\circ}\text{C}$) at 149.1 mbsf, 17.05°C ($\pm 0.05^{\circ}\text{C}$) at 196.6 mbsf, and 20.00°C ($\pm 0.05^{\circ}\text{C}$) at 244.1 mbsf.

Interpretations

The calculated surface thermal gradient (from bottom water and the sediment temperature at 25.6 mbsf) is $186^{\circ}\text{C}/\text{km}$. This gradient decreases between 25.6 and 44.6 mbsf to $71^{\circ}\text{C}/\text{km}$. There is a distinct gradient inversion between 44.6 and 63.6 mbsf. These temperatures are believed to be accurate because a) all APC measurements were made with the same tool and earlier results did not suggest malfunction; b) the measurements at 44.6 and 63.6 mbsf were taken 9.5 m ahead of the bit (like all APC temperatures), well away from any likely drilling disturbance; and c) the curves extrapolated to yield the sediment temperatures at 44.6 and 63.6 mbsf (Figs. 31 and 32) are some of the most complete seen on Leg 110. Thus the data are accepted as accurately reflecting temperatures in the sediment column at Site 676.

The final APC tool and the first T-probe measurements are colinear with bottom water, and fit a straight line with a gradient of $92^{\circ}\text{C}/\text{km}$. The bottom four T-probe measurements were fitted with a linear-least-squares best-fitting line that yields a gradient of $60^{\circ}\text{C}/\text{km}$ for the lower 140 mbsf of Hole 676A (Fig. 35). These last two gradients intersect close to 100 mbsf.

Table 7. Compressional wave velocity, Hole 676A.

Core 110-676A-	Sec.	Int. (cm)	Depth (mbsf)	Vel(A)* (km/s)	Vel(B)* (km/s)
2	2	70	8.40		1.52
2	4	70	11.40		1.51
3	2	70	17.90		1.51
3	4	70	20.90		1.56
3	6	70	23.90		1.55
4	2	70	27.40		1.53
4	4	70	30.40		1.54
4	6	70	33.40		1.58
5	4	80	40.00		1.53
5	6	80	43.00	1.56	1.57
6	2	87	46.57		1.60
6	4	84	49.54		1.57
6	6	69	52.39		1.58
7	2	65	55.85		1.53
7	4	65	58.85	1.63	1.62
7	6	65	61.85	1.61	
8	2	65	65.35	1.55	1.56
8	4	65	68.35	1.63	1.65
8	6	65	71.35	1.57	1.58
9	2	62	74.82	1.55	1.55
9	4	60	77.80	1.59	1.61
9	6	65	80.85	1.58	
10	2	65	83.65	1.57	1.58
10	4	66	86.66	1.59	1.60
10	6	65	89.65	1.60	1.61
11	2	65	93.85	1.59	1.58
11	4	67	96.87	1.61	1.61
11	6	62	99.82	1.61	1.63
12	2	69	103.39	1.53	1.58
12	4	68	106.38	1.59	1.59
13	2	69	112.89	1.57	1.57
13	4	68	115.88	1.60	1.59
13	6	70	118.90	1.59	1.58
15	2	99	132.19	1.60	1.60
16	2	19	140.89		1.52
16	4	57	144.27		1.62
17	2	7	150.27	1.59	1.58
17	4	84	154.04	1.57	1.58
17	6	10	156.30	1.59	1.59
18	2	70	160.40		1.55
18	4	80	163.50	1.59	1.60
18	6	69	166.39	1.58	1.58
19	2	70	169.90	1.63	1.64
19	4	80	173.00	1.57	1.58
20	4	78	182.48	1.57	1.57
20	6	132	186.02	1.58	1.70
21	2	60	188.80	1.59	1.60
21	4	29	191.49	1.58	1.60
26	1	35	234.55		1.60
27	2	67	245.87		1.60
27	4	54	248.74	1.66	1.60
27	6	64	251.84		1.63
28	2	60	255.30	1.59	1.58
28	6	45	261.15	1.58	1.61
30	2	68	274.38	1.61	1.59
30	4	110	277.80	1.91	1.63
30	5	54	278.74	1.58	1.60
30	6	77	280.47	1.57	1.60
31	2	70	283.90	1.60	1.71
31	4	135	287.55	1.63	1.62
31	6	70	289.90	1.60	1.60
32	2	81	293.51	1.59	1.58
32	4	77	296.47	1.61	1.63
32	6	77	299.47	1.58	1.60
33	2	90	303.10	1.57	1.57
33	4	77	305.97	1.59	1.61
33	6	85	309.05		1.61
33	6	85	309.05	1.59	

*Velocity measured parallel (Vel A) and perpendicular (Vel B) to core axis.

After accounting for changes in thermal conductivity (Physical Properties section, this chapter; Fig. 36) by computing the integrated thermal resistance at each sediment-temperature depth (see Heat Flow section, Site 672), heat flow values were calculated (Fig. 37). The calculated surface heat flow at Site 676 is

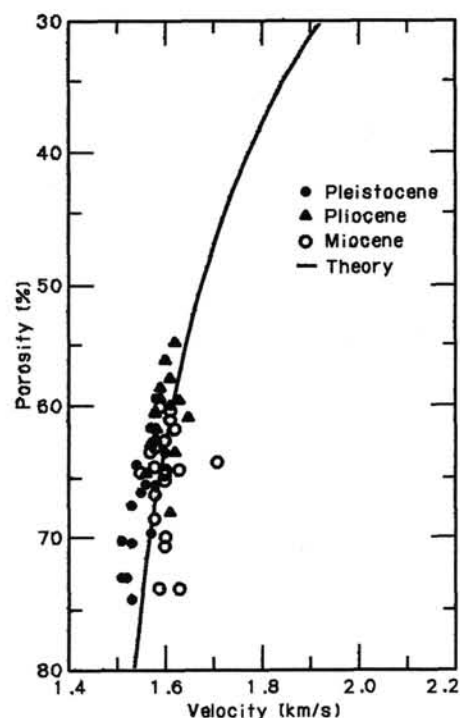


Figure 22. Compressional wave velocity vs. porosity at Site 676. Solid line represents theoretical relationship for unlithified sediments.

202 mW/m², which is lower than that measured at the surface of Site 674 (218 mW/m²; Heat Flow section, Site 674 chapter), but still one of the highest values measured in the region (Speed et al., 1984; Langseth et al., 1986). The lowermost APC temperature and the uppermost two T-probe temperatures are still colinear with a heat flow of 117 mW/m². The lowermost four T-probe measurements are colinear with a heat flow of 75 mW/m².

In comparison to the thermal regime predicted by cooling plate models (e.g., Anderson and Skilbeck, 1982; Lister, 1977) and thermal models of active margins (e.g., Hsui and Toksoz, 1979), all the above gradients are anomalous. The deepest confirmed gradient of 60°C/km (with heat flow of 75 mW/m²) is 30% higher than that predicted by either type of model. In addition, the extremely high surface gradient and thermal inversion noted earlier require that unusual processes be active in the sediments near the deformation front.

One possibility is that recent thrusting has displaced warm sediments to the surface from depth. Simple thermal modeling suggests that such an event would need to have occurred in the last several hundred years for the sediment to still be in thermal disequilibrium.

An alternative explanation is that warm fluid is flowing along a frontal thrust somewhere between 25.6 and 44.6 mbsf and raising sediment temperatures both below and above this conduit. In either case, the thermal structure of the sediments is in a transient state.

The second hypothesis is supported by the presence of a jump in porosity, bulk density, and water content at around 38 mbsf (Physical Properties section, this chapter), a repeated magnetic susceptibility section starting at 29–32 mbsf (Paleomagnetism section, this chapter) and a methane anomaly (Geochemistry section, this chapter). The changes in physical properties and the repeating magnetic susceptibility signature suggest the presence of a thrust fault between 29 and 38 mbsf. The methane anomaly is consistent with the migration of warm fluid along a high permeability conduit.

Table 8. Thermal conductivity, Hole 676A.

Core 110-676A-	Sec.	Int. (cm)	Depth (mbsf)	Thermal conductivity	
				Cal/cm·°C·s ($\times 10^{-3}$)	W/m·°C
1	2	75	2.25	2.47	1.030
1	4	75	5.25	2.40	1.010
2	4	75	11.45	2.49	1.040
3	4	75	20.95	2.92	1.220
4	4	75	30.45	2.94	1.230
5	2	75	36.95	2.66	1.110
6	2	75	46.45	2.68	1.120
7	2	70	55.90	2.70	1.130
8	2	70	65.40	2.95	1.230
9	2	75	74.95	2.74	1.150
9	6	70	80.90	3.30	1.380
10	2	70	83.70	3.29	1.380
10	4	70	86.70	3.26	1.370
11	2	70	93.90	3.14	1.320
11	4	70	96.90	3.29	1.380
12	2	50	103.20	3.19	1.340
12	4	50	106.20	3.29	1.380
13	2	75	112.95	3.08	1.290
13	4	75	115.95	3.37	1.410
15	2	58	131.78	3.12	1.310
16	4	75	144.45	3.14	1.320
17	2	80	151.00	2.30	1.250
17	4	80	154.00	2.89	1.210
18	2	70	160.40	2.78	1.160
18	4	80	163.50	3.09	1.290
19	2	80	170.00	2.87	1.200
19	4	80	173.00	2.82	1.180
20	2	70	179.40	2.73	1.143
20	4	80	182.50	2.96	1.239
21	2	68	188.88	2.85	1.193
21	4	28	191.48	2.89	1.209
22	2	77	198.47	2.66	1.110
22	4	77	201.47	2.71	1.130
23	2	75	207.95	2.82	1.180
23	4	75	210.95	3.02	1.270
24	2	75	217.45	3.01	1.260
24	4	75	220.45	2.91	1.220
26	2	33	236.03	2.65	1.110
26	2	70	236.40	2.65	1.109
27	2	60	245.80	2.85	1.190
27	4	56	248.76	2.68	1.124
28	2	70	255.40	2.65	1.110
28	4	70	258.40	2.67	1.117
30	2	70	274.40	2.44	1.020
30	4	100	277.70	2.26	0.945
31	2	70	283.90	2.73	1.142
31	6	70	289.90	2.77	1.158
32	2	80	293.50	2.87	1.202
32	4	80	296.50	2.39	1.001
33	2	80	303.00	2.86	1.200
33	4	80	306.00	2.92	1.220

LOGGING RESULTS

Operations

On August 14th, from 0730 to 1500, Site 676 was the scene of the final logging operations of Leg 110. The soft claystone formation penetrated by Hole 676A did not offer a transition to competent rock as a likely place to set the pipe, so the choice was made to leave the bit at 122 mbsf, a few meters beyond the depth at which piston coring ceased. With the hole filled by 137 barrels (about 21,000 L) of 9.7 lb/gal (1160 kg/m³) bentonite mud, a Schlumberger DIL-LSS-CAL-GR tool string (described in the Site 671 chapter) was sent down. After a number of passes into the open hole, the string finally stopped at an impassable obstruction at 162 mbsf. While the hole conditions did not appear to present insurmountable difficulties, there was not enough time available to pull the logging tools, add more pipe to the drill string, push on past the obstacle, and once again lower the logging tools. Thus, a continuous open hole log was run up from the obstruction to the bit (covering Cores 110-676A-17X through -14X), and logging operations were ended.

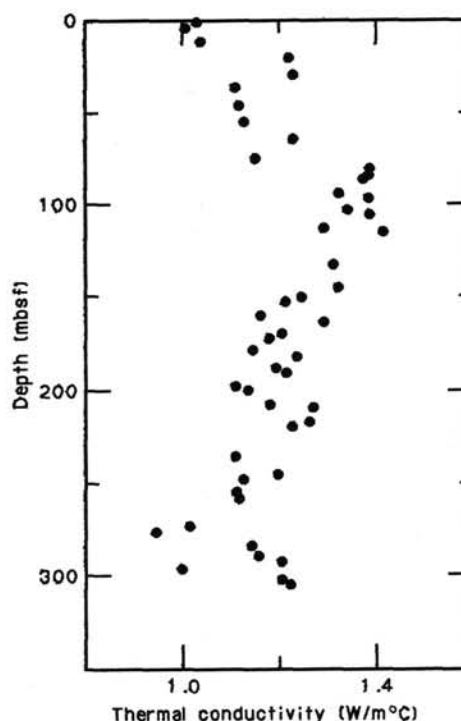


Figure 23. Thermal conductivity vs. depth at Site 676.

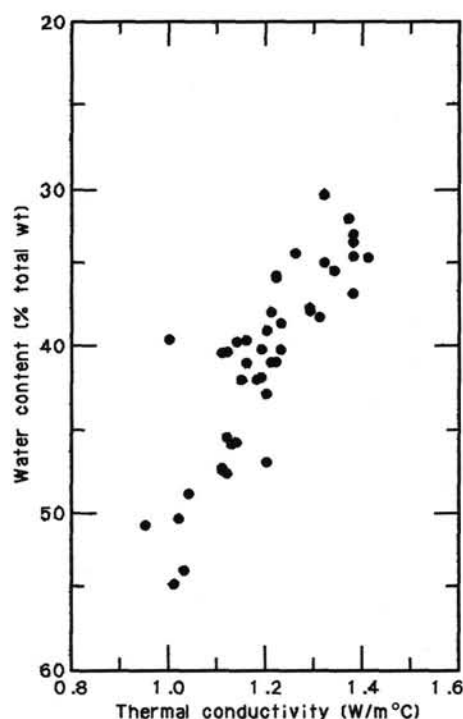


Figure 24. Thermal conductivity vs. water content (% total weight) at Site 676.

Results

Figure 38 displays the results of the logging, along with the locations of cores in the logged interval. All of the measurements fall within a section that is predominantly calcareous mud and marl (see Lithostratigraphy section). The caliper curve (displayed in track 1) shows the most variation of any of the curves,

Table 9. Sediment formation factor in Hole 676A.
F-horizontal: electrodes positioned across core.
F-vertical: electrodes positioned along core axis.

Core 110-676A-	Sec.	Int. (cm)	Depth (mbsf)	F-horiz.	F-vert.
1	2	70	2.20	2.18	2.36
1	4	77	5.27	2.30	2.50
2	2	70	8.40	2.50	2.80
2	4	70	11.40	2.70	2.80
2	6	70	14.40	3.10	3.10
3	2	70	17.90	3.10	3.40
3	4	70	20.90	3.60	4.00
3	6	68	23.88	3.50	3.80
4	2	68	27.38	3.10	3.30
4	4	68	30.38	3.70	4.00
4	6	68	33.38	3.70	4.00
5	2	82	37.02	3.20	4.50
5	4	77	39.97	2.75	3.00
5	6	62	42.82	3.00	3.50
6	2	83	46.53	3.75	3.75
6	4	68	49.38	4.28	4.72
6	6	83	52.53	3.89	3.89
7	2	65	55.85	4.13	4.38
7	4	60	58.80	4.42	4.82
7	6	60	61.80	5.00	5.25
8	2	60	65.30	4.25	4.50
8	4	60	68.30	4.44	4.72
8	6	60	71.30	4.72	5.22
9	2	60	74.80	4.25	4.50
9	4	62	77.82	4.50	4.63
9	6	60	80.80	5.13	5.31
10	2	60	83.60	4.17	4.44
10	4	60	86.60	4.00	4.70
10	6	65	89.65	4.78	5.00
11	2	60	93.80	4.56	4.89
11	4	60	96.80	5.28	5.28
11	6	60	99.80	4.89	5.11
12	2	60	103.30	5.00	5.11
12	4	60	106.30	5.11	5.33
13	2	60	112.80	4.11	4.56
13	4	60	115.80	5.00	5.22
13	6	60	118.80	4.30	4.70
15	1	62	130.32	4.50	4.25
15	2	63	131.83	6.50	5.75
16	4	85	144.55	5.33	5.33
17	5	120	155.90	3.96	4.17

starting at a near-bit-size value of 10.5 in. at 150 mbsf, increasing to values in the range of 13–15 in. between 149 and 135 mbsf, dropping abruptly to 5 in. between 135 and 133 mbsf and then oscillating between 10 and 15 in. from 133 mbsf to the drill bit at 122 mbsf. This large variation of hole size is a good indicator of the poor hole conditions, with the constriction at 133 mbsf probably arising from an accumulation of fill falling below the drill bit.

The measure of natural background radiation (the GR curve) is also displayed in track 1. Two observations can be made about the behavior of this curve. First, there is a general decrease in radioactivity up the hole, with the peak value of 65 API units at 151 mbsf dropping to 35 API units at 127 mbsf; this decrease apparently corresponds to a general increase in the carbonate content across this section (see Lithostratigraphy section). Second, the locations of ash layers (indicated in the lithologic column) correspond in general to slight increases in the radiation curve, but the changes are so small (on the order of 2–4 API units) that a direct cause-and-effect correlation cannot be made with confidence.

The resistivity curves (ILD, ILM, and SFLU), which are displayed in track 2, provide what is, perhaps, the most interesting variation in properties over the logged interval. From the bottom of the section at 160 mbsf up to 135 mbsf, there is a gradual, but steady, increase in ILM and ILD resistivity from approximately 3 ohm-m to approximately 4 ohm-m, with the oscil-

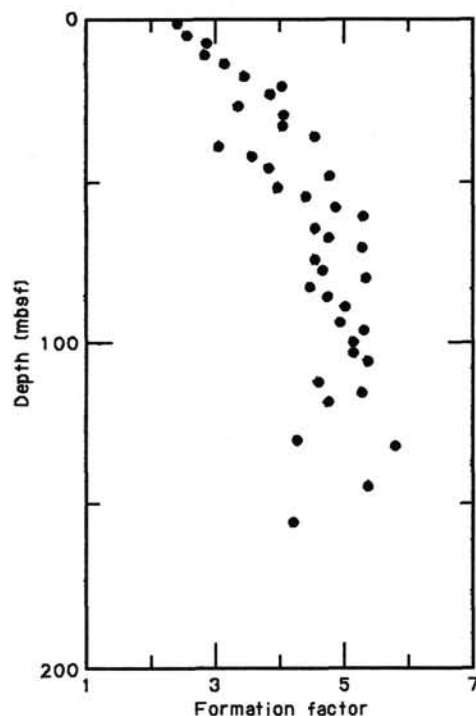


Figure 25. Formation factor vs. depth at Site 676.

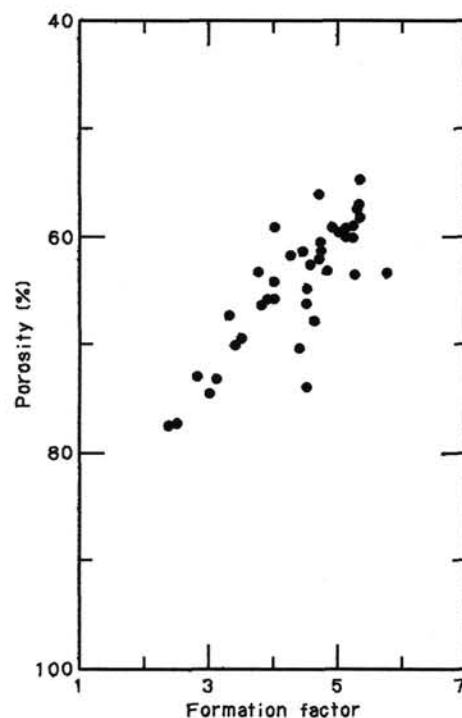


Figure 26. Formation factor vs. porosity at Site 676.

lations in the curve corresponding, in general, to changes in hole diameter. These values are generally consistent with the values measured at similar depths in Holes 672A and 671C. From 135 to 130 mbsf there is a rapid decrease to a value of 1 ohm-m, a value that is maintained all the way into the bit at 122 mbsf. This decrease does not correspond to any change in hole diameter, so only four possibilities can account for it.

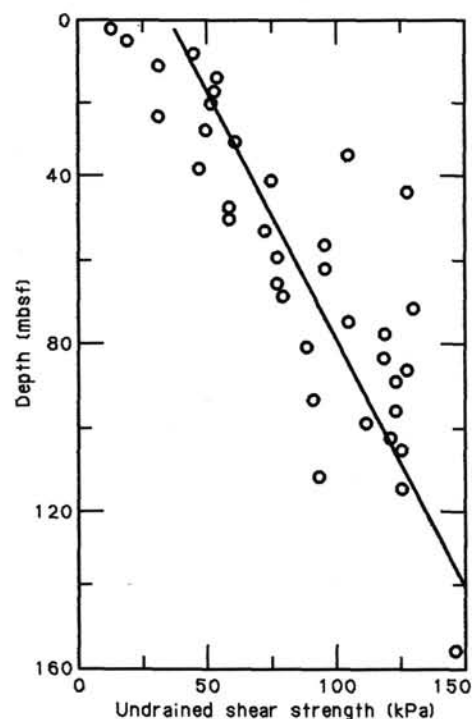


Figure 27. Undrained shear strength vs. depth at Site 676. The solid line represents a linear least-squares fit to the data.

The first, and least likely, possibility is that there is a major increase in pore-water salinity; there have not been any recorded changes of this type in any of the Leg 110 holes. An anomalous mud accumulation is another possibility, but since the mud has only 75% of the salinity of sea water, an accumulation would cause an *increase* in resistivity. If there was an absence of mud above the hole constriction (as might have been caused by the pumping that was necessary to get the tool string through the bottom hole assembly), then the predicted result would be normal resistivity values above the constriction and anomalously *high* values below the constriction. This explanation conflicts with the consistency of the measurements below the constriction and with measurements recorded by logs in the other Leg 110 holes. A third possibility is that there is a sudden increase in porosity at this depth. The physical properties data (see Physical Properties section) show a small increase in porosity, but the sonic velocity measurement (discussed below), which is usually a good indicator of porosity, does not show any major variation here. Thus, a large porosity change appears unlikely. Finally, it is possible that there is a change in the resistivity of the formation without a concomitant change in the porosity or other physical parameters. This could easily be accomplished through improved interconnectedness of pores via microfractures that would not show up as large changes in porosity, or through a change in electrical properties owing to mineralogical variations. The actual cause of this resistivity change is not clear, although a drop in values of shipboard measurements of formation factor (See Physical Properties section) confirms this change.

The results of the sonic velocity measurement are displayed as slowness values in track 3. Despite some problems with cycle-skipping, the values of slowness remain remarkably constant for both the long-spacing (DTL) measurement and the short-spacing (DT) measurement. The peak value of slowness is approximately 182 $\mu\text{s}/\text{ft}$ (1.68 km/s), occurring at 140 mbsf, and the lowest value is approximately 175 $\mu\text{s}/\text{ft}$ (1.74 km/s), occurring at 139, 138, and 130 mbsf. Thus, given the relatively unspectacular nature of the variations in this log, the only additional observation that can be made about the slowness values is that

Table 10. Vane shear strength, Hole 676A.

Core 110-676A-	Sec.	Int. (cm)	Depth (mbsf)	Peak (kPa)	Residual (kPa)
1	2	75	2.25	11.99	6.92
1	4	76	5.26	17.98	10.14
2	2	75	8.45	43.81	23.06
2	3	0	9.20	31.00	14.53
2	4	75	11.45	29.98	23.06
2	6	80	14.50	53.05	41.50
3	2	75	17.95	51.88	20.74
3	3	0	18.70	46.11	29.98
3	4	75	20.95	50.72	27.66
3	6	75	23.95	29.97	19.61
4	2	75	27.45	48.43	23.06
4	3	0	28.20	69.17	25.37
4	4	75	30.45	59.94	25.36
4	6	75	33.45	103.75	41.50
5	2	68	36.88	46.11	32.28
5	3	0	37.70	94.53	43.81
5	4	75	39.95	73.78	20.75
5	6	75	42.95	126.81	50.72
6	2	76	46.46	57.64	25.36
6	4	75	49.45	57.64	27.67
6	6	75	52.45	71.47	41.50
7	2	70	55.90	94.53	
7	3	0	56.70	87.61	48.42
7	4	70	58.90	76.08	41.50
7	6	70	61.90	94.53	50.72
8	2	70	65.40	76.08	27.67
8	4	70	68.40	78.39	43.94
8	6	70	71.40	129.12	29.98
9	2	70	74.90	103.75	
9	3	0	75.70	85.30	39.19
9	4	60	77.80	117.96	80.69
9	6	72	80.92	87.62	48.43
10	2	0	83.00	124.50	57.64
10	2	70	83.70	117.58	43.80
10	4	70	86.70	126.81	23.06
10	6	70	89.70	122.20	55.32
11	2	70	93.90	89.92	39.19
11	4	0	96.20	133.72	62.25
11	4	70	96.90	122.20	53.03
11	6	70	99.90	110.67	53.03
12	2	0	102.70	124.50	59.94
12	2	75	103.45	119.89	41.50
12	4	75	106.45	124.50	39.19
13	2	75	112.95	92.22	39.19
13	4	75	115.95	124.50	46.11
17	5	130	156.00	145.23	43.81
18	3	0	161.20	177.67	48.42

they are slightly lower (higher velocity) than the slowness values measured in Holes 671C and 672A (a difference of approximately 15 $\mu\text{s}/\text{ft}$ or 0.05 km/s). This is probably a reflection of the higher carbonate content in this logged section, since calcite has a characteristic velocity that is higher than silica.

Conclusions

Results from the logged interval in Hole 676A indicate that: a) the decrease in the gamma-ray reading in the upper part of the logged hole (130 mbsf) can be related to an increase of the carbonate content of the formation, b) the effects of the bioturbation on the different ash layers leads to an uncertain correlation with the local peaks in the gamma-ray curve, c) the rapid decrease in resistivity observed in the upper part of the log can be related either to improved interconnectedness of pores via microfractures or to a change in electrical properties owing to mineralogical variations, and d) the slowness curve shows a uniform and unspectacular trend, with velocities ranging from 1.68 km/s to 1.74 km/s.

SUMMARY AND CONCLUSIONS

Site 676 is located on the lower slope of the deformation front, 250 m west and 20–25 m above the adjacent Atlantic abyssal plain. The main objective of this site was to document

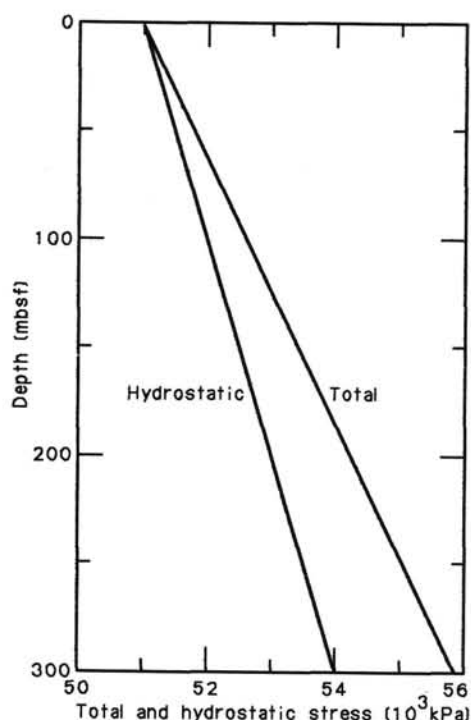


Figure 28. Total and hydrostatic stress vs. depth at Site 676.

the present structural and hydrologic processes related to the seaward propagation of the accretionary complex.

Site 676 penetrated three main lithologic units (Fig. 39):

Unit 1 (0–162 mbsf) is composed of uppermost Miocene to lower Pleistocene calcareous mudstone and claystone, marl, and ash layers. Conspicuous folding occurs between 25 and 55 mbsf within the Pleistocene section. Bedding dips in this interval are locally as steep as 75° . These structures are probably related to the frontal thrust of the deformation front. A second discrete thrust fault with folded scaly fabric occurs at 155 mbsf at the Miocene/Pliocene boundary. It is interesting to note that sub-vertical veins and numerous steeply dipping normal faults were described at the same age boundary at reference Site 672.

Unit 2 (162–263 mbsf) is made up of claystone and mudstone with ash beds. Calcareous intervals are present only in the upper section where upper Miocene nannofossil flora have been encountered. The lower part of this unit shows traces of radiolarians which cannot be dated. The detailed biozonation in the upper section revealed an unexpected repetition of about 30 m of strata which apparently results from thrust faulting. A reinterpretation of the seismic stratigraphy data suggests that this thrust is probably a very recent fault propagating upward and forward from the décollement.

Unit 3 (263–310 mbsf) is composed of claystone, siliceous mudstone, and ash layers, and is of early Miocene age according to its radiolarian content. At a depth of 270 to 280 mbsf this unit shows a zone of incipient horizontal shearing, and a biostratigraphically documented thrust fault has been penetrated at

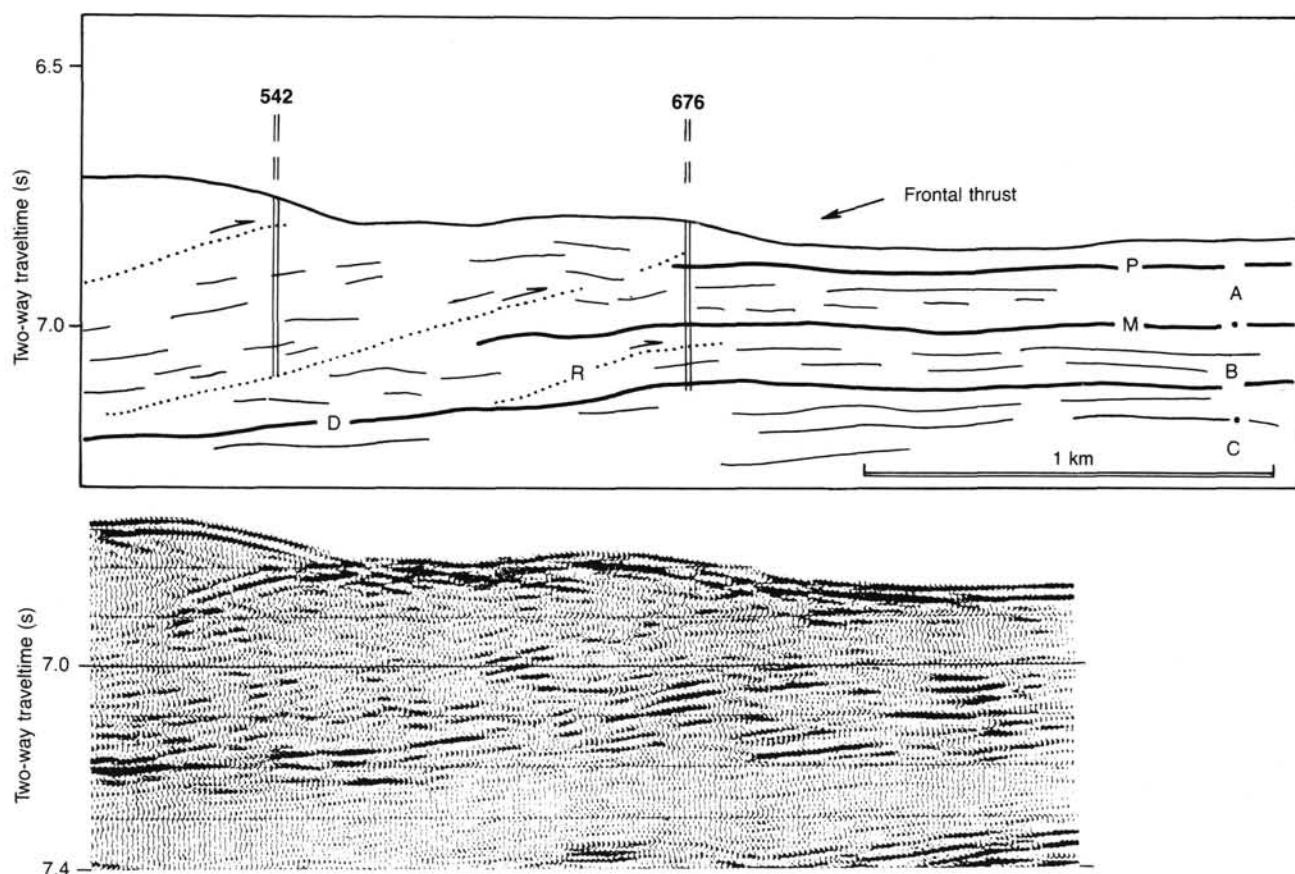


Figure 29. Interpreted line drawing (top) and seismic section (bottom) of seismic profile CRV 128 at Site 676. P: Top of Pliocene; M: Top of Miocene; D: décollement; R: Seismic reflector interpreted as the trace of a deep thrust fault; A, B, C, and D are seismic sequences.

Table 11. Temperature measurement instruments used at Site 676.

Tool	Thermistor housing	Thermistor resolution	Recorder program
APC Tool	Steel annular cylinder ID: 0.0617 m OD: 0.0786 m	0.02°C	15-s recording interval
T-probe	Steel cylindrical probe 0.0125 m dia	0.05°C	60-s recording interval

Table 12. Temperature measurement summary at Site 676.

Depth (mbsf)	Tool	Equilibrium T (est error) (°C)	Sediment/water temperature
0.0	APC tool/T-probe	2.18 (0.05)	water
25.6	APC tool	6.95 (0.10)	sediment
44.6	APC tool	8.30 (0.05)	sediment
63.6	APC tool	8.00 (0.05)	sediment
73.4	T-probe	9.05 (0.05)	sediment
101.6	T-probe	11.50 (0.05)	sediment
149.1	T-probe	13.95 (0.05)	sediment
196.6	T-probe	17.05 (0.05)	sediment
244.1	T-probe	20.00 (0.10)	sediment

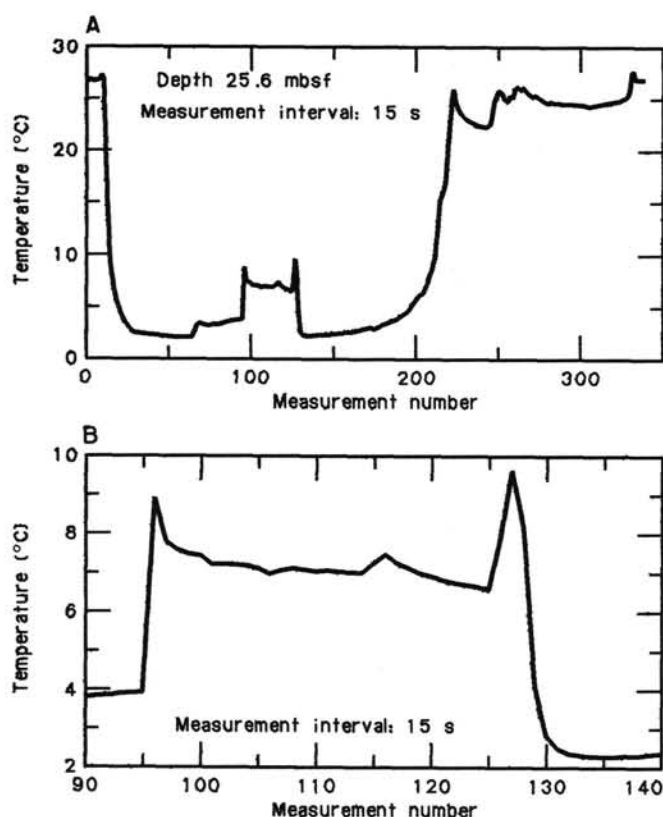


Figure 30. A. Temperature vs. time record for first deployment of APC tool, Core 110-676A-3H. B. Detail of record of APC tool deployment in same core, showing sediment temperature.

a depth of 291 mbsf. Both features may represent the seaward propagation of the décollement zone.

The physical properties at Site 676 show trends very similar to those at Site 672. The upper Pliocene and Pleistocene section (0–150 mbsf) decreases in porosity downsection from 80 to 55 %

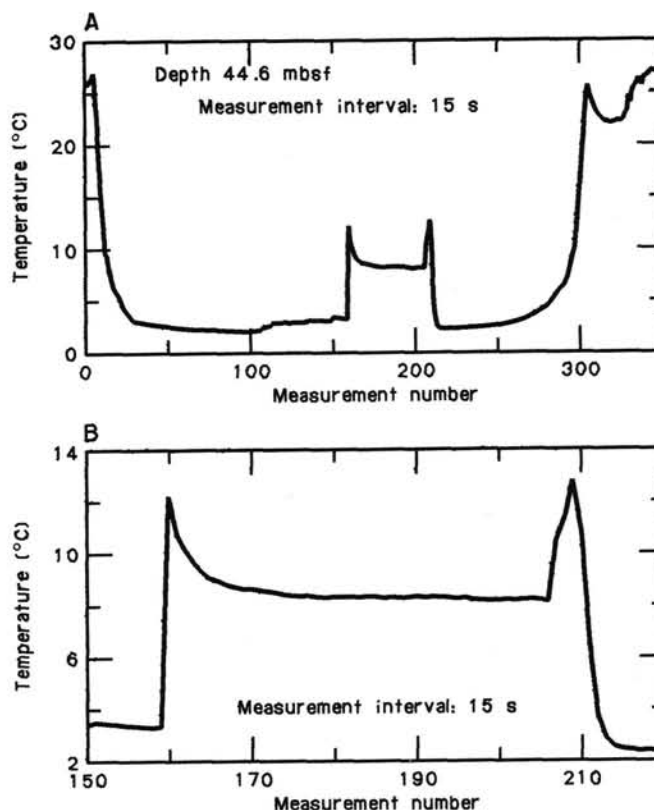


Figure 31. A. Temperature vs. time record for second deployment of APC tool, Core 110-676A-5H. B. Detail of record of APC tool deployment, same core, showing sediment temperature.

(Fig. 39). The Miocene section (150–310 mbsf) shows higher porosities (about 70%) with a maximum at 275 mbsf. As at Site 672, this porosity high is correlative with an incipient shear zone. The nearly identical porosity values between Sites 676 and 672 suggest little-to-no compaction owing to lateral stresses affected the Neogene sediments as they were incorporated into the accretionary prism. However, a sharp increase in porosity downsection (60 to 75%) at a depth of about 35 mbsf is correlated with the frontal thrust where more-consolidated sediments have recently overthrust less-consolidated lithologies. The magnetic susceptibility measurements in this upper section also depict the repetition of Pleistocene strata. A prominent high-temperature anomaly between 25 and 45 mbsf, as well as an anomalously high methane content in pore water at 33 mbsf, strongly suggest that relatively warm fluid is flowing along this frontal thrust (Fig. 39).

In spite of the clear methane anomaly, no decrease in pore-water chloride content occurs at the depth of the frontal thrust. Low chlorinities are restricted to a depth of 250 mbsf, i.e., about 25 m above the incipient shear zone of the future décollement. This lack of correlation and the absence of any methane at this lower depth is unexplained. High pore-water methane content does occur at four different depths (Fig. 39). Three of these anomalies correlate well within the limits of the sampling intervals with the three main structural features so far observed: the upper high value at 33 mbsf coincides with the frontal thrust; the high methane content at 190 mbsf is close to the thrust repeating an upper Miocene section; and the deeper high value at 286 mbsf is almost perfectly correlated with the thrust fault in the décollement zone.

The results from Site 676 are of prime importance in understanding how the accretionary complex is propagating. In this single vertical section we found not one, but at least three zones

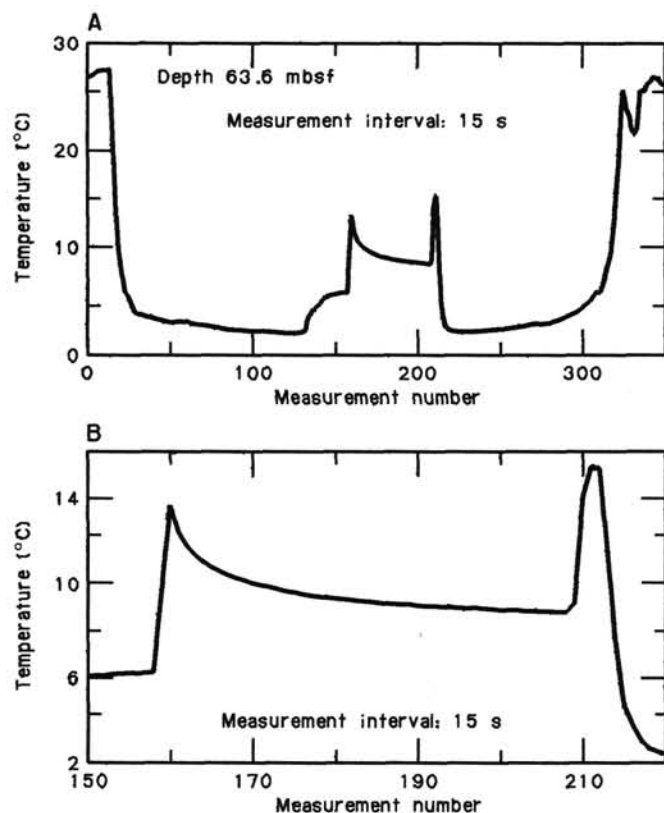


Figure 32. A. Temperature vs. time record for third deployment of APC tool, Core 110-676A-7H. B. Detail of record of APC tool deployment, same core, showing sediment temperature.

of active deformation. The frontal thrust at 35 mbsf projects upward to the present deformation front on the seafloor. The frontal thrust is characterized by tight folding of Pleistocene sediments and flow of warm fluids with high methane content. The deeper thrust zone at 205 mbsf could be the lower boundary of the next accreted package, as suggested on seismic line A1D, 3 km to the south (see Background and Objectives section). The deepest tectonic features observed in Hole 676A sediments are an incipient shear zone at 270–280 mbsf and a thrust fault at 251 mbsf. They define a décollement zone that correlates with the décollement zone at Sites 675 and 671 and a similar zone of incipient shearing at Site 672.

REFERENCES

- Anderson, R. N., and Skilbeck, J. N., 1982. Oceanic heat flow. In Emiliani, C. (Ed.), *The Oceanic Lithosphere, The Sea, Volume 7*: New York (Wiley and Sons): 489–524.
- Bally, A. W., 1983. Seismic expression of structural styles. *AAPG Stud. Geol.*, Ser. 15, V. 3.
- Berggren, W. A., 1977. Late Neogene planktonic foraminiferal biostratigraphy of the Rio Grande Rise (South Atlantic). *Mar. Micropaleontology*, 2, 3: 265–313.
- Berggren, W. A., Kent, D. V., and Van Couvering, J. A., 1984. Neogene geochronology and chronostratigraphy. In: Snelling, N. J., *The geochronology and the geologic record*. *Geol. Soc. London, Mem.* 10: 141–195.
- Bolli, H. M., Premoli Silva, I., 1973. Oligocene to Recent planktonic foraminifera and stratigraphy of the Leg 15 Sites in the Caribbean Sea. In Edgar, N. T., Saunders, J. B., et al., *Init. Repts. DSDP*, 15: Washington (U.S. Govt. Printing Office), 475–497.
- Boulegue, J., Le Pichon, X., and Iiyama, J. T., 1985. Prevision des tremblements de terre dans la région de Tokai, Japan. *C. R. Acad. Sci. Paris*: 301.

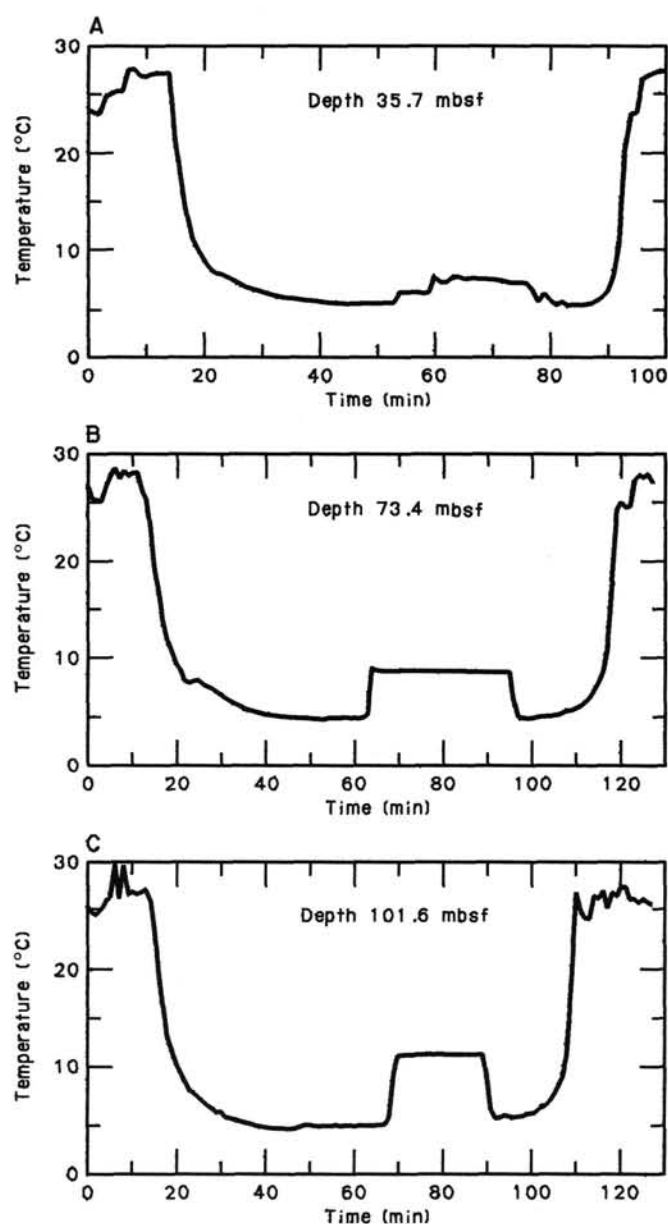


Figure 33. A. Temperature vs. time record for first deployment of T-probe, after Core 110-676A-4H. B. Temperature vs. time record for second deployment of T-probe, after Core 110-676A-8H. C. Temperature vs. time record for third deployment of T-probe, after Core 110-676A-11H.

- Gartner, S., 1977. Calcareous nannofossil biostratigraphy and revised zonation of the Pleistocene. *Mar. Micropaleontology*, 2: 1–25.
- Hemleben, C., and Auras, A., 1984. Variations in the calcite dissolution pattern on the Barbados Ridge complex at Sites 541 and 543, Deep Sea Drilling Project Leg 78A. In: Biju-Duval, B., Moore J. C., et al., *Init. Repts. DSDP*, 78A: Washington (U.S. Govt. Printing Office), 471–508.
- Hsui, A. T., and Toksoz, M. N., 1979. The evolution of thermal structures beneath a subduction zone. *Tectonophysics*, 60: 43–60.
- Kulm, L. D., Suess, E., Moore, J. C., Carson, B., Lewis, B. T., Ritger, S. D., Kadko, D. C., Thornberg, T. M., Embley, R. W., Rugh, W. D., Massoth, G. J., Langseth, M. G., Cochran, G. R., and Scamman, R. L., 1986. Oregon subduction zone: venting, fauna, and carbonates. *Science*, 231: 561–566.
- Kuster, G. T., and Toksöz, M. N., 1974. Velocity and attenuation of seismic waves in two-phase media. Part 1. Theoretical formulation. *Geophysics*, 39:587–606.

- Langseth, M., Westbrook, G., and Hobart, M., 1986. Geothermal transects of the lower trench slope of the Barbados accretionary prism, [paper presented at the 11th Annual Caribbean Geological Conference, Bridgetown, Barbados].
- Lister, C. R. B., 1977. Estimates for heat flow and deep rock properties based on boundary layer theory. *Tectonophysics*, 41: 157-171.
- Masle A. and Biscarrat, P. A., 1979. The Sulu Sea, a marginal basin in Southeast Asia. In Watkins, J. S., Montadert, L. and Dickerson, P. W. (Eds.), *Geological and geophysical investigations of continental margins*. *Am. Assoc. Petrol. Geol. Mem.*, 29.
- Masle, A., Biju-Duval, B., de Clarens, P., and Munsch, H., 1986. Growth of accretionary prisms; tectonic processes from Caribbean examples. In Wezel, D. (Ed.), *The origin of arcs. Developments in Geotectonics*: New York (Elsevier Scientific Publ. Co.) 395-400.
- Moore, J. C., and Biju-Duval, B., 1984. Tectonic synthesis, Deep Sea Drilling Project Leg 78A: Structural evolution of offscraped and underthrust sediments, northern Barbados Ridge Complex. In Biju-

- Duval, B., Moore, J. C., et al., *Init. Repts. DSDP 78A*: Washington (U.S. Govt. Printing Office), 601-621.
- Okada, H., and Bukry, D., 1980. Supplementary modification and introduction of code numbers to the low latitude coccolith biostratigraphic zonation (Bukry 1973, 1975). *Mar. Micropaleontology*, 5: 321-325.
- Riedel, W. R., and Sanfilippo, A., 1978. Stratigraphy and evolution of tropical Cenozoic radiolarians. *Micropaleontology*, 24: 61-96.
- Speed, R. C., Westbrook, G. K., Biju-Duval, B., Ladd, J. W., Masle, A., Moore, J. C., Saunders, J. B., Schoonmaker, J. E., and Stein, S., 1984. *Atlas 10, Ocean Margin Drilling Program; Lesser Antilles and Adjacent Ocean Floor*: Woods Hole (Marine Science Institute Publication), 27 sheets.
- Westbrook, J. K., and Smith, M. J., 1983. Long décollements and mud volcanoes: evidence from the Barbados Ridge Complex for the role of high pore fluid pressure in the development of an accretionary complex. *Geology*, 11: 279-283.

Ms 110A-110

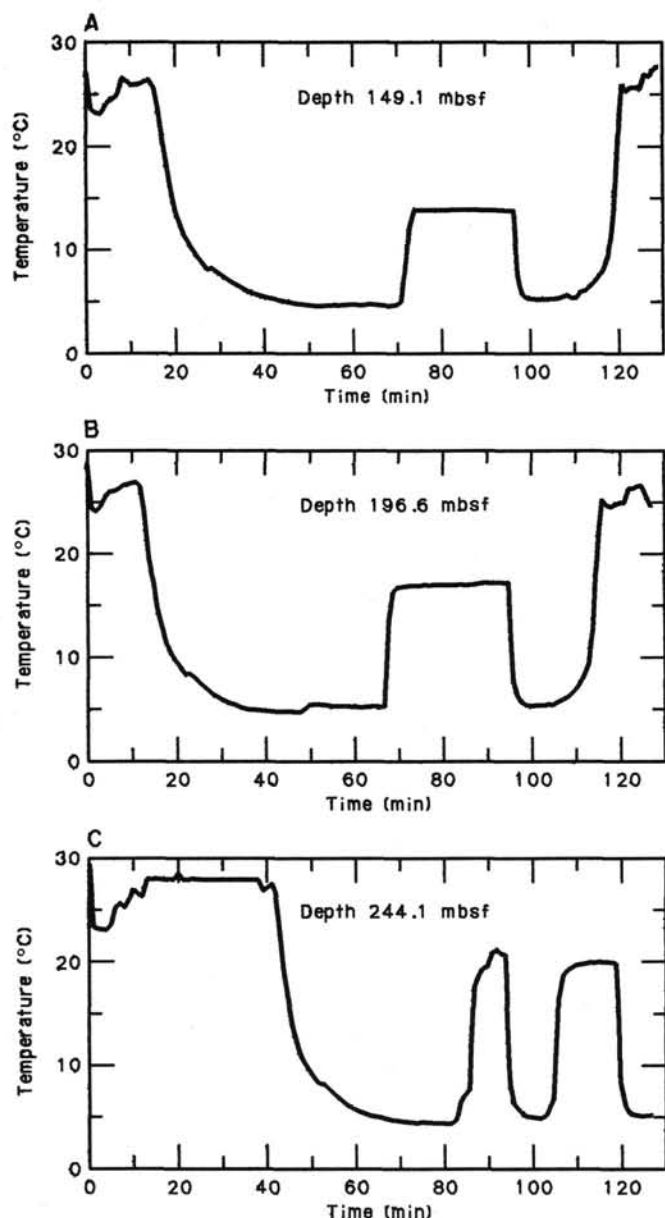


Figure 34. A. Temperature vs. time record for fourth deployment of T-probe, after Core 110-676A-16X. B. Temperature vs. time record for fifth deployment of T-probe, after Core 110-676A-21X. C. Temperature vs. time record for sixth deployment of T-probe, after Core 110-676A-26X.

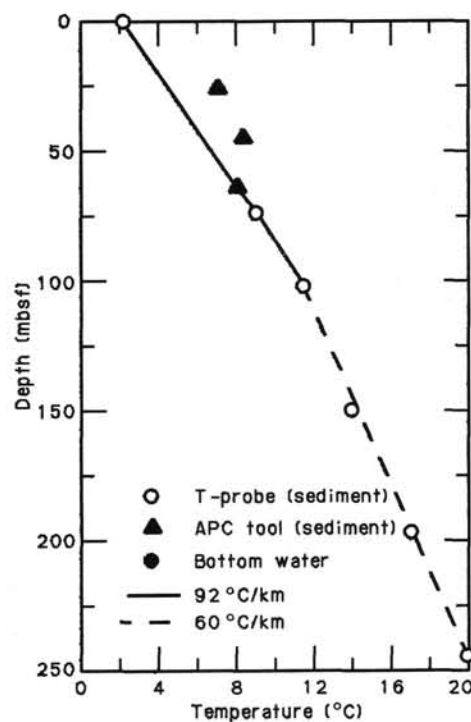


Figure 35. Plot of downhole temperatures in Hole 676A. The thermal gradient for the upper section (depth < 25.6 m) is 186 °C/km. The thermal gradient for the middle section (63.6 mbsf < depth < 101.4 mbsf) is 92 °C/km. The thermal gradient in the lower sediment section (depth > 101.4 m) is 60 °C/km.

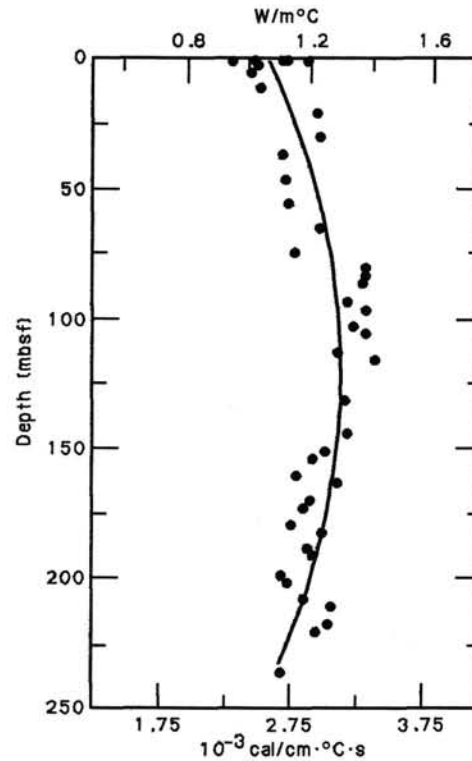


Figure 36. Plot of sediment thermal conductivity determined by the needle-probe method for cores from Hole 676A.

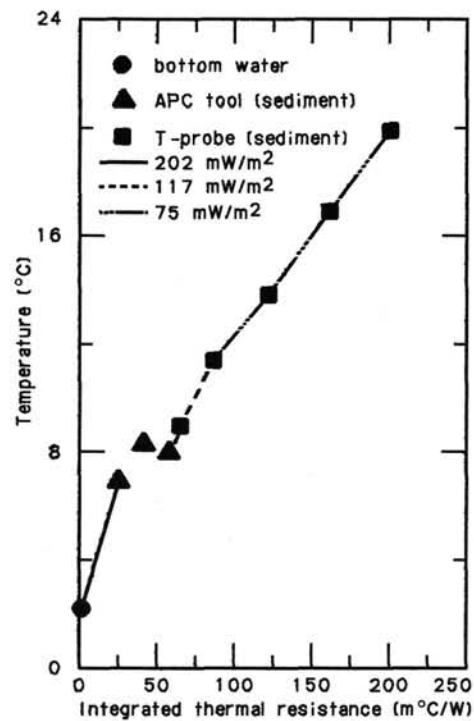


Figure 37. Plot of downhole temperatures vs. integrated thermal resistance at Site 673. linear least-squares best-fitted heat flow for the lower section (depth > 101.4 m) is 75 mW/m², heat flow for the middle section (63.6 mbsf < depth < 101.4 mbsf) is 117 mW/m², heat flow for the upper section (depth < 25.6 m) is 202 mW/m².

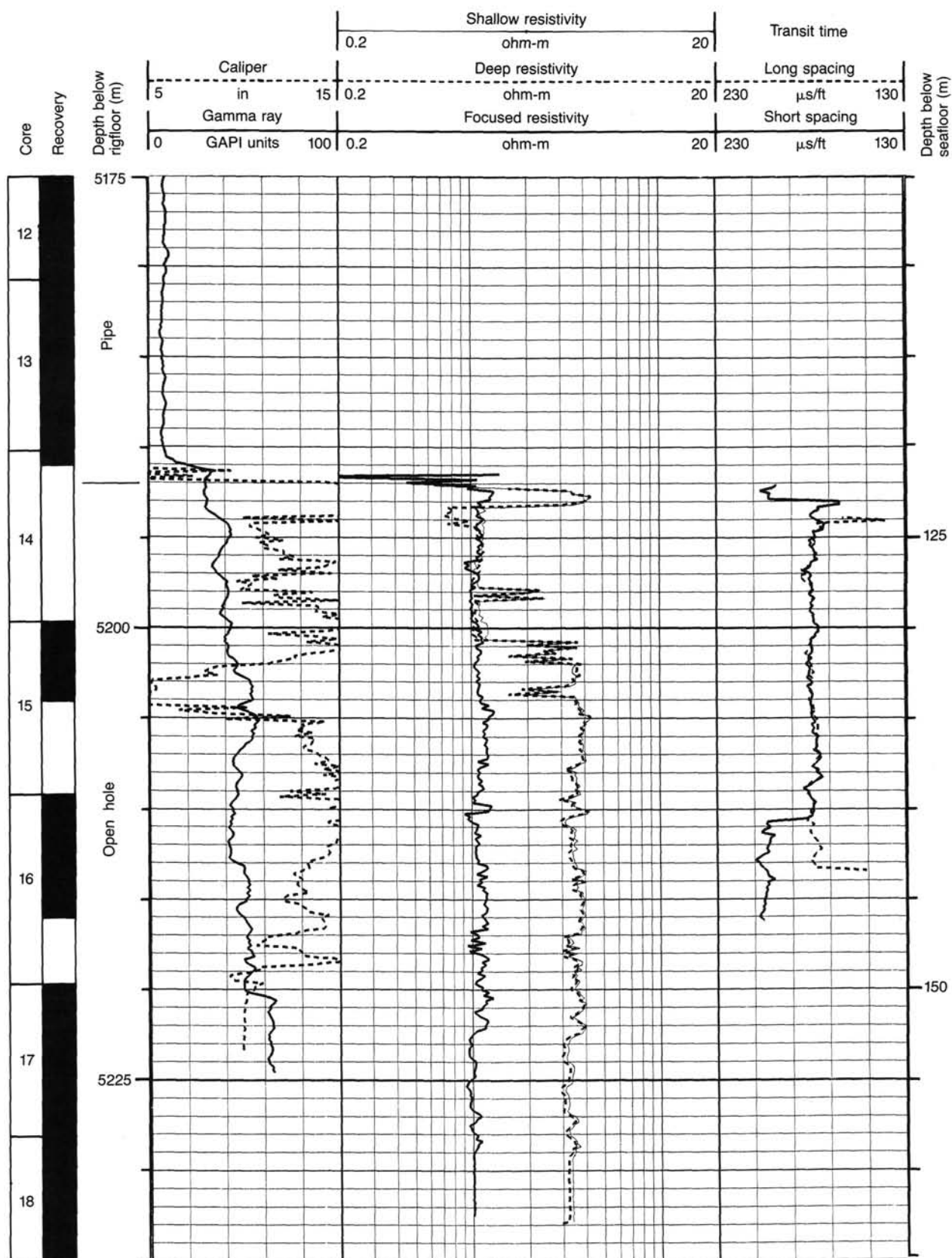


Figure 38. Results of the logging run in Hole 676A with the corresponding core locations and recoveries. The gamma-ray (GR) and caliper curves are on track 1. The deep induction curve (ILD), the medium induction curve (ILM), and the spherical focused curve (SFL) are on track 2. the DT and DTL curves of the long spacing sonic are on track 3. The position of the drill pipe is also shown on this figure.

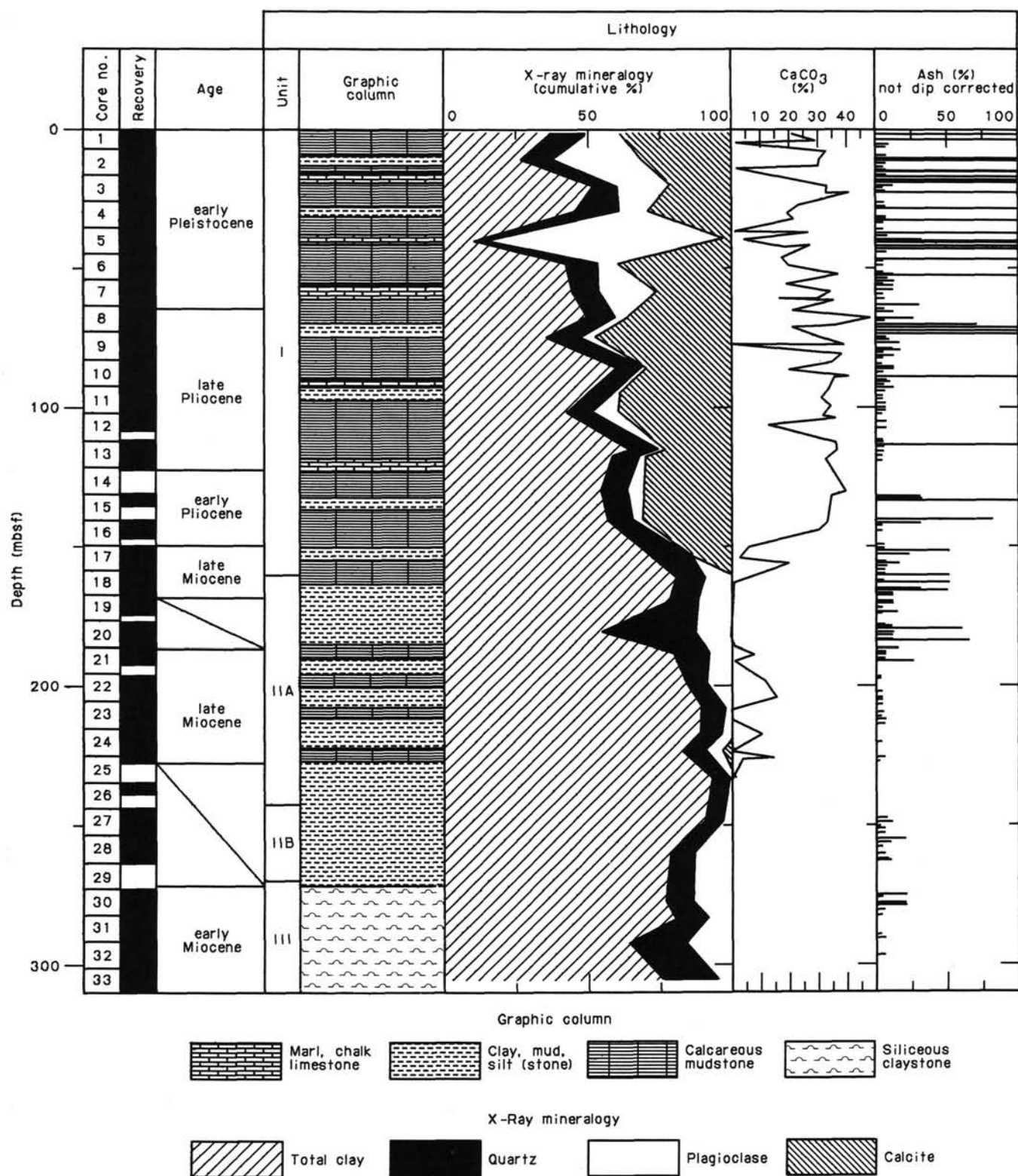


Figure 39. Site summary diagram, Site 676.

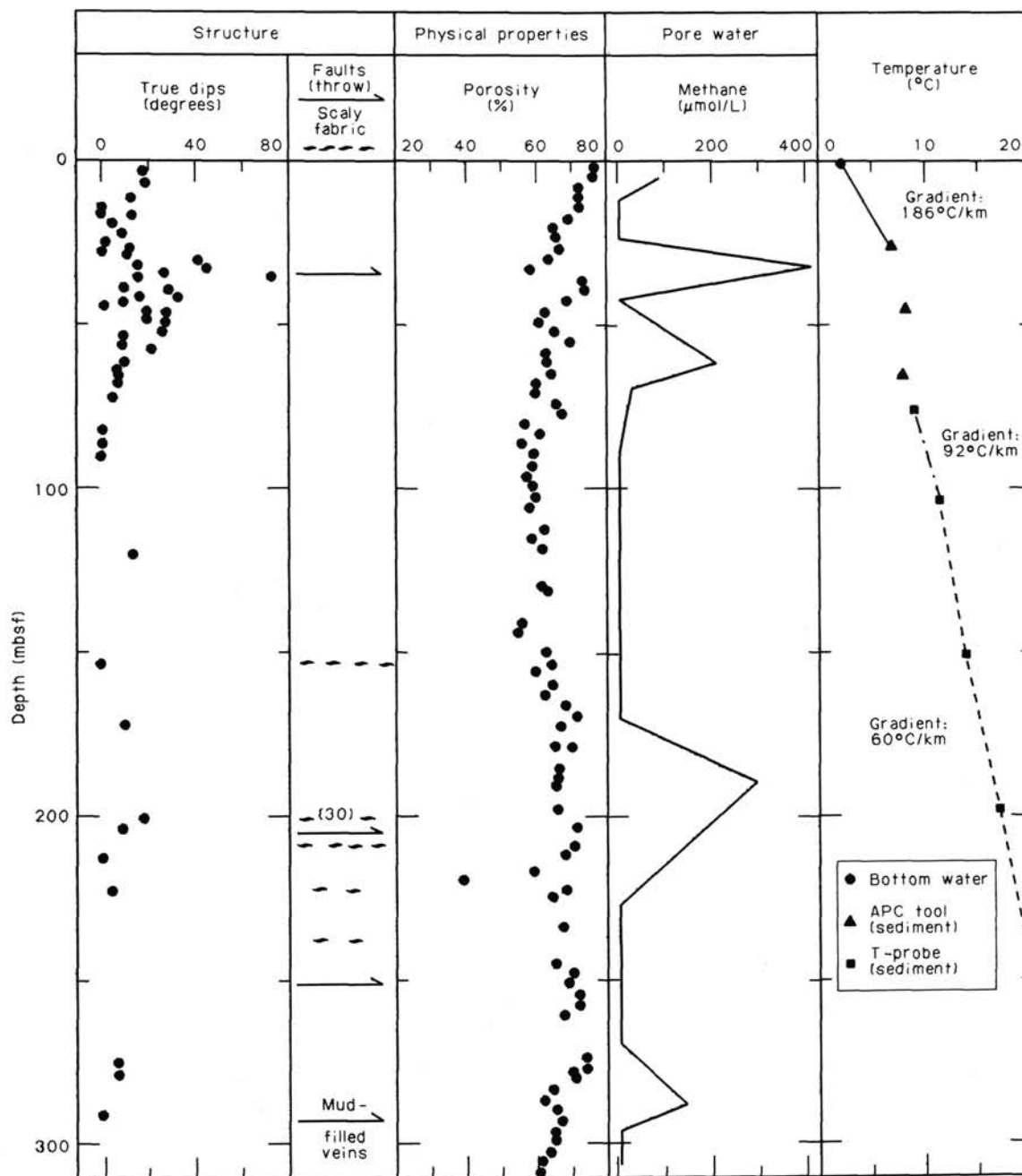
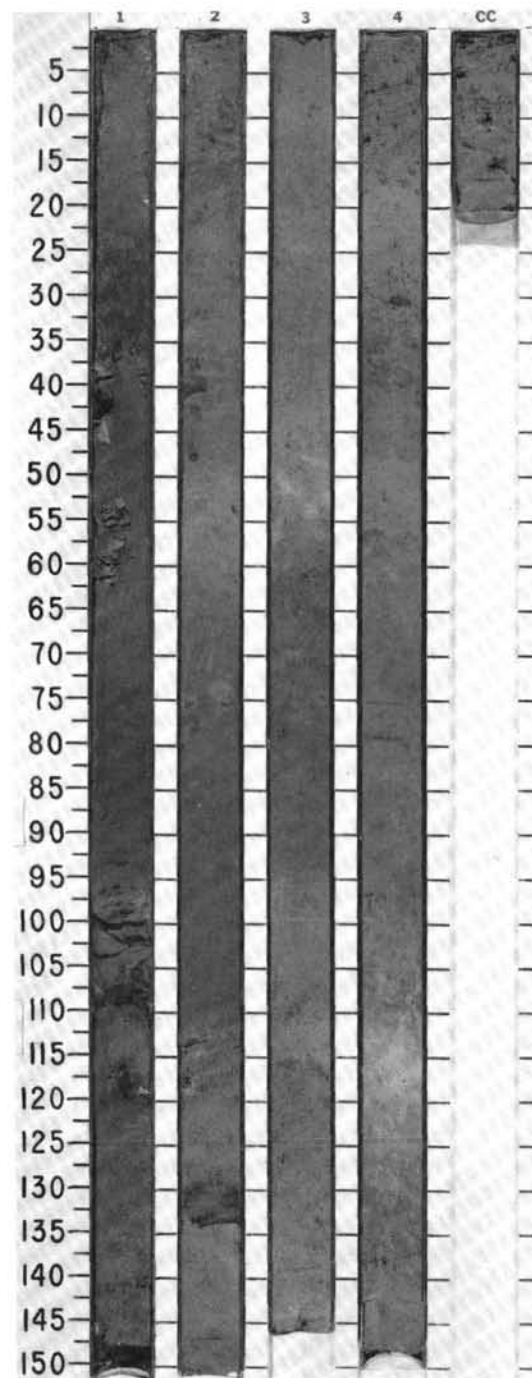


Figure 39 (continued).

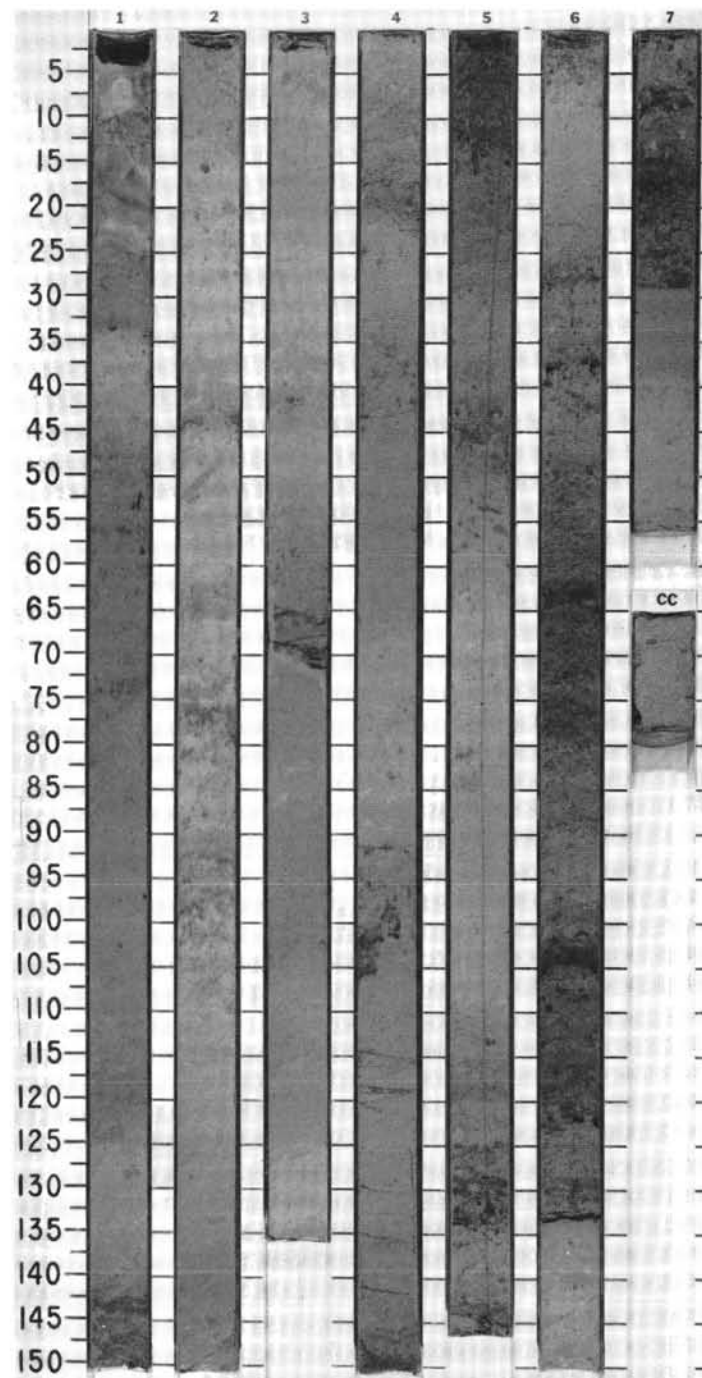
SITE 676 HOLE A CORE 1 H CORED INTERVAL 5059.6-5065.8 mbsl; 0.0-6.2 mbsf

TIME-ROCK UNIT	BIOSTRAT. ZONE/ FOSSIL CHARACTER				PALEOMAGNETICS	PHYS. PROPERTIES	CHEMISTRY	SECTION	METERS	GRAPHIC LITHOLOGY	DRILLING DISTURB.	SED. STRUCTURES	SAMPLES	LITHOLOGIC DESCRIPTION
	FORAMINIFERS	NANNOFOSSILS	RADIOLARIANS	DIAZONES										
PLEISTOCENE														
R/P	<i>Globorotalia truncatulinoides</i> Zone													CALCAREOUS CLAY, CALCAREOUS MUD, and MARL
	indet.												*	Light brown to brown (10YR5/4, 10YR4/4), moderately bioturbated CALCAREOUS CLAY, CALCAREOUS MUD, and MARL; very gradational contacts.
vR/M	indet.												**	Minor lithology: well-preserved vitric to crystalline ash beds. Bedding generally subhorizontal.
														SMEAR SLIDE SUMMARY (%):
														1, 1 D 1, 79 D 1, 100 M 1, 105 M 2, 80 D 2, 130 M
														TEXTURE:
													*	Sand 15 Tr 70 80 6 60
													*	Silt 7 8 30 20 24 40
													*	Clay 78 92 — — 70 —
													*	COMPOSITION:
													*	Quartz Tr — 3 10 6 10
													*	Feldspar 2 Tr 5 14 — 27
													*	Rock fragments — Tr — — — 20
													*	Clay 68 68 — — 67 —
													*	Volcanic glass — — 86 60 4 20
													*	Accessory minerals
													*	Orthopyroxene Tr Tr 1 — 1 Tr
													*	Clinopyroxene — — 1 2 — 6
													*	Hornblende 1 Tr 4 10 — 10
													*	Foraminifers 15 — Tr 8 —
													*	Nannofossils 10 25 — Tr 13 2
													*	Diatoms — Tr — — —
													*	Radiolarians 1 1 — — —
													*	Sponge spicules 3 4 — — Tr —
													*	Bioclasts — 2 — — —

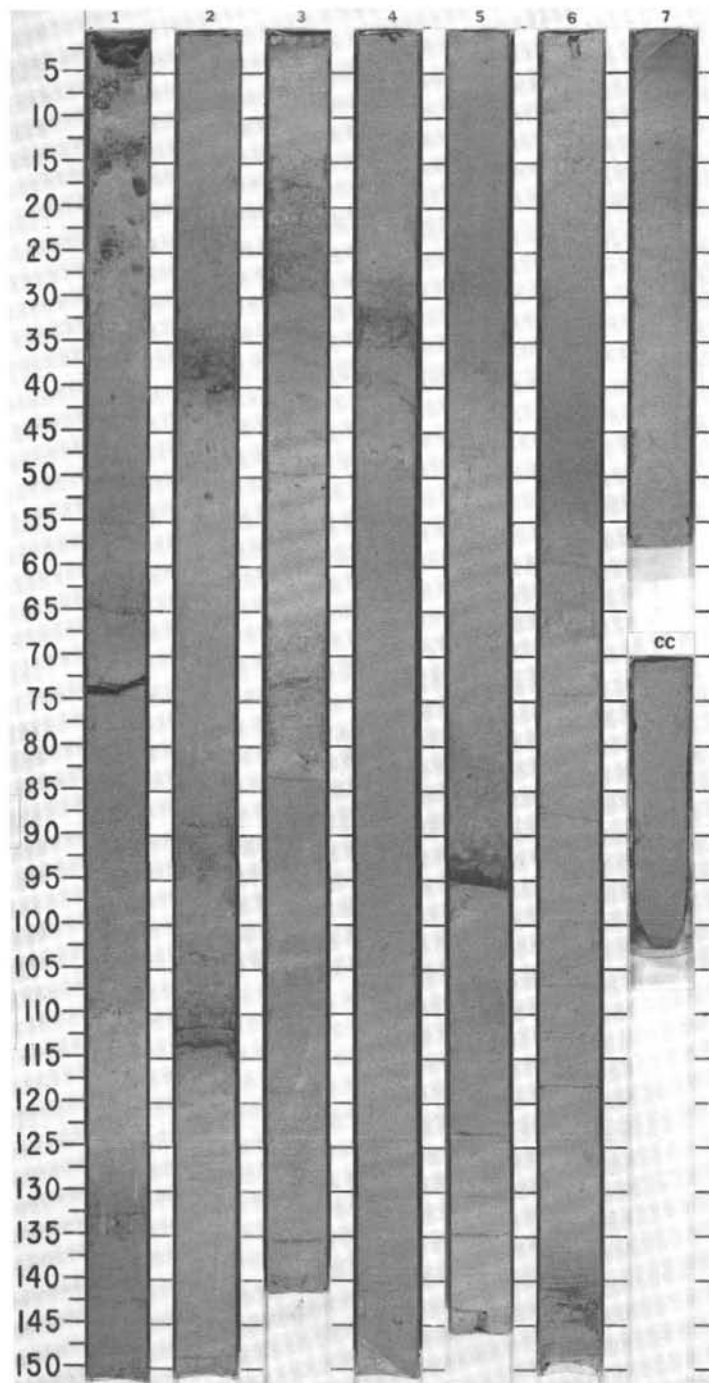


SITE 676 HOLE A CORE 2 H CORED INTERVAL 5065.8-5075.3 mbsl; 6.2-15.7 mbsf

TIME-ROCK UNIT	BIOSTRAT. ZONE/ FOSSIL CHARACTER	PALEOMAGNETICS	PHYS. PROPERTIES	CHEMISTRY	SECTION	METERS	GRAPHIC LITHOLOGY	DRILLING DISTURB.	SED. STRUCTURES	SAMPLES	LITHOLOGIC DESCRIPTION
	FORAMINIFERS NANNOFOSSILS RADIOLARIANS DIATOMS										
LOWER PLEISTOCENE	<i>G. truncatulinoides</i> Zone (<i>G. hessi</i> subzone) <i>Pseudoemiliania lacunosa</i> Zone Barren										
						</					

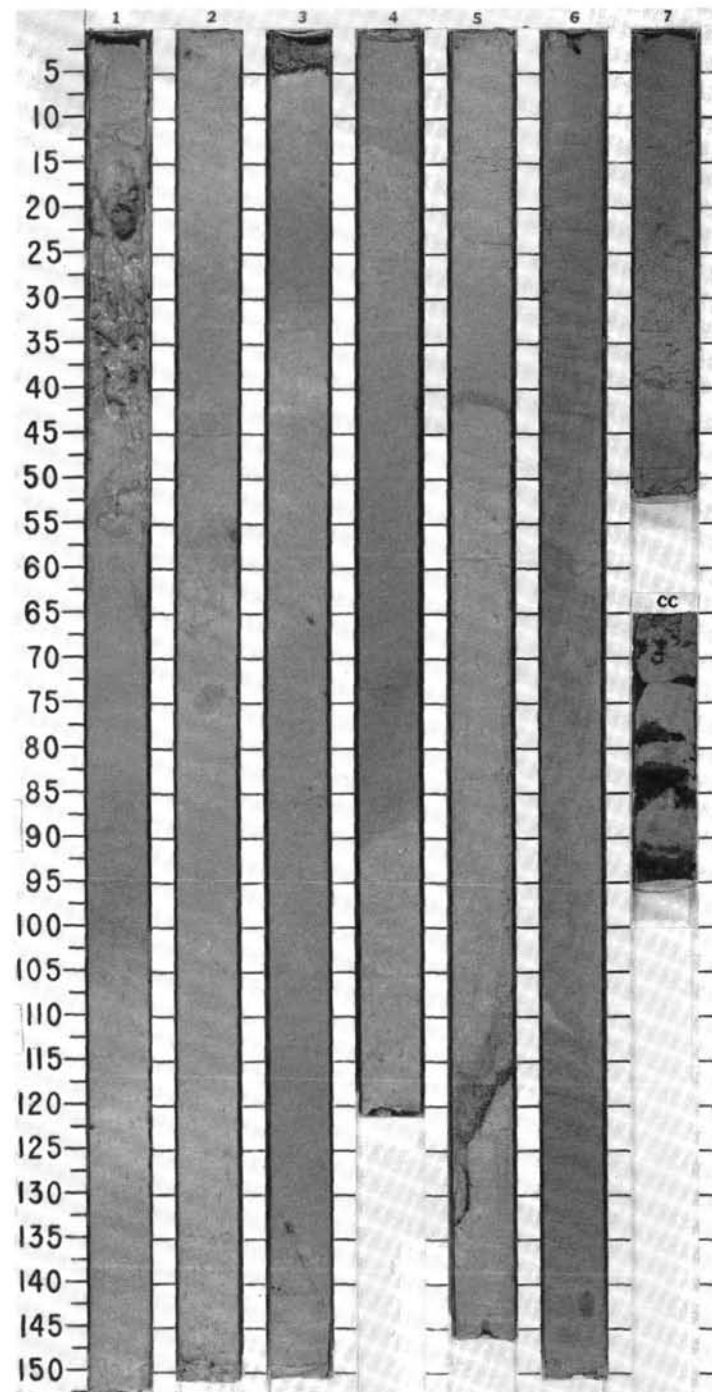


SITE 676

[illegible]

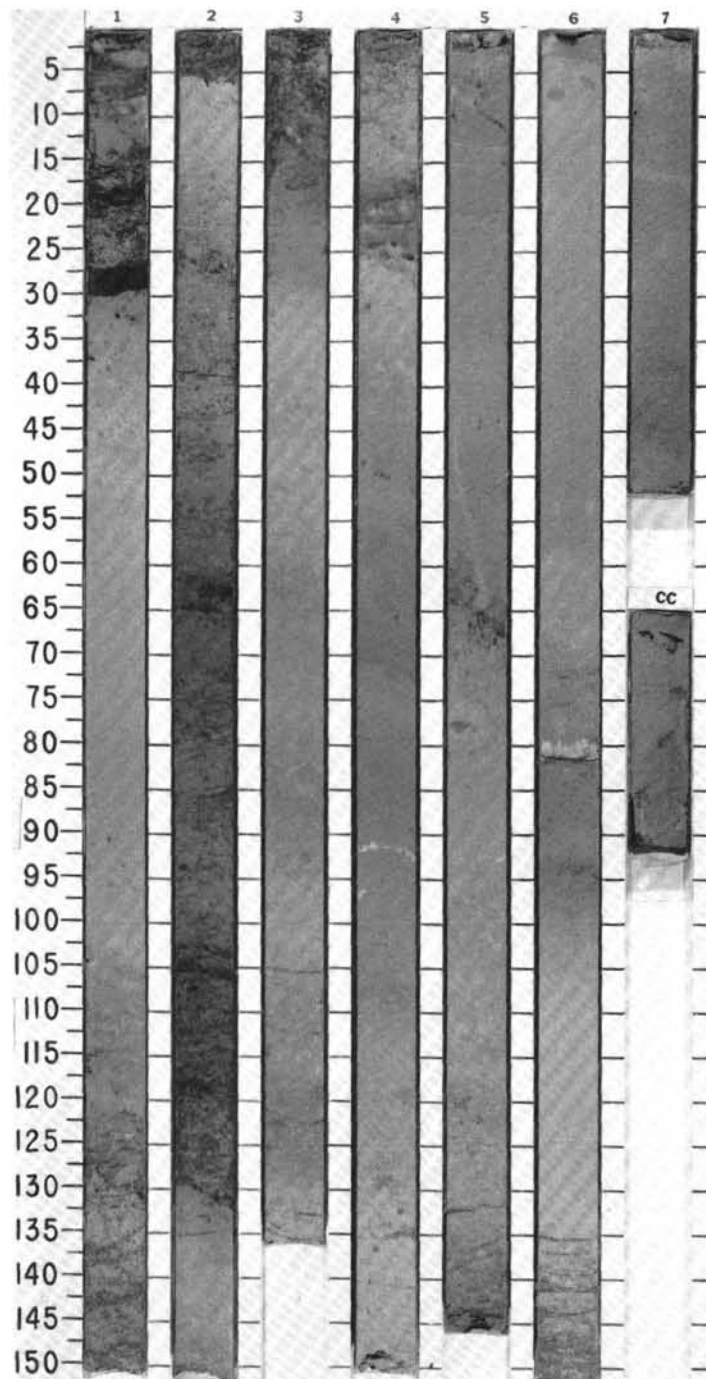
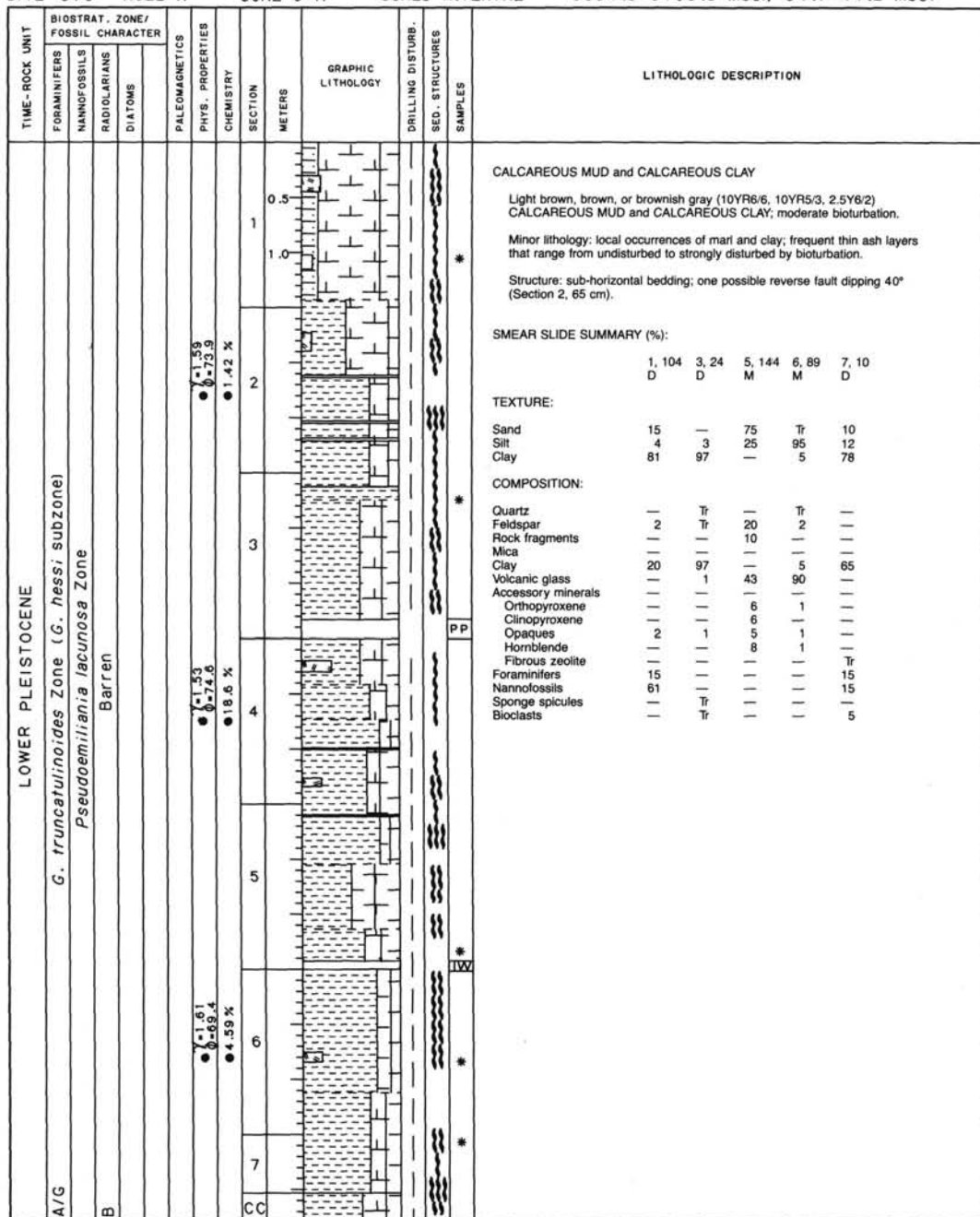
SITE 676 HOLE A CORE 4 H CORED INTERVAL 5084.8-5094.3 mbsl; 25.2-34.7 mbsf

TIME-ROCK UNIT	BIOSTRAT. ZONE/ FOSSIL CHARACTER				PALEOMAGNETICS	PHYS. PROPERTIES	CHEMISTRY	SECTION	METERS	GRAPHIC LITHOLOGY	DRILLING DISTURB. SED. STRUCTURES	SAMPLES	LITHOLOGIC DESCRIPTION																																																																																																																																																								
	FORAMINIFERS	NANNOFOSSILS	RADIOLARIANS	DIAZONIS																																																																																																																																																																	
C/M	G. truncatulinoides Zone (G. hessi subzone)												CALCAREOUS MUD or MARL Light brownish gray (2.5Y6/2) to light olive-gray (5Y6/2) CALCAREOUS MUD or MARL; moderate bioturbation. Minor lithology: thin ash beds (Section 3, 0-50 cm, and Section 5, 110-145 cm). Structure: fanned bedding dips (from 0-70°), suggesting small-scale folding around a steeply dipping axial surface. SMEAR SLIDE SUMMARY (%): <table><tr><td>1,2</td><td>1,3</td><td>1,122</td><td>3,74</td><td>5,123</td><td>6,148</td></tr><tr><td>M</td><td>M</td><td>D</td><td>D</td><td>M</td><td>D</td></tr></table> TEXTURE: <table><tr><td>Sand</td><td>58</td><td>40</td><td>10</td><td>—</td><td>60</td><td>—</td></tr><tr><td>Silt</td><td>20</td><td>18</td><td>5</td><td>18</td><td>40</td><td>10</td></tr><tr><td>Clay</td><td>22</td><td>42</td><td>85</td><td>82</td><td>—</td><td>90</td></tr></table> COMPOSITION: <table><tr><td>Quartz</td><td>—</td><td>—</td><td>—</td><td>—</td><td>5</td><td>—</td></tr><tr><td>Feldspar</td><td>45</td><td>34</td><td>4</td><td>—</td><td>40</td><td>4</td></tr><tr><td>Rock fragments</td><td>1</td><td>—</td><td>—</td><td>—</td><td>28</td><td>—</td></tr><tr><td>Clay</td><td>22</td><td>42</td><td>76</td><td>62</td><td>20</td><td>89</td></tr><tr><td>Volcanic glass</td><td>20</td><td>5</td><td>—</td><td>—</td><td>—</td><td>—</td></tr><tr><td>Accessory minerals(?)</td><td>3</td><td>1</td><td>—</td><td>Tr</td><td>—</td><td>—</td></tr><tr><td>Fibrous zeolite</td><td>—</td><td>—</td><td>—</td><td>Tr</td><td>—</td><td>—</td></tr><tr><td>Orthopyroxene</td><td>5</td><td>5</td><td>—</td><td>—</td><td>2</td><td>1</td></tr><tr><td>Clinopyroxene</td><td>—</td><td>—</td><td>—</td><td>—</td><td>3</td><td>1</td></tr><tr><td>Opauques</td><td>—</td><td>—</td><td>Tr</td><td>—</td><td>—</td><td>Tr</td></tr><tr><td>Hornblende</td><td>3</td><td>3</td><td>2</td><td>—</td><td>2</td><td>—</td></tr><tr><td>Olivine</td><td>—</td><td>—</td><td>1</td><td>—</td><td>—</td><td>—</td></tr><tr><td>Mn oxide</td><td>—</td><td>10</td><td>—</td><td>—</td><td>—</td><td>—</td></tr><tr><td>Foraminifers</td><td>—</td><td>—</td><td>5</td><td>10</td><td>—</td><td>—</td></tr><tr><td>Nannofossils</td><td>—</td><td>—</td><td>10</td><td>25</td><td>—</td><td>1</td></tr><tr><td>Sponge spicules</td><td>—</td><td>—</td><td>—</td><td>—</td><td>—</td><td>1</td></tr><tr><td>Bioclasts</td><td>—</td><td>—</td><td>2</td><td>3</td><td>—</td><td>3</td></tr></table>	1,2	1,3	1,122	3,74	5,123	6,148	M	M	D	D	M	D	Sand	58	40	10	—	60	—	Silt	20	18	5	18	40	10	Clay	22	42	85	82	—	90	Quartz	—	—	—	—	5	—	Feldspar	45	34	4	—	40	4	Rock fragments	1	—	—	—	28	—	Clay	22	42	76	62	20	89	Volcanic glass	20	5	—	—	—	—	Accessory minerals(?)	3	1	—	Tr	—	—	Fibrous zeolite	—	—	—	Tr	—	—	Orthopyroxene	5	5	—	—	2	1	Clinopyroxene	—	—	—	—	3	1	Opauques	—	—	Tr	—	—	Tr	Hornblende	3	3	2	—	2	—	Olivine	—	—	1	—	—	—	Mn oxide	—	10	—	—	—	—	Foraminifers	—	—	5	10	—	—	Nannofossils	—	—	10	25	—	1	Sponge spicules	—	—	—	—	—	1	Bioclasts	—	—	2	3	—	3
	1,2	1,3	1,122	3,74	5,123	6,148																																																																																																																																																															
M	M	D	D	M	D																																																																																																																																																																
Sand	58	40	10	—	60	—																																																																																																																																																															
Silt	20	18	5	18	40	10																																																																																																																																																															
Clay	22	42	85	82	—	90																																																																																																																																																															
Quartz	—	—	—	—	5	—																																																																																																																																																															
Feldspar	45	34	4	—	40	4																																																																																																																																																															
Rock fragments	1	—	—	—	28	—																																																																																																																																																															
Clay	22	42	76	62	20	89																																																																																																																																																															
Volcanic glass	20	5	—	—	—	—																																																																																																																																																															
Accessory minerals(?)	3	1	—	Tr	—	—																																																																																																																																																															
Fibrous zeolite	—	—	—	Tr	—	—																																																																																																																																																															
Orthopyroxene	5	5	—	—	2	1																																																																																																																																																															
Clinopyroxene	—	—	—	—	3	1																																																																																																																																																															
Opauques	—	—	Tr	—	—	Tr																																																																																																																																																															
Hornblende	3	3	2	—	2	—																																																																																																																																																															
Olivine	—	—	1	—	—	—																																																																																																																																																															
Mn oxide	—	10	—	—	—	—																																																																																																																																																															
Foraminifers	—	—	5	10	—	—																																																																																																																																																															
Nannofossils	—	—	10	25	—	1																																																																																																																																																															
Sponge spicules	—	—	—	—	—	1																																																																																																																																																															
Bioclasts	—	—	2	3	—	3																																																																																																																																																															
B	Pseudoemiliania lacunosa Zone																																																																																																																																																																				
	Barren																																																																																																																																																																				
CC																																																																																																																																																																					



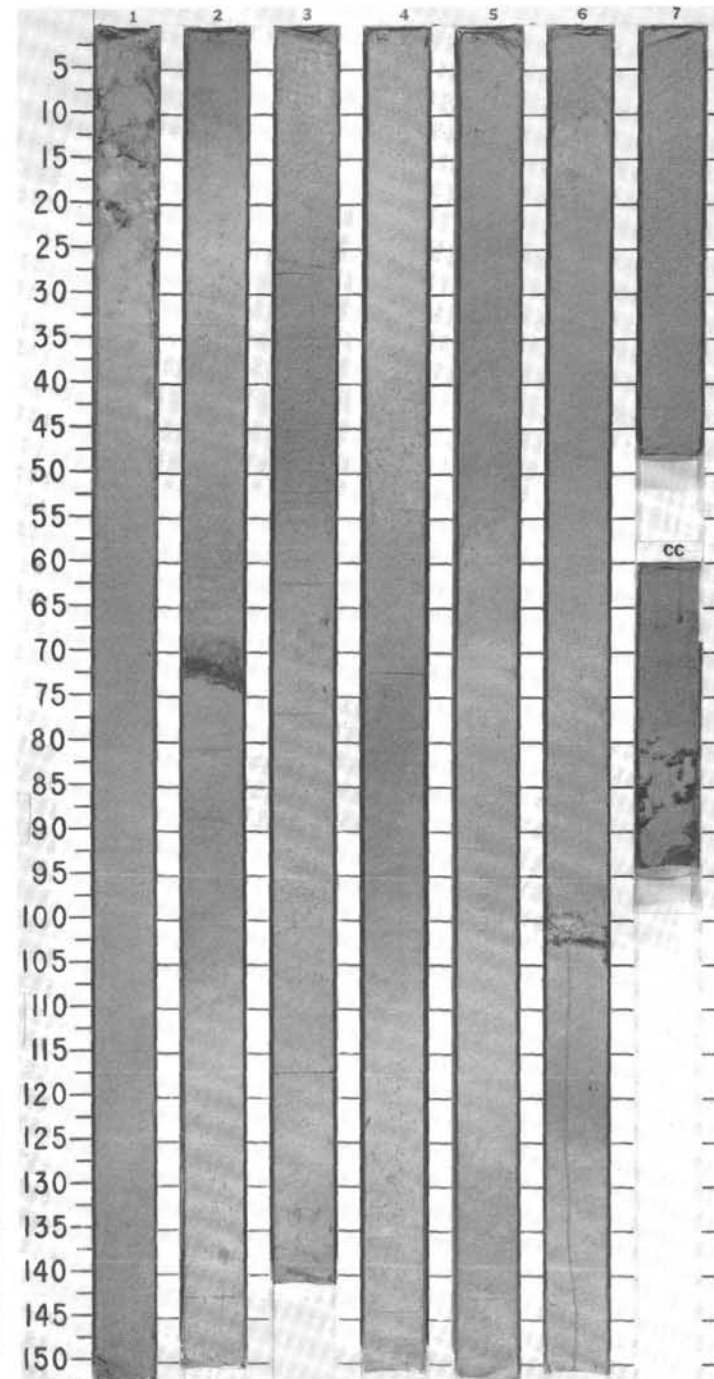
SITE 676

SITE 676 HOLE A CORE 5 H CORED INTERVAL 5094.3-5103.8 mbsl; 34.7-44.2 mbsf



SITE 676 HOLE A CORE 6 H CORED INTERVAL 5103.8-5113.3 mbsl; 44.2-53.7 mbsf

LOWER PLEISTOCENE																																																																																																																										
TIME-ROCK UNIT	BIOSTRAT. ZONE/ FOSSIL CHARACTER				PALEOMAGNETICS	PHYS. PROPERTIES	CHEMISTRY	SECTION	METERS	GRAPHIC LITHOLOGY	DRILLING DISTURB.	SED. STRUCTURES	SAMPLES	LITHOLOGIC DESCRIPTION																																																																																																												
	FORAMINIFERS	NANNOFOSSILS	RADIOLARIANS	DIATOMS																																																																																																																						
A/M	<i>G. truncatulinoides</i> Zone (<i>G. hessi</i> subzone)													<p>CALCAREOUS MUD and CALCAREOUS CLAY</p> <p>Light brownish gray to pale olive (2.5Y6/6, 10YR6/6, 5Y6/3) CALCAREOUS MUD and CALCAREOUS CLAY; moderately bioturbated.</p> <p>Minor lithology: common ash beds with sharp contacts; disseminated by bioturbation. Bedding dips range from sub-horizontal to 40° (Section 2).</p> <p>SMEAR SLIDE SUMMARY (%):</p> <table><tr><td></td><td>1, 70</td><td>2, 74</td><td>3, 138</td><td>4, 46</td><td>6, 101</td></tr><tr><td></td><td>D</td><td>M</td><td>D</td><td>D</td><td>M</td></tr></table> <p>TEXTURE:</p> <table><tr><td>Sand</td><td>2</td><td>50</td><td>Tr</td><td>—</td><td>70</td></tr><tr><td>Silt</td><td>98</td><td>50</td><td>3</td><td>10</td><td>30</td></tr><tr><td>Clay</td><td>—</td><td>—</td><td>97</td><td>90</td><td>—</td></tr></table> <p>COMPOSITION:</p> <table><tr><td>Quartz</td><td>—</td><td>—</td><td>—</td><td>Tr</td><td>—</td></tr><tr><td>Feldspar</td><td>Tr</td><td>30</td><td>Tr</td><td>—</td><td>40</td></tr><tr><td>Rock fragments</td><td>—</td><td>44</td><td>—</td><td>—</td><td>14</td></tr><tr><td>Mica</td><td>—</td><td>—</td><td>—</td><td>—</td><td>—</td></tr><tr><td>Clay</td><td>78</td><td>—</td><td>81</td><td>75</td><td>—</td></tr><tr><td>Volcanic glass</td><td>—</td><td>15</td><td>—</td><td>—</td><td>30</td></tr><tr><td>Accessory minerals (?)</td><td>1</td><td>5</td><td>1</td><td>—</td><td>2</td></tr><tr><td>Orthopyroxene</td><td>—</td><td>4</td><td>—</td><td>—</td><td>10</td></tr><tr><td>Clinopyroxene</td><td>—</td><td>2</td><td>—</td><td>—</td><td>2</td></tr><tr><td>Hornblende</td><td>—</td><td>—</td><td>—</td><td>—</td><td>2</td></tr><tr><td>Foraminifers</td><td>1</td><td>—</td><td>1</td><td>5</td><td>—</td></tr><tr><td>Nannofossils</td><td>20</td><td>—</td><td>15</td><td>20</td><td>—</td></tr><tr><td>Bioclasts</td><td>—</td><td>—</td><td>2</td><td>—</td><td>—</td></tr></table>		1, 70	2, 74	3, 138	4, 46	6, 101		D	M	D	D	M	Sand	2	50	Tr	—	70	Silt	98	50	3	10	30	Clay	—	—	97	90	—	Quartz	—	—	—	Tr	—	Feldspar	Tr	30	Tr	—	40	Rock fragments	—	44	—	—	14	Mica	—	—	—	—	—	Clay	78	—	81	75	—	Volcanic glass	—	15	—	—	30	Accessory minerals (?)	1	5	1	—	2	Orthopyroxene	—	4	—	—	10	Clinopyroxene	—	2	—	—	2	Hornblende	—	—	—	—	2	Foraminifers	1	—	1	5	—	Nannofossils	20	—	15	20	—	Bioclasts	—	—	2	—	—
	1, 70	2, 74	3, 138	4, 46	6, 101																																																																																																																					
	D	M	D	D	M																																																																																																																					
Sand	2	50	Tr	—	70																																																																																																																					
Silt	98	50	3	10	30																																																																																																																					
Clay	—	—	97	90	—																																																																																																																					
Quartz	—	—	—	Tr	—																																																																																																																					
Feldspar	Tr	30	Tr	—	40																																																																																																																					
Rock fragments	—	44	—	—	14																																																																																																																					
Mica	—	—	—	—	—																																																																																																																					
Clay	78	—	81	75	—																																																																																																																					
Volcanic glass	—	15	—	—	30																																																																																																																					
Accessory minerals (?)	1	5	1	—	2																																																																																																																					
Orthopyroxene	—	4	—	—	10																																																																																																																					
Clinopyroxene	—	2	—	—	2																																																																																																																					
Hornblende	—	—	—	—	2																																																																																																																					
Foraminifers	1	—	1	5	—																																																																																																																					
Nannofossils	20	—	15	20	—																																																																																																																					
Bioclasts	—	—	2	—	—																																																																																																																					
B	<i>Pseudosmilania lacunosa</i> Zone																																																																																																																									
	Barren																																																																																																																									



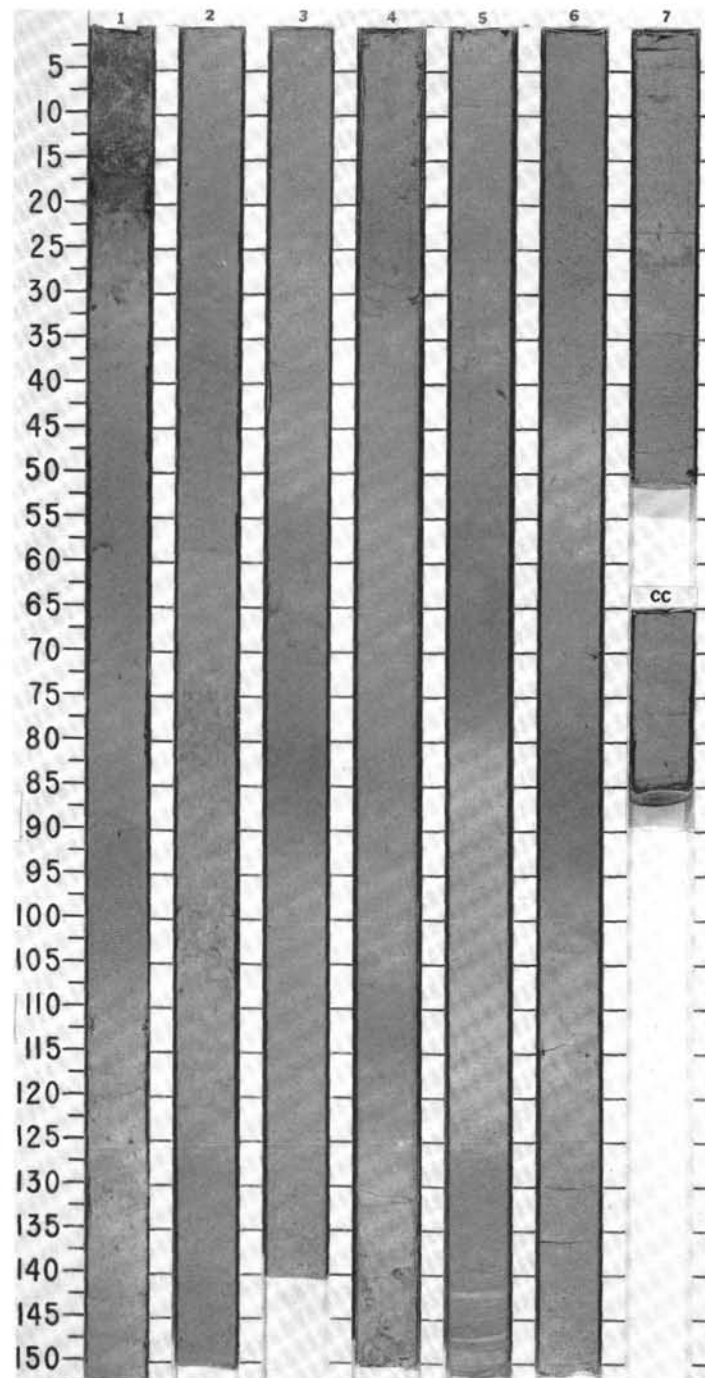
SITE 676

SITE 676 HOLE A CORE 8 H CORED INTERVAL 5122.8-5132.3 mbsl; 63.2-72.7 mbsf

TIME-ROCK UNIT	BIOSTRAT. ZONE/ FOSSIL CHARACTER				SECTION	METERS	GRAPHIC LITHOLOGY	DRILLING DISTURB.	SED. STRUCTURES	SAMPLES	LITHOLOGIC DESCRIPTION
	FORAMINIFERS	NANNOFOSSILS	RADIOLARIANS	DIATOMS							
PALEOMAGNETICS				PHYS. PROPERTIES	CHEMISTRY						
UPPER PLIOCENE Zone	C/M	<i>Globorotalia fosaensis</i> Zone (PL6)	CN12d -c	Barren							
UPPER PLIOCENE Zone	B	<i>Globorotalia fosaensis</i> Zone (PL6)	CN12d -c	Barren							
UPPER PLIOCENE Zone	C/M	<i>Globorotalia fosaensis</i> Zone (PL6)	CN12d -c	Barren							
UPPER PLIOCENE Zone	B	<i>Globorotalia fosaensis</i> Zone (PL6)	CN12d -c	Barren							
UPPER PLIOCENE Zone	C/M	<i>Globorotalia fosaensis</i> Zone (PL6)	CN12d -c	Barren							
UPPER PLIOCENE Zone	B	<i>Globorotalia fosaensis</i> Zone (PL6)	CN12d -c	Barren							
UPPER PLIOCENE Zone	C/M	<i>Globorotalia fosaensis</i> Zone (PL6)	CN12d -c	Barren							
UPPER PLIOCENE Zone	B	<i>Globorotalia fosaensis</i> Zone (PL6)	CN12d -c	Barren							
UPPER PLIOCENE Zone	C/M	<i>Globorotalia fosaensis</i> Zone (PL6)	CN12d -c	Barren							
UPPER PLIOCENE Zone	B	<i>Globorotalia fosaensis</i> Zone (PL6)	CN12d -c	Barren							
UPPER PLIOCENE Zone	C/M	<i>Globorotalia fosaensis</i> Zone (PL6)	CN12d -c	Barren							
UPPER PLIOCENE Zone	B	<i>Globorotalia fosaensis</i> Zone (PL6)	CN12d -c	Barren							
UPPER PLIOCENE Zone	C/M	<i>Globorotalia fosaensis</i> Zone (PL6)	CN12d -c	Barren							
UPPER PLIOCENE Zone	B	<i>Globorotalia fosaensis</i> Zone (PL6)	CN12d -c	Barren							
UPPER PLIOCENE Zone	C/M	<i>Globorotalia fosaensis</i> Zone (PL6)	CN12d -c	Barren							
UPPER PLIOCENE Zone	B	<i>Globorotalia fosaensis</i> Zone (PL6)	CN12d -c	Barren							
UPPER PLIOCENE Zone	C/M	<i>Globorotalia fosaensis</i> Zone (PL6)	CN12d -c	Barren							
UPPER PLIOCENE Zone	B	<i>Globorotalia fosaensis</i> Zone (PL6)	CN12d -c	Barren							
UPPER PLIOCENE Zone	C/M	<i>Globorotalia fosaensis</i> Zone (PL6)	CN12d -c	Barren							
UPPER PLIOCENE Zone	B	<i>Globorotalia fosaensis</i> Zone (PL6)	CN12d -c	Barren							
UPPER PLIOCENE Zone	C/M	<i>Globorotalia fosaensis</i> Zone (PL6)	CN12d -c	Barren							
UPPER PLIOCENE Zone	B	<i>Globorotalia fosaensis</i> Zone (PL6)	CN12d -c	Barren							
UPPER PLIOCENE Zone	C/M	<i>Globorotalia fosaensis</i> Zone (PL6)	CN12d -c	Barren							
UPPER PLIOCENE Zone	B	<i>Globorotalia fosaensis</i> Zone (PL6)	CN12d -c	Barren							
UPPER PLIOCENE Zone	C/M	<i>Globorotalia fosaensis</i> Zone (PL6)	CN12d -c	Barren							
UPPER PLIOCENE Zone	B	<i>Globorotalia fosaensis</i> Zone (PL6)	CN12d -c	Barren							
UPPER PLIOCENE Zone	C/M	<i>Globorotalia fosaensis</i> Zone (PL6)	CN12d -c	Barren							
UPPER PLIOCENE Zone	B	<i>Globorotalia fosaensis</i> Zone (PL6)	CN12d -c	Barren							
UPPER PLIOCENE Zone	C/M	<i>Globorotalia fosaensis</i> Zone (PL6)	CN12d -c	Barren							
UPPER PLIOCENE Zone	B	<i>Globorotalia fosaensis</i> Zone (PL6)	CN12d -c	Barren							
UPPER PLIOCENE Zone	C/M	<i>Globorotalia fosaensis</i> Zone (PL6)	CN12d -c	Barren							
UPPER PLIOCENE Zone	B	<i>Globorotalia fosaensis</i> Zone (PL6)	CN12d -c	Barren							
UPPER PLIOCENE Zone	C/M	<i>Globorotalia fosaensis</i> Zone (PL6)	CN12d -c	Barren							
UPPER PLIOCENE Zone	B	<i>Globorotalia fosaensis</i> Zone (PL6)	CN12d -c	Barren							
UPPER PLIOCENE Zone	C/M	<i>Globorotalia fosaensis</i> Zone (PL6)	CN12d -c	Barren							
UPPER PLIOCENE Zone	B	<i>Globorotalia fosaensis</i> Zone (PL6)	CN12d -c	Barren							
UPPER PLIOCENE Zone	C/M	<i>Globorotalia fosaensis</i> Zone (PL6)	CN12d -c	Barren							
UPPER PLIOCENE Zone	B	<i>Globorotalia fosaensis</i> Zone (PL6)	CN12d -c	Barren							
UPPER PLIOCENE Zone	C/M	<i>Globorotalia fosaensis</i> Zone (PL6)	CN12d -c	Barren							
UPPER PLIOCENE Zone	B	<i>Globorotalia fosaensis</i> Zone (PL6)	CN12d -c	Barren							
UPPER PLIOCENE Zone	C/M	<i>Globorotalia fosaensis</i> Zone (PL6)	CN12d -c	Barren							
UPPER PLIOCENE Zone	B</										

SITE 676 HOLE A CORE 9 H CORED INTERVAL 5132.3-5141.8 mbsl; 72.7-82.2 mbsf

UPPER PLIOCENE														
TIME-ROCK UNIT	BIOSTRAT. ZONE/ FOSSIL CHARACTER				PALEOMAGNETICS	PHYS. PROPERTIES	CHEMISTRY	SECTION	METERS	GRAPHIC LITHOLOGY	DRILLING DISTURB.	SED. STRUCTURES	SAMPLES	LITHOLOGIC DESCRIPTION
	FORAMINIFERS	NANNOFOSSILS	RADIOLARIANS	DIAZONES										
A/M	Gibborotalia miocenica Zone (PL50)													
B	CN12b Barren													



SITE 676 HOLE A CORE 10 H CORED INTERVAL 5141.8-5151.3 mbsl; 82.2-91.7 mbsf

TIME-ROCK UNIT	BIOSTRAT. ZONE/ FOSSIL CHARACTER				SECTION METERS	GRAPHIC LITHOLOGY	DRILLING DISTURB.	SED. STRUCTURES	SAMPLES	LITHOLOGIC DESCRIPTION	
	FORAMINIFERS	NANNOFOSSILS	RADIOLARIANS	DIATOMS							
PALEOMAGNETICS					PHYS. PROPERTIES	CHEMISTRY					
UPPER PLIOCENE	C/M	<i>Globorotalia miocenica</i> Zone (PL5)	CN12a	Barren							
B											
PALEOMAGNETICS											
PHYS. PROPERTIES											
CHEMISTRY											
SECTION											
METERS											
VOID											
1											
2											
3											
4											
5											
6											
7											
CC											

CALCAREOUS MUD and MARL

Olive-gray (5Y6/2, 5Y6/1, 5Y5/3, 2.5Y6/2, 2.5Y6/1) CALCAREOUS MUD and MARL; bioturbated throughout; 5-10% foraminifers disseminated throughout core.

Minor lithology: 2-10% disseminated ash. One discrete gray (N4) ash bed at Section 5, 83-84 cm.

Structure: faults at Section 2, 78-85 cm (dips 50°); 105-116 cm (dips 60°), 113-132 cm (dips 75°). Bedding dips are sub-horizontal (0-3°).

SMEAR SLIDE SUMMARY (%):

	5, 83	6, 110
	M	D

TEXTURE:

Sand	5	2
Silt	60	8
Clay	35	90

COMPOSITION:

Quartz	—	5
Plagioclase	30	1
Pumice	3	—
Clay	6	58
Volcanic glass	55	1
Accessory minerals	—	—
Pyrite	—	1
Hematite (?)	1	—
Opauques	5	—
Foraminifers	—	4+
Nannofossils	—	30

CALCAREOUS MUD and MARL

Olive-gray (5Y6/2, 5Y6/1, 5Y5/3, 2.5Y6/2, 2.5Y6/1) CALCAREOUS MUD and MARL; bioturbated throughout; 5-10% foraminifers disseminated throughout core.

Minor lithology: 2-10% disseminated ash. One discrete gray (N4) ash bed at Section 5, 83-84 cm.

Structure: faults at Section 2, 78-85 cm (dips 50°); 105-116 cm (dips 60°); 113-132 cm (dips 75°). Bedding dips are sub-horizontal (0-3°).

SMEAR SLIDE SUMMARY (%):

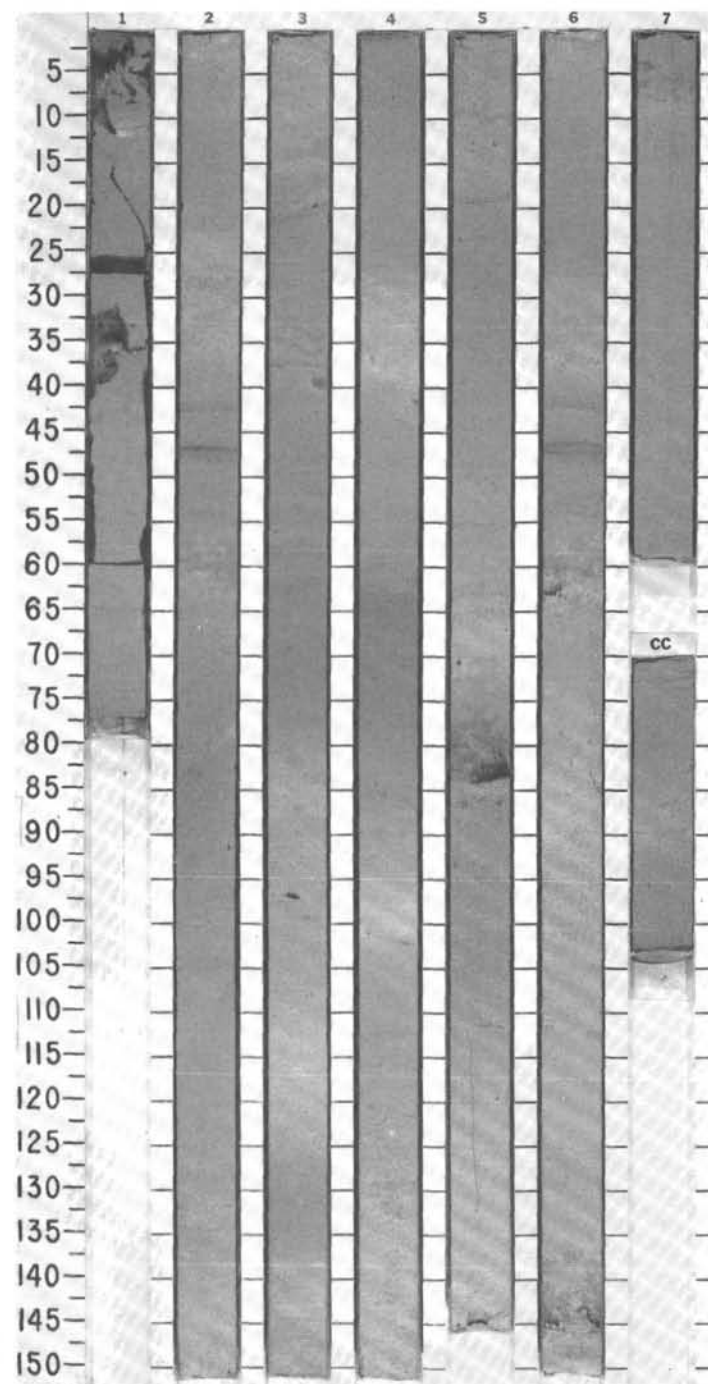
5, 83	6, 110
M	D

TEXTURE:

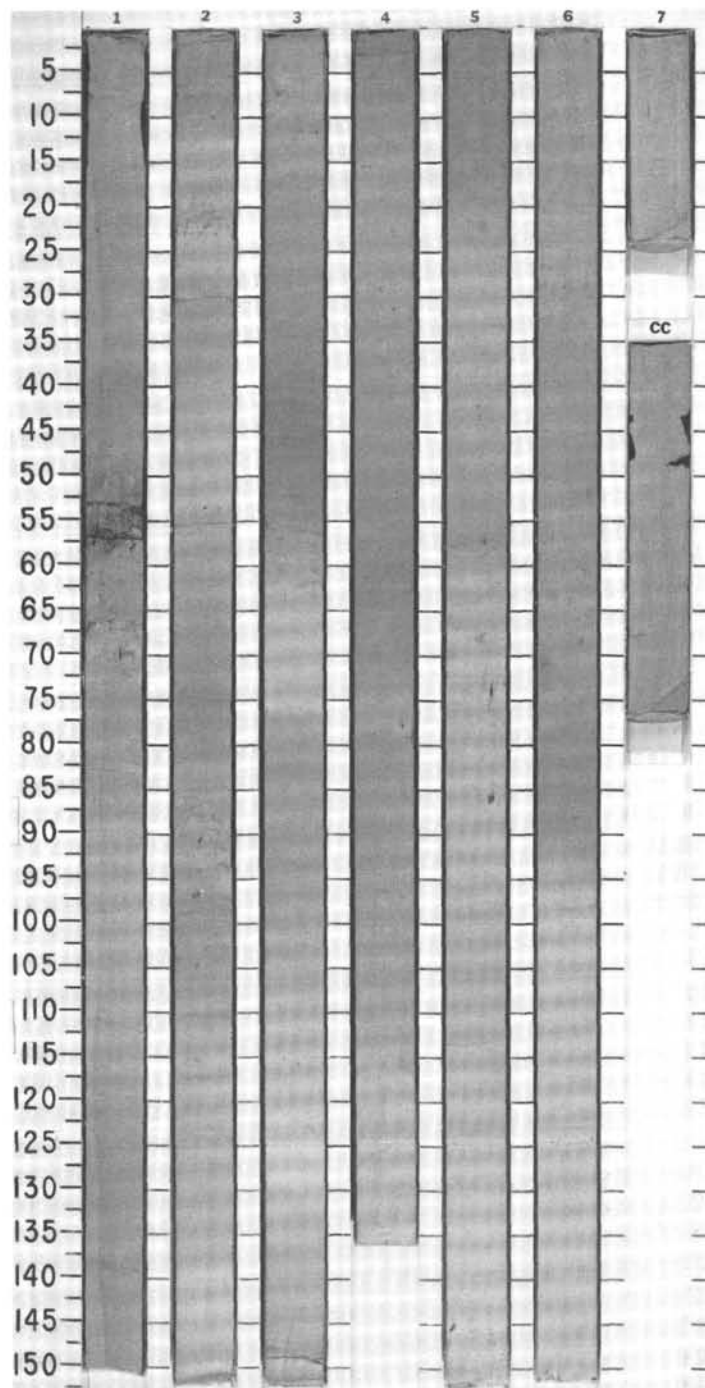
Sand	5	2
Silt	60	8
Clay	35	90

COMPOSITION:

Quartz	—	5
Plagioclase	30	1
Pumice	3	—
Clay	6	58
Volcanic glass	55	1
Accessory minerals	—	—
Pyrite	—	1
Hematite (?)	1	—
Opauques	5	—
Foraminifers	—	4+
Nannofossils	—	30

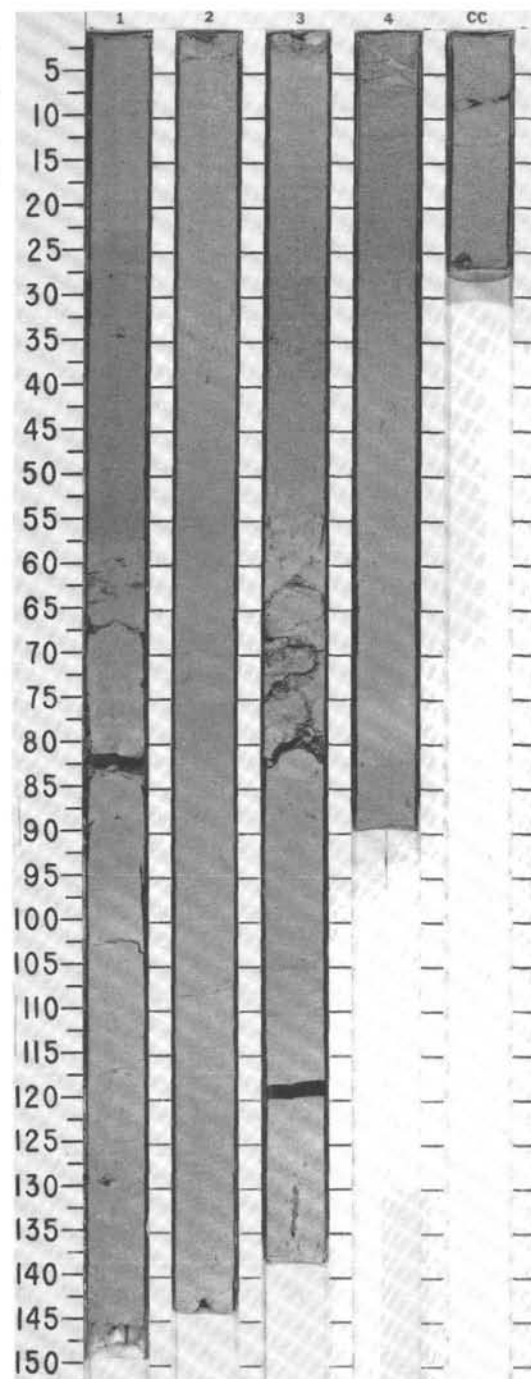


SITE 676 HOLE A CORE 11 H CORED INTERVAL 5151.3-5160.8 mbsl; 91.7-101.2 mbsf

[illegible]

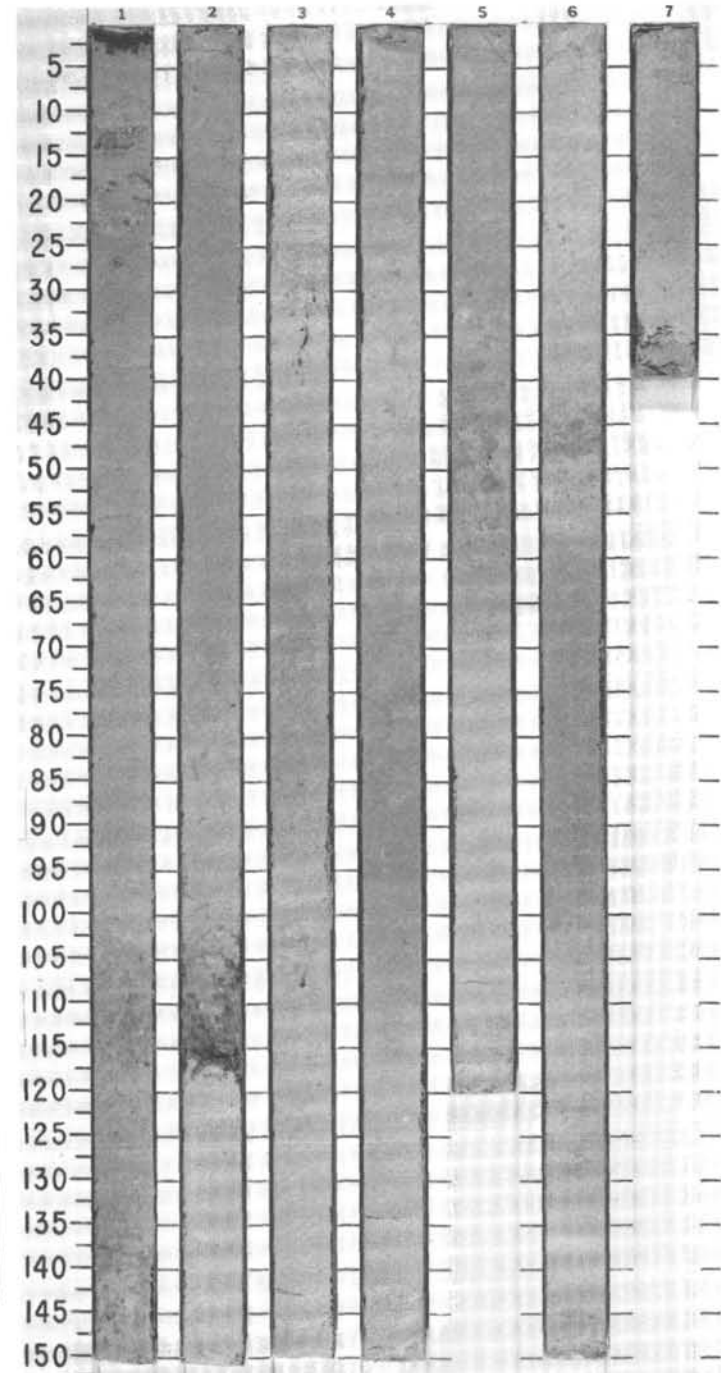
SITE 676 HOLE A CORE 12 X CORED INTERVAL 5160.8-5170.3 mbsl; 101.2-110.7 mbsf

TIME-ROCK UNIT	BIOSTRAT. ZONE/ FOSSIL CHARACTER				SECTION METERS	GRAPHIC LITHOLOGY	DRILLING DISTURB. SED. STRUCTURES	SAMPLES	LITHOLOGIC DESCRIPTION
	FORAMINIFERS	NANNOFOSSILS	RADIOLARIANS	DIAATOMS					
UPPER PLIOCENE	C/P	<i>Globorotalia miocenica</i> Zone (PL3)							
	B	CN12a							
		Barren							
					</				



SITE 676 HOLE A CORE 13 X CORED INTERVAL 5170.3-5179.8 mbsl; 110.7-120.2 mbsf

TIME-ROCK UNIT	BIOSTRAT. ZONE/ FOSSIL CHARACTER							SECTION	METERS	GRAPHIC LITHOLOGY	DRILLING DISTURB.	SED. STRUCTURES	SAMPLES	LITHOLOGIC DESCRIPTION
					PALEOMAGNETICS	PHYS. PROPERTIES	CHEMISTRY							
	FORAMINIFERS	NANNOFOSSILS	RADIOLARIANS	DIAZONIS										
UPPER / LOWER PLIOCENE														
A/G	Glabrotalia miocenica Zone (PL3)													
	CN11													
B	Barren													

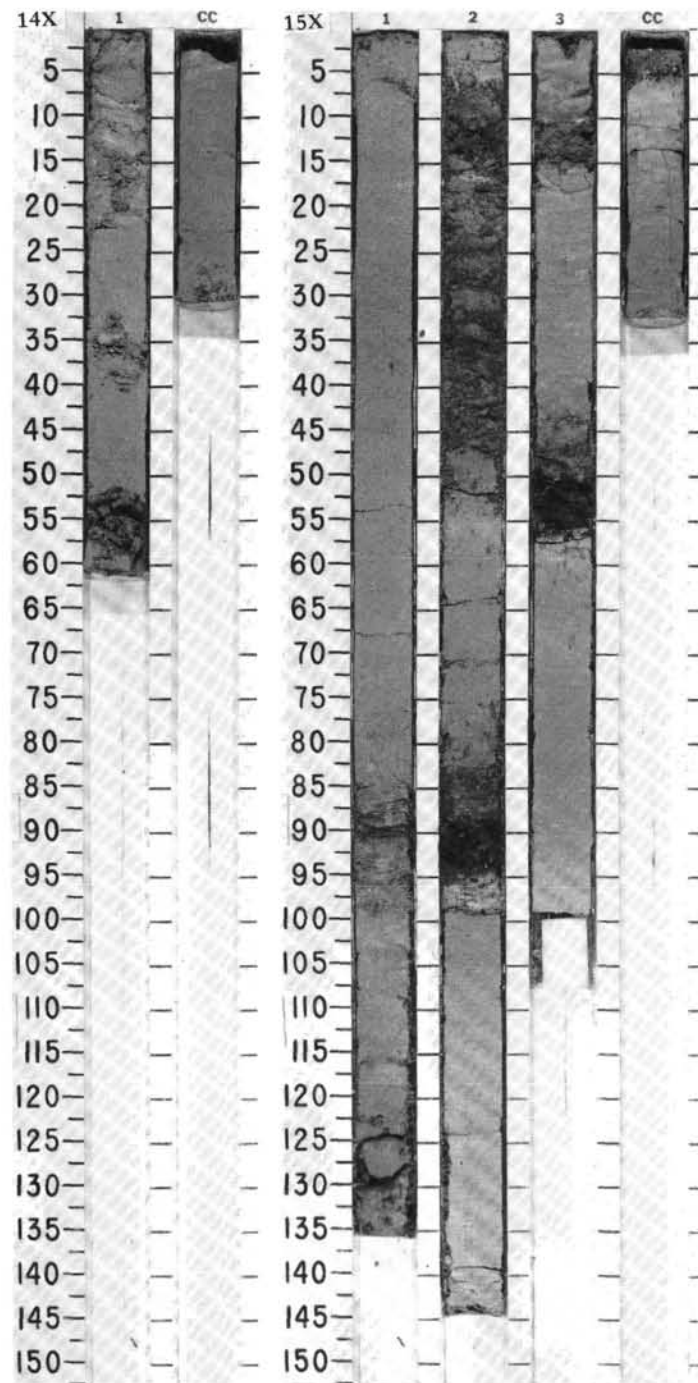


SITE 676 HOLE A CORE 14 X CORED INTERVAL 5179.3-5189.3 mbsl; 120.2-129.7 mbsf

TIME-ROCK UNIT	BIOSTRAT. ZONE/ FOSSIL CHARACTER				PALEOMAGNETICS	PHYS. PROPERTIES	CHEMISTRY	SECTION	METERS	GRAPHIC LITHOLOGY	DRILLING DISTURB.	SED. STRUCTURES	SAMPLES	LITHOLOGIC DESCRIPTION
	FORAMINIFERS	NANNOFOSSILS	RADIOLARIANS	DIATOMS										
LOWER PLIOCENE	<i>Globorotalia margaritae</i> Zone (PL2) A/G							1	0.5				*	<p>MARL</p> <p>Light gray to light olive-gray (5Y7/2, 5Y6/2) MARL, moderately bioturbated with scattered darker altered ashy blebs. Bedding dips slightly (10-15').</p> <p>SMEAR SLIDE SUMMARY (%):</p> <p>1, 27</p> <p>TEXTURE:</p> <p>Silt 10 Clay 90</p> <p>COMPOSITION:</p> <p>Clay 67 Accessory minerals Tr Foraminifers 5 Nannofossils 25 Bioclasts 3</p>
	CN11	Barren						CC						

SITE 676 HOLE A CORE 15 X CORED INTERVAL 5189.3-5198.8 mbsl; 129.7-139.2 mbsf

TIME-ROCK UNIT		BIOSTRAT. ZONE/ FOSSIL CHARACTER				PALEOMAGNETICS		PHYS. PROPERTIES		CHEMISTRY	SECTION	METERS	GRAPHIC LITHOLOGY	DRILLING DISTURB.	SED. STRUCTURES	SAMPLES	LITHOLOGIC DESCRIPTION																																																						
		FORAMINIFERS	NANNOFOSSILS	RADIOLARIANS	DIATOMS																																																																		
C/M	LOWER PLIOCENE	<i>Globorotalia margaritae</i> Zone (PL2) CN11				● 1.70 ● 63.4	● 1.70 ● 61.7	● 39.78 %	1	0.5 1.0				*		MARL Gray to pale olive-gray (5Y6/2, 5Y6/1, 5Y5/1) MARL, moderately bioturbated. Minor lithology: frequent strongly bioturbated dark gray (N4) altered (opaque mineral-rich) ash beds. Bedding dips sub-horizontally.																																																							
																	2				*																																																		
																							3				*																																												
																													CC				*																																						
B	Barren																																																																						
SMEAR SLIDE SUMMARY (%):																																																																							
<table><tr><td></td><td>1, 66 D</td><td>3, 52 M</td><td>3, 90 D</td><td>cc, 26 D</td></tr><tr><td>TEXTURE:</td><td></td><td></td><td></td><td></td></tr><tr><td>Sand</td><td>10</td><td>20</td><td>2</td><td>—</td></tr><tr><td>Silt</td><td>15</td><td>70</td><td>10</td><td>10</td></tr><tr><td>Clay</td><td>75</td><td>10</td><td>88</td><td>90</td></tr></table>																		1, 66 D	3, 52 M	3, 90 D	cc, 26 D	TEXTURE:					Sand	10	20	2	—	Silt	15	70	10	10	Clay	75	10	88	90																														
	1, 66 D	3, 52 M	3, 90 D	cc, 26 D																																																																			
TEXTURE:																																																																							
Sand	10	20	2	—																																																																			
Silt	15	70	10	10																																																																			
Clay	75	10	88	90																																																																			
COMPOSITION:																																																																							
<table><tr><td>Feldspar</td><td>Tr</td><td>40</td><td>Tr</td><td>—</td></tr><tr><td>Rock fragments</td><td>—</td><td>10</td><td>—</td><td>—</td></tr><tr><td>Clay</td><td>61</td><td>—</td><td>59</td><td>75</td></tr><tr><td>Volcanic glass</td><td>—</td><td>33</td><td>—</td><td>—</td></tr><tr><td>Calcite/dolomite</td><td>—</td><td>5</td><td>—</td><td>—</td></tr><tr><td>Accessory minerals(?)</td><td>—</td><td>10</td><td>1</td><td>Tr</td></tr><tr><td>Glaucoite</td><td>—</td><td>1</td><td>—</td><td>—</td></tr><tr><td>Orthopyroxene</td><td>—</td><td>1</td><td>—</td><td>—</td></tr><tr><td>Foraminifers</td><td>12</td><td>—</td><td>10</td><td>1</td></tr><tr><td>Nannofossils</td><td>23</td><td>—</td><td>30</td><td>25</td></tr><tr><td>Bioclasts</td><td>2</td><td>—</td><td>—</td><td>4</td></tr></table>																	Feldspar	Tr	40	Tr	—	Rock fragments	—	10	—	—	Clay	61	—	59	75	Volcanic glass	—	33	—	—	Calcite/dolomite	—	5	—	—	Accessory minerals(?)	—	10	1	Tr	Glaucoite	—	1	—	—	Orthopyroxene	—	1	—	—	Foraminifers	12	—	10	1	Nannofossils	23	—	30	25	Bioclasts	2	—	—	4
Feldspar	Tr	40	Tr	—																																																																			
Rock fragments	—	10	—	—																																																																			
Clay	61	—	59	75																																																																			
Volcanic glass	—	33	—	—																																																																			
Calcite/dolomite	—	5	—	—																																																																			
Accessory minerals(?)	—	10	1	Tr																																																																			
Glaucoite	—	1	—	—																																																																			
Orthopyroxene	—	1	—	—																																																																			
Foraminifers	12	—	10	1																																																																			
Nannofossils	23	—	30	25																																																																			
Bioclasts	2	—	—	4																																																																			



SITE 676 HOLE A CORE 16 X CORED INTERVAL 5198.8-5208.3 mbsl; 139.2-148.7 mbsf

TIME-ROCK UNIT	BIOSTRAT. ZONE/ FOSSIL CHARACTER				SECTION	METERS	GRAPHIC LITHOLOGY	DRILLING DISTURB.	SED. STRUCTURES	SAMPLES	LITHOLOGIC DESCRIPTION
	FORAMINIFERS	NANNOFOSSILS	RADIOLARIANS	DIATOMS							
PALEOMAGNETICS											
PHYS. PROPERTIES											
CHEMISTRY											
LOWER PLIOCENE					1	0.5 1.0		XX 			

LOWER PLIOCENE

Globorotalia margaritae Zone (PL1)

CN10c

Barren

● = 1.83

● = 56.0

● = 32.94 %

● = 1.82

● = 54.7

● = 29.94 %

MARL

Light yellowish brown to light olive-gray (2.5Y6/4, 5Y6/4), homogeneous MARL; strongly bioturbated.

Minor lithology: minor ash beds, strongly bioturbated and altered to greenish blue color (10G8, 10G6). Bedding dips sub-horizontal.

SMEAR SLIDE SUMMARY (%):

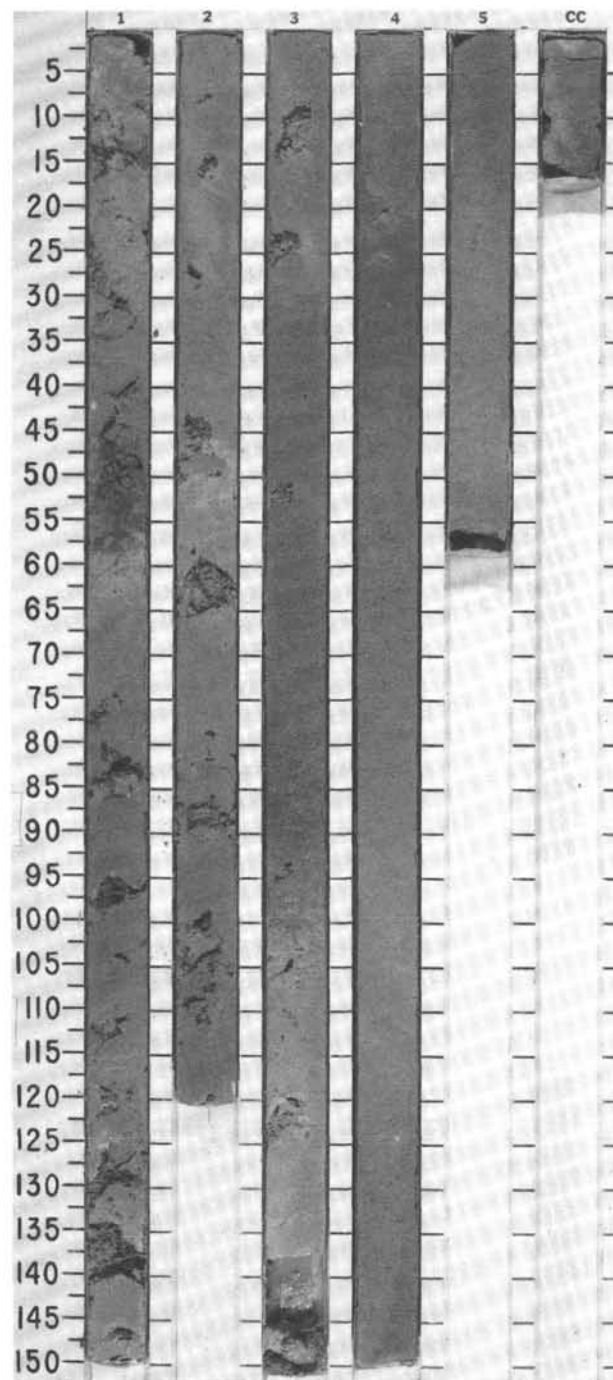
1, 55	1, 55	2, 88	4, 78	4, 138
M	M	D	D	D

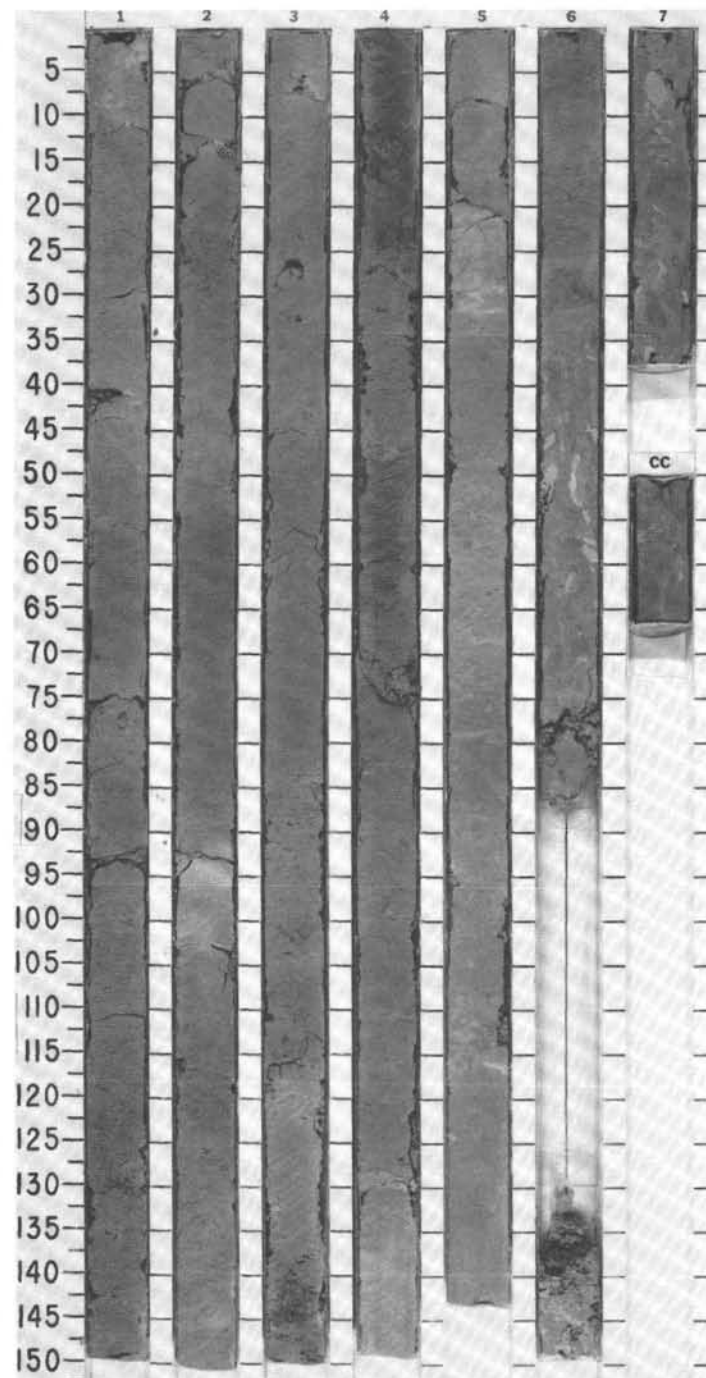
TEXTURE:

Sand	40	—	—	—	—
Silt	20	4	15	10	15
Clay	40	96	85	90	85

COMPOSITION:

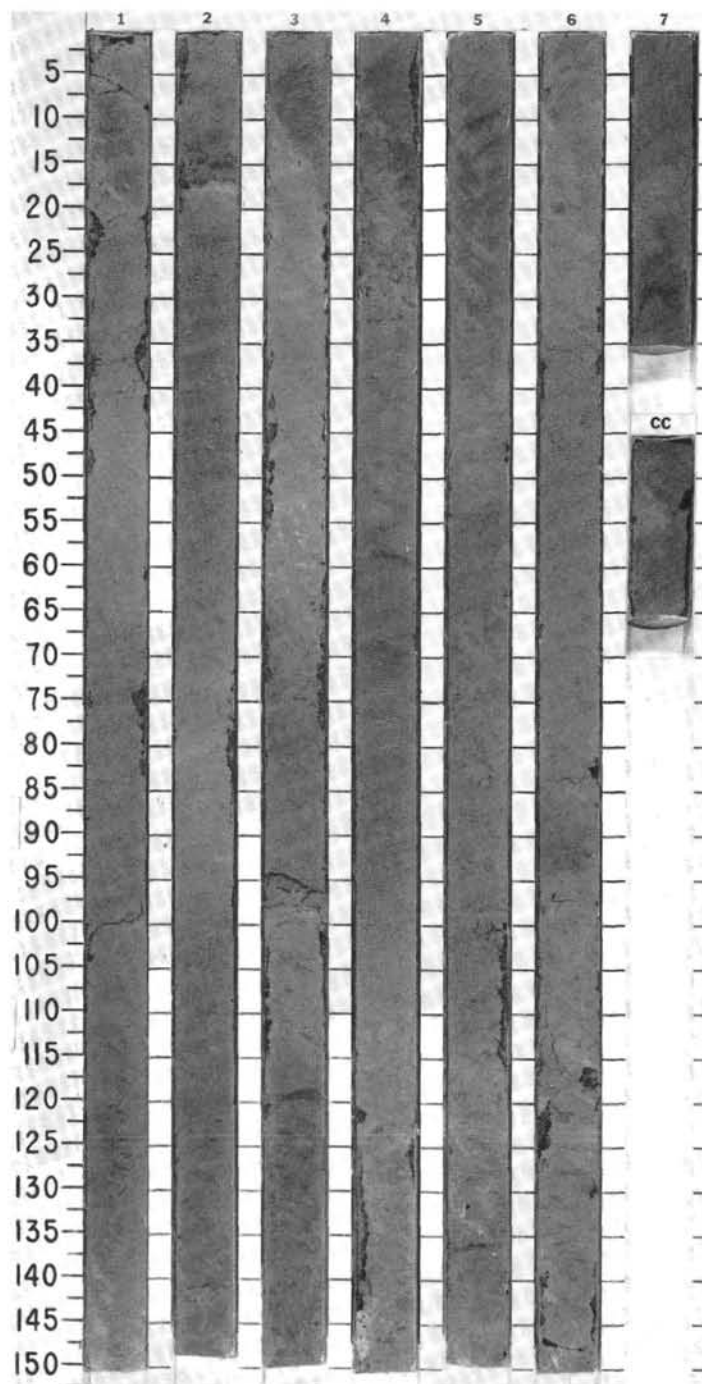
Quartz	Tr	—	—	—	—
Feldspar	40	Tr	—	Tr	—
Clay	20	51	58	72	69
Volcanic glass	30	—	—	—	—
Accessory minerals	—	—	—	—	—
Fibrous zeolite	—	—	Tr	—	—
Mn-oxide	8	1	1	1	—
Orthopyroxene	Tr	—	—	—	—
Hematite	Tr	—	—	—	—
Hornblende	2	—	—	—	—
Foraminifers	—	3	—	—	—
Nannofossils	—	45	40	25	30
Fish remains	Tr	—	—	—	—
Bioclasts	—	—	1	2	1

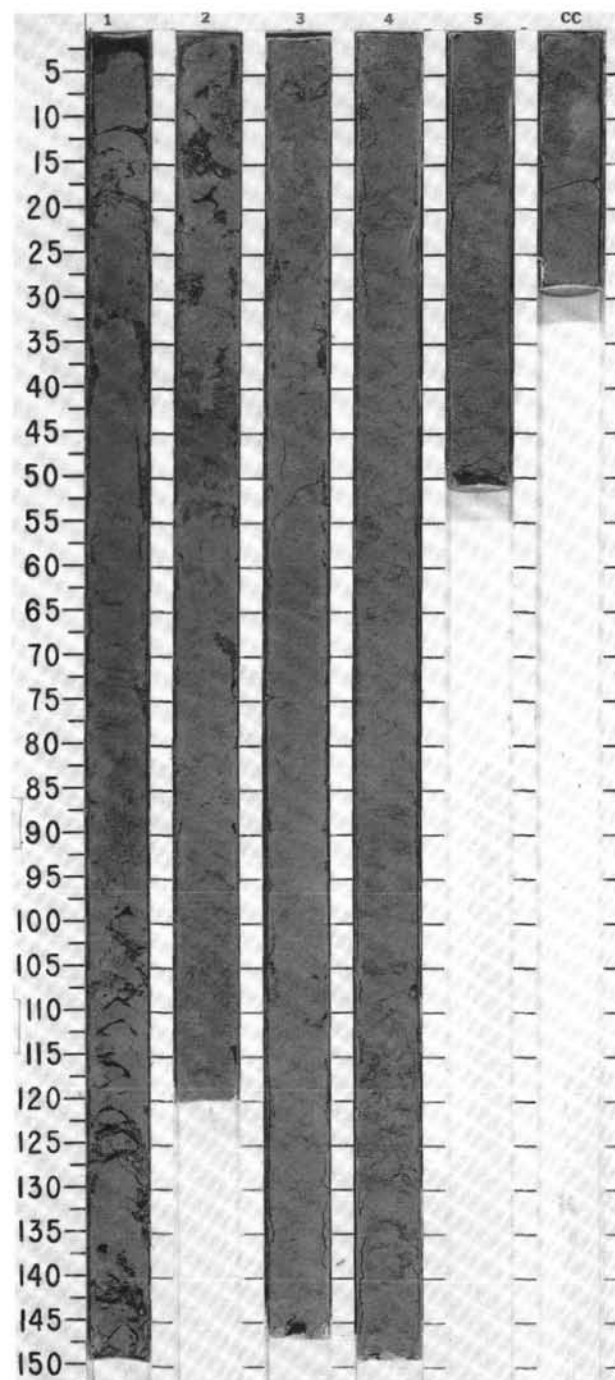


[illegible]

SITE 676 HOLE A CORE 18 X CORED INTERVAL 5217.8-5227.3 mbsl; 158.2-167.7 mbsf

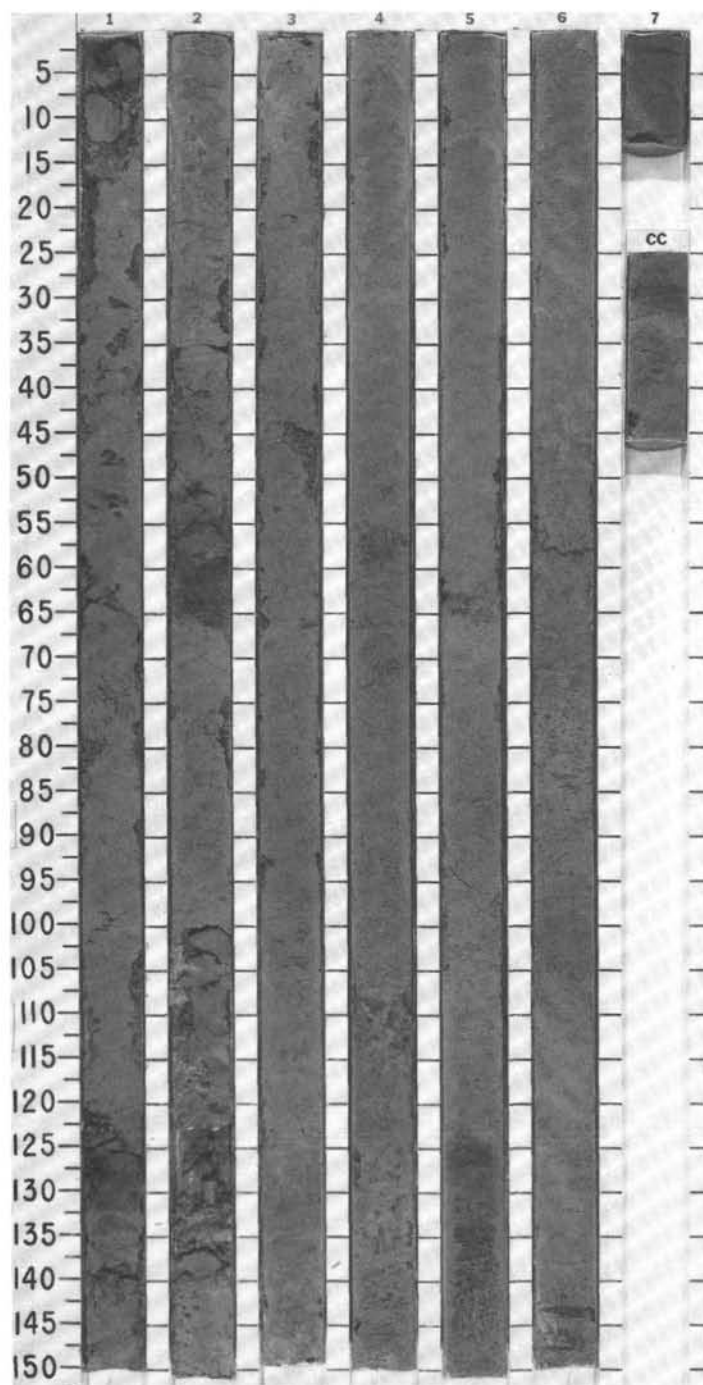
TIME - ROCK UNIT	BIOSTRAT. ZONE/ FOSSIL CHARACTER				PALEOMAGNETICS	PHYS. PROPERTIES	CHEMISTRY	SECTION	METERS	GRAPHIC LITHOLOGY	DRILLING DISTURB.	SED. STRUCTURES	SAMPLES	LITHOLOGIC DESCRIPTION																																																															
	FORAMINIFERS																																																																												
	NANNOFOSSILS																																																																												
	RADIOLARIANS																																																																												
DIATOMS																																																																													
UPPER MIOCENE																																																																													
B	Barren	CN9b	Barren			● 1.62 ● 0.54 %	● 0.34 %	1	0.5						MUDSTONE Olive-brown (2.5Y5/2, 2.5Y6/2), olive-gray 5Y4/2, 5Y5/2), and brown (10YR5/4) MUDSTONE, slightly calcareous to carbonate-free, moderately bioturbated. Minor lithology: gray (N4, N5) ash layers, strongly bioturbated (Sections 1, 2, 4, and 5). Structure: scaly fabric, dipping moderately to steeply (Section 1, 100-120 cm; Section 3, 119-131 cm; Section 6, 1-150 cm; Section 7, 28-34 cm); possibly drilling-induced. Shear fracture (dipping 65°) is offset by normal faults (dipping 20°) with vertical slickensides (Section 2, 110-130 cm). SMEAR SLIDE SUMMARY (%): <table><tr><td>2, 33</td><td>3, 65</td><td>4, 16</td></tr><tr><td>D</td><td>D</td><td>M</td></tr></table> TEXTURE: <table><tr><td>Sand</td><td>—</td><td>—</td><td>5</td></tr><tr><td>Silt</td><td>15</td><td>5</td><td>50</td></tr><tr><td>Clay</td><td>85</td><td>95</td><td>45</td></tr></table> COMPOSITION: <table><tr><td>Quartz</td><td>7</td><td>1</td><td>2</td></tr><tr><td>Feldspar</td><td>—</td><td>1</td><td>20</td></tr><tr><td>Clay</td><td>75</td><td>70</td><td>36</td></tr><tr><td>Volcanic glass</td><td>Tr</td><td>2</td><td>20</td></tr><tr><td>Calcite/dolomite</td><td>3</td><td>1</td><td>—</td></tr><tr><td>Accessory minerals</td><td>—</td><td>—</td><td>—</td></tr><tr><td>Opacities</td><td>3</td><td>5</td><td>20</td></tr><tr><td>Pyroxene</td><td>Tr</td><td>—</td><td>Tr</td></tr><tr><td>Hornblende</td><td>Tr</td><td>—</td><td>—</td></tr><tr><td>Hematite (?)</td><td>—</td><td>—</td><td>2</td></tr><tr><td>Nannofossils</td><td>12</td><td>20</td><td>—</td></tr></table>	2, 33	3, 65	4, 16	D	D	M	Sand	—	—	5	Silt	15	5	50	Clay	85	95	45	Quartz	7	1	2	Feldspar	—	1	20	Clay	75	70	36	Volcanic glass	Tr	2	20	Calcite/dolomite	3	1	—	Accessory minerals	—	—	—	Opacities	3	5	20	Pyroxene	Tr	—	Tr	Hornblende	Tr	—	—	Hematite (?)	—	—	2	Nannofossils	12	20	—
2, 33	3, 65	4, 16																																																																											
D	D	M																																																																											
Sand	—	—	5																																																																										
Silt	15	5	50																																																																										
Clay	85	95	45																																																																										
Quartz	7	1	2																																																																										
Feldspar	—	1	20																																																																										
Clay	75	70	36																																																																										
Volcanic glass	Tr	2	20																																																																										
Calcite/dolomite	3	1	—																																																																										
Accessory minerals	—	—	—																																																																										
Opacities	3	5	20																																																																										
Pyroxene	Tr	—	Tr																																																																										
Hornblende	Tr	—	—																																																																										
Hematite (?)	—	—	2																																																																										
Nannofossils	12	20	—																																																																										
B						● 1.70 ● 0.52 %	● 0.67 %	2	1.0																																																																				
								3																																																																					
								4																																																																					
								5																																																																					
								6																																																																					
								7																																																																					
CC																																																																													



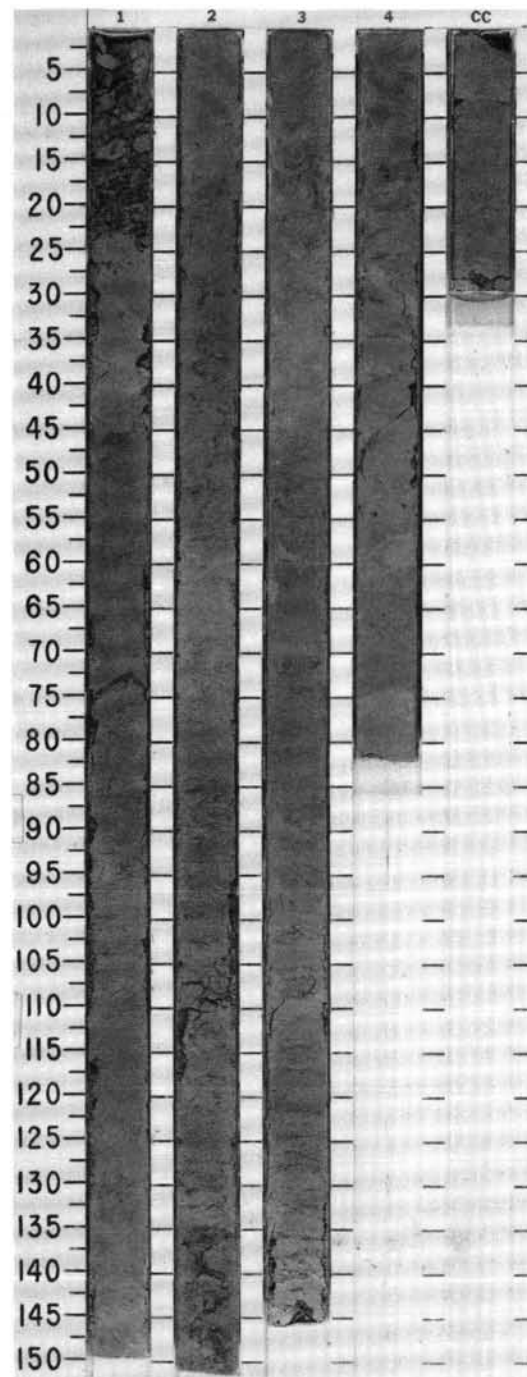
[illegible]

SITE 676 HOLE A CORE 20 X CORED INTERVAL 5236.8-5246.3 mbsl; 177.2-186.7 mbsf

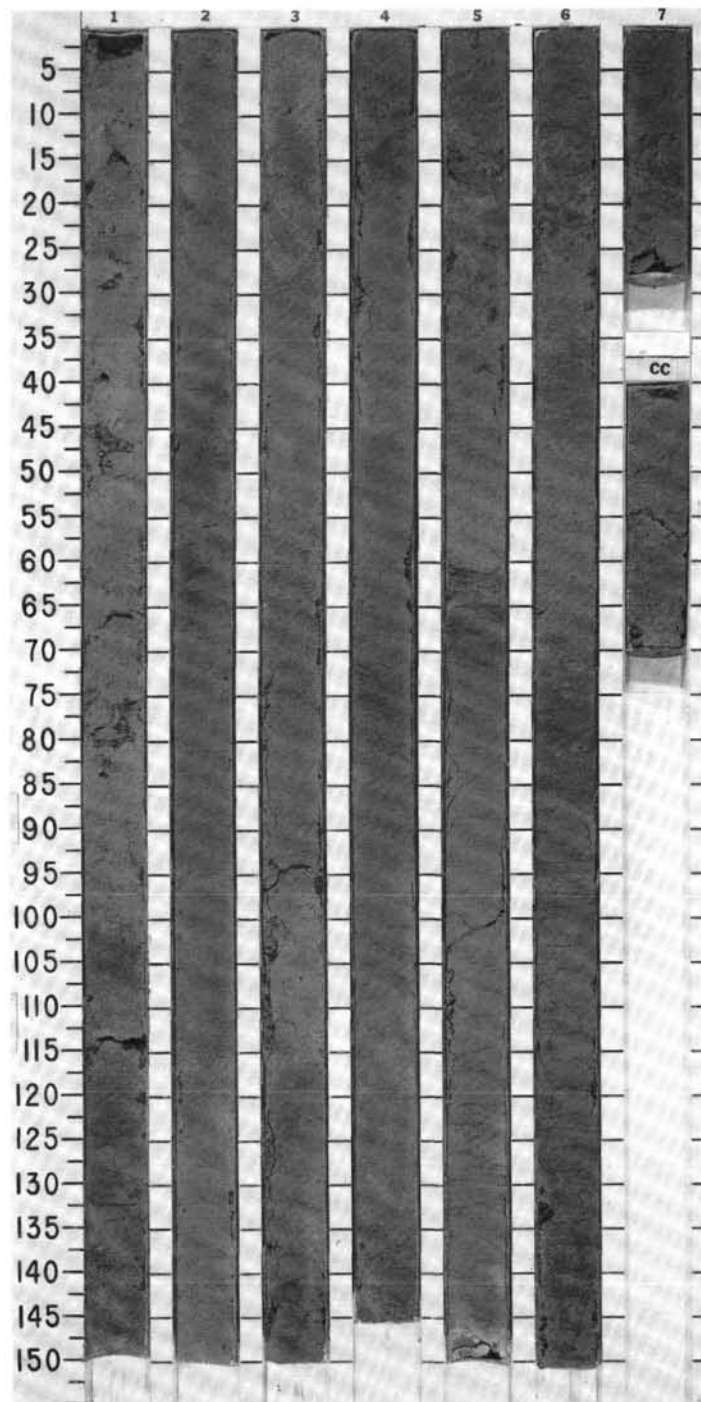
TIME-ROCK UNIT	BIOSTRAT. ZONE/ FOSSIL CHARACTER				PALEOMAGNETICS	PHYS. PROPERTIES	CHEMISTRY	SECTION	METERS	GRAPHIC LITHOLOGY	DRILLING DISTURB.	SED. STRUCTURES	SAMPLES	LITHOLOGIC DESCRIPTION
	FORAMINIFERS	NANNOFOSSILS	RADIOLARIANS	DIATOMS										
?	Barren	Barren	Barren			$\gamma = 1.56$ $\delta = 70.0$ $\bullet 0.17\%$		1	0.5 1.0					MUDSTONE, CLAYSTONE, and ASHY MUDSTONE Greenish gray (5GY5/2, 5GY5/1, 10Y5/2) MUDSTONE, CLAYSTONE, and ASHY MUDSTONE. Most of core is moderately to intensely bioturbated with common <i>Planolites</i> and one <i>Zoophycos</i> burrow (Section 1, 7-13 cm). 2-3% gray ash disseminated throughout most of core. Minor lithology: strongly bioturbated dark gray (N4) ash layers occur in Sections 2 and 4. The layer at Section 4, 110 cm, has been bioturbated and burrowed more than 35 cm downsection. Structure: steeply dipping to vertical (70-90°) poorly to moderately developed scaly fabrics occur in Sections 4, 5, and 7.
B						$\gamma = 1.69$ $\delta = 65.1$ $\bullet 0.25\%$		2						SMEAR SLIDE SUMMARY (%): 3, 83 3, 131 5, 63 cc, 8 D D M M TEXTURE: Sand — Tr 2 — Silt 5 20 70 15 Clay 95 80 28 85 COMPOSITION: Quartz Tr — 1 — Plagioclase 1 3 15 5 Pumice — Tr — — Clay 93 83 27 85 Volcanic glass 1 10 50 10 Accessory minerals — — — — Glauconite (?) 1 1 — — Opauques 3 3 7 — Hematite (?) Tr — — — Sponge spicules 1 — — — Fish remains Tr — — —
B								3						
B								4						
B								5						
								6						
								7						
								CC						



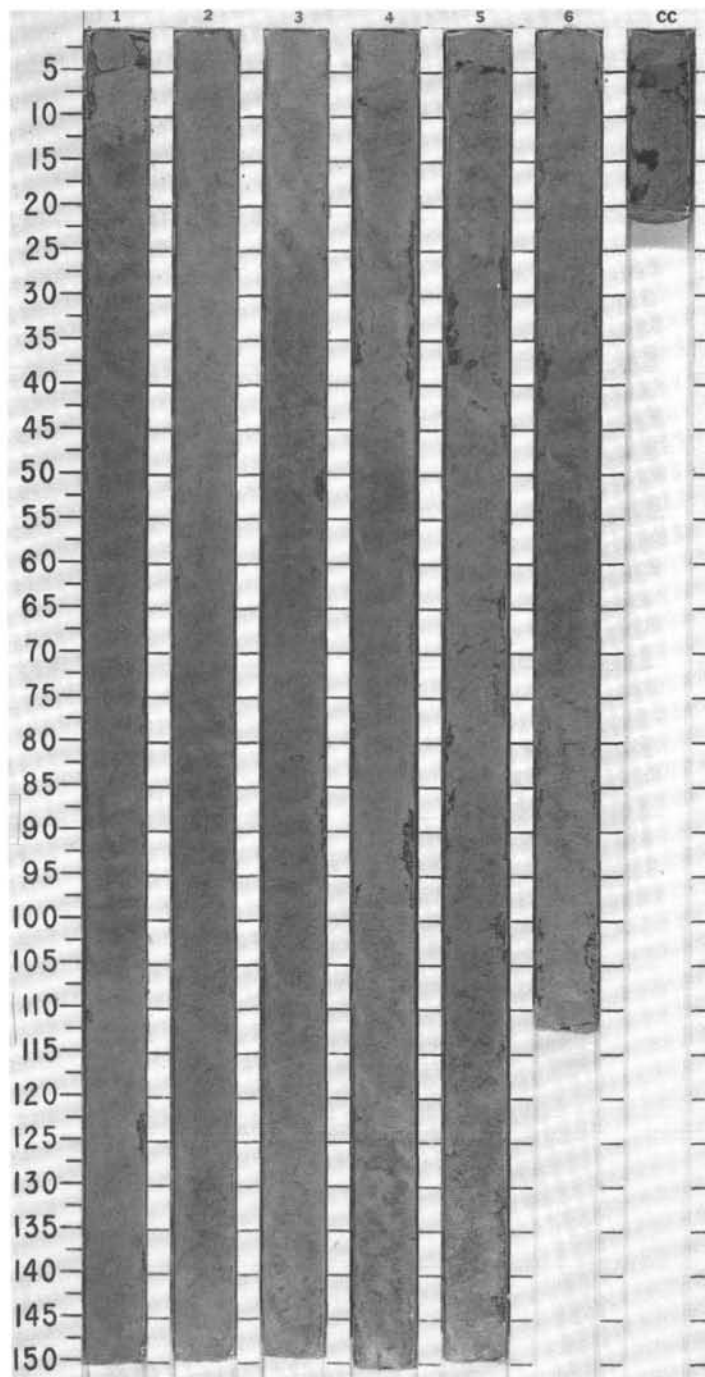
TIME-ROCK UNIT		BIOSTRAT. ZONE/ FOSSIL CHARACTER				PALEOMAGNETICS	PHYS. PROPERTIES	CHEMISTRY	SECTION	METERS	GRAPHIC LITHOLOGY	DRILLING DISTURB.	SED. STRUCTURES	SAMPLES	LITHOLOGIC DESCRIPTION
B		Barren	CN8b	Barren					1	0.5				*	MUDSTONE
B		Barren						2	1.0						Olive-gray (5Y5/2, 10Y5/2), olive (5Y5/3), and greenish gray (5G5/1) MUDSTONE with variable amounts of ash (up to 30%) disseminated throughout; moderately to strongly bioturbated. Structure: faults dip steeply (60-90°) in Section 2, 0-58 cm.
								3							SMEAR SLIDE SUMMARY (%): TEXTURE: COMPOSITION:
								4							1, 64 4, 53 D D Silt 25 50 Clay 75 50 Quartz 19 27 Feldspar 3 8 Clay 70 45 Volcanic glass 4 20 Clinopyroxene Tr — Nannofossils 4 —



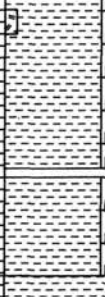
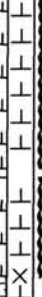
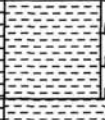



UPPER MIOCENE														
TIME-ROCK UNIT	BIOSTRAT. ZONE / FOSSIL CHARACTER				PALEOMAGNETICS	PHYS. PROPERTIES	CHEMISTRY	SECTION	METERS	GRAPHIC LITHOLOGY	DRILLING DISTURB.	SED. STRUCTURES	SAMPLES	LITHOLOGIC DESCRIPTION
	FORAMINIFERS	NANNOFOSSILS	RADIOLARIANS	DIATOMS										
P/R	indet.	CN9a	Barren											
B														



SITE 676 HOLE A CORE 24 X CORED INTERVAL 5274.8-5284.3 mbsl; 215.2-224.7 mbsf

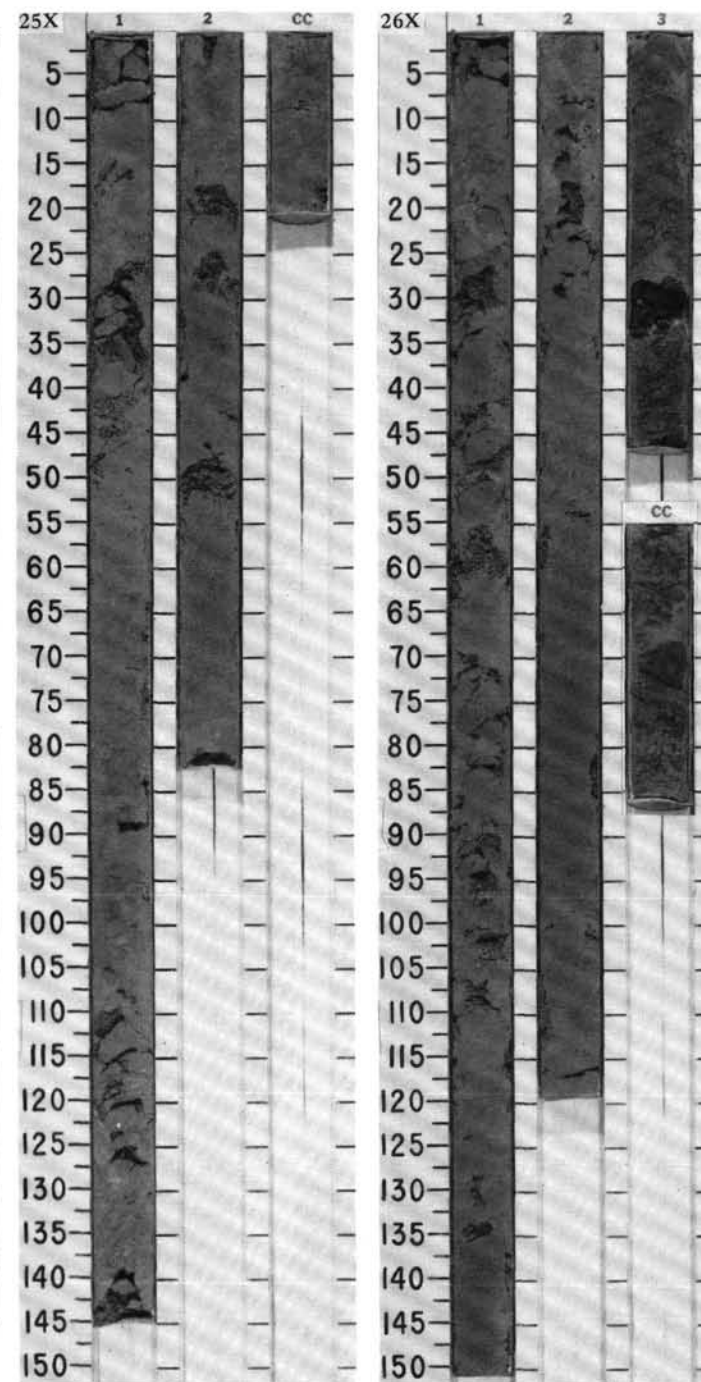
[illegible]

SITE 676 HOLE A CORE 25 X CORED INTERVAL 5284.3-5293.8 mbsl; 224.7-234.2 mbsf

TIME-ROCK UNIT	BIOSTRAT. ZONE/ FOSSIL CHARACTER				PALEOMAGNETICS	PHYS. PROPERTIES	CHEMISTRY	SECTION	METERS	GRAPHIC LITHOLOGY	DRILLING DISTURB. SED. STRUCTURES	SAMPLES	LITHOLOGIC DESCRIPTION
	FORAMINIFERS	NANNOFOSSILS	RADIOLARIANS	DIAZONES									
?	indet.	indet.	Barren			$\gamma = 1.67$ $\delta = 64.3$	$\bullet 14.43 \%$	1	0.5			*	CLAYSTONE Grayish-green to dusky yellow-green (5GY5/4, 10GY5/2), carbonate-free CLAYSTONE; moderately bioturbated and homogeneous. Locally developed weak scaly fabric. SMEAR SLIDE SUMMARY (%): 1, 20 M 1, 67 D cc, 16 D TEXTURE: Sand Tr 1 — Silt 10 12 8 Clay 90 87 92 COMPOSITION: Quartz 1 — 3 Feldspar 1 — 2 Clay 80 85 89 Volcanic glass 5 — 1 Calcite/dolomite 2 2 1 Accessory minerals (?) 1 5 1 Orthopyroxene — Tr — Foraminifers — 1 — Nannofossils 10 7 3
P/R								2	1.0			*	
B								CC				*	

SITE 676 HOLE A CORE 26 X CORED INTERVAL 5293.8-5303.3 mbsl; 234.2-243.7 mbsf

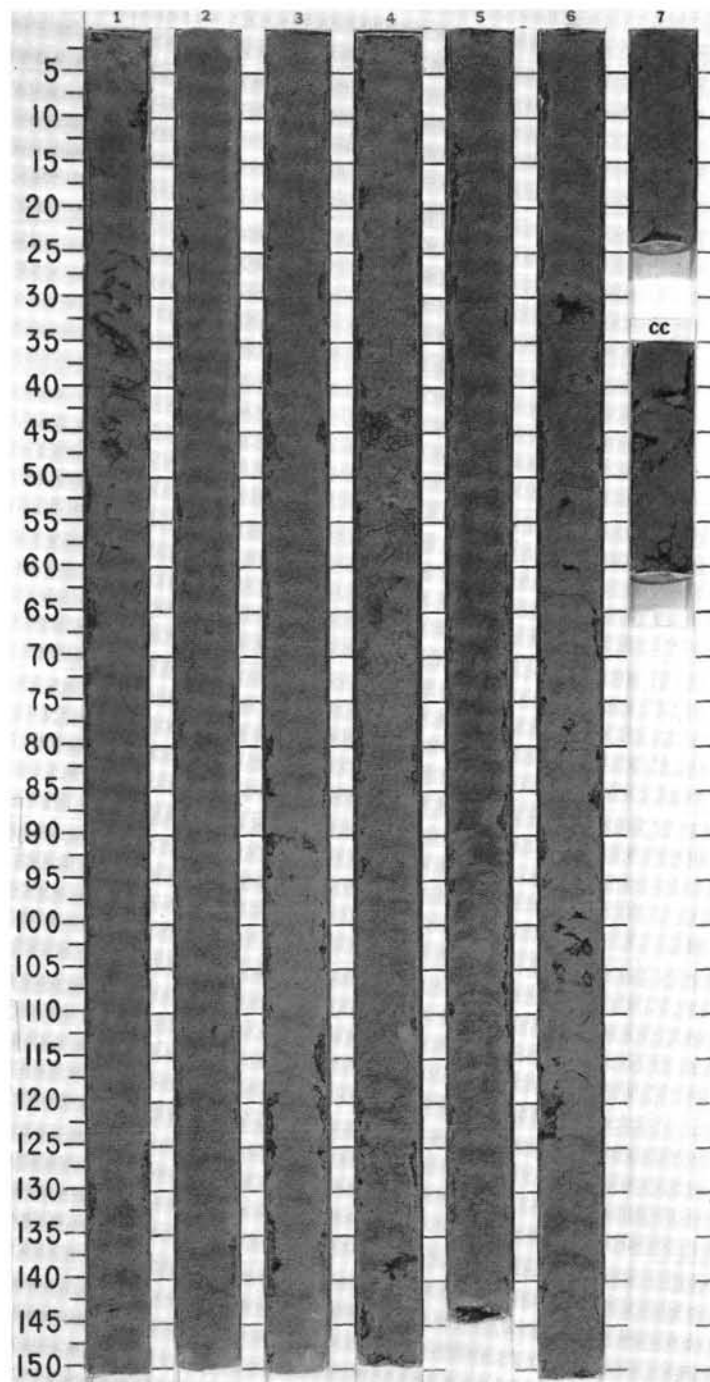
TIME-ROCK UNIT	BIOSTRAT. ZONE/ FOSSIL CHARACTER				PALEOMAGNETICS	PHYS. PROPERTIES	CHEMISTRY	SECTION	METERS	GRAPHIC LITHOLOGY	DRILLING DISTURB.	SED. STRUCTURES	SAMPLES	LITHOLOGIC DESCRIPTION
	FORAMINIFERS	NANNOFOSSILS	RADIOLARIANS	DIAZONES										
?	Barren	Barren	Barren			$\gamma = 1.63$ $\delta = 67.4$	$\bullet 0.0 \%$	1	0.5				*	CLAYSTONE Olive-gray to greenish gray (5G5/2, 10Y5/2) to brownish gray (2.5Y5/2), carbonate-free CLAYSTONE; mild to strong bioturbation. Locally developed scaly fabric dips 30-45°.
B								2	1.0				*	
B								3					OG	
B								CC					*	



SITE 676

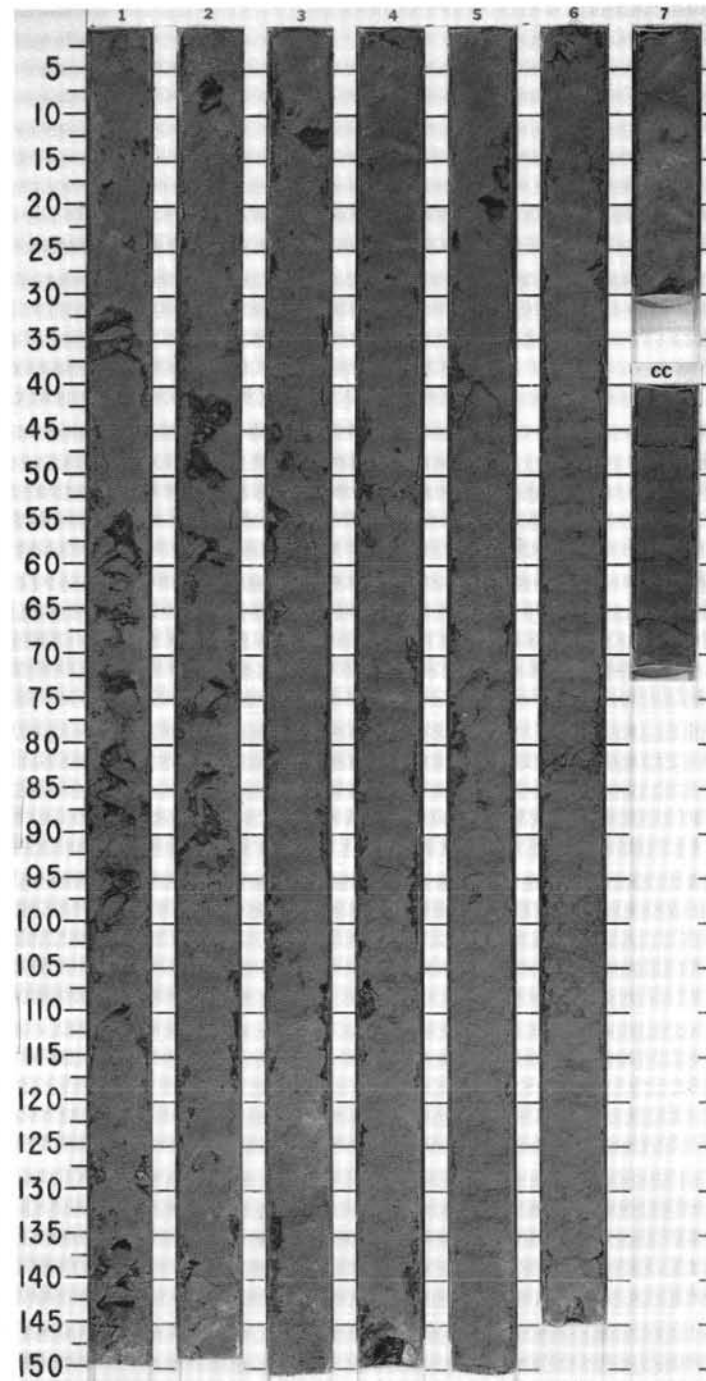
SITE 676 HOLE A CORE 27 X CORED INTERVAL 5303.3-5312.8 mbsl; 243.7-253.2 mbsf

TIME-ROCK UNIT	BIOSTRAT. ZONE/ FOSSIL CHARACTER				PALEOMAGNETICS	PHYS. PROPERTIES	CHEMISTRY	SECTION	METERS	GRAPHIC LITHOLOGY	DRILLING DISTURB.	SED. STRUCTURES	SAMPLES	LITHOLOGIC DESCRIPTION
	FORAMINIFERS	NANNOFOSSILS	RADIOLARIANS	DIAZONIS										
?	Barren								0.5					
B	Barren							1	1.0				*	CLAYSTONE and ASHY MUDSTONE
B	Barren							2					*	Olive-gray (10Y4/2, 5Y5/2, 5Y4/2) and olive (5Y5/3, 5Y5/4) CLAYSTONE and ASHY MUDSTONE; moderately to intensely bioturbated; clinoptilolite(?) spherules noted in Section 2.
B	Barren							3						SMEAR SLIDE SUMMARY (%):
								4						1, 86 2, 74 4, 56
								5						D D M
								6						TEXTURE:
								7						Silt 10 5 15
CC														Clay 90 95 85
														COMPOSITION:
														Quartz Tr Tr —
														Feldspar 1 1 2
														Clay 93 94 87
														Volcanic glass 2 2 8
														Calcite/dolomite 2 1 1
														Accessory minerals — — —
														Opales 2 2 2
														Radiolarians Tr — —
														Sponge spicules — Tr —

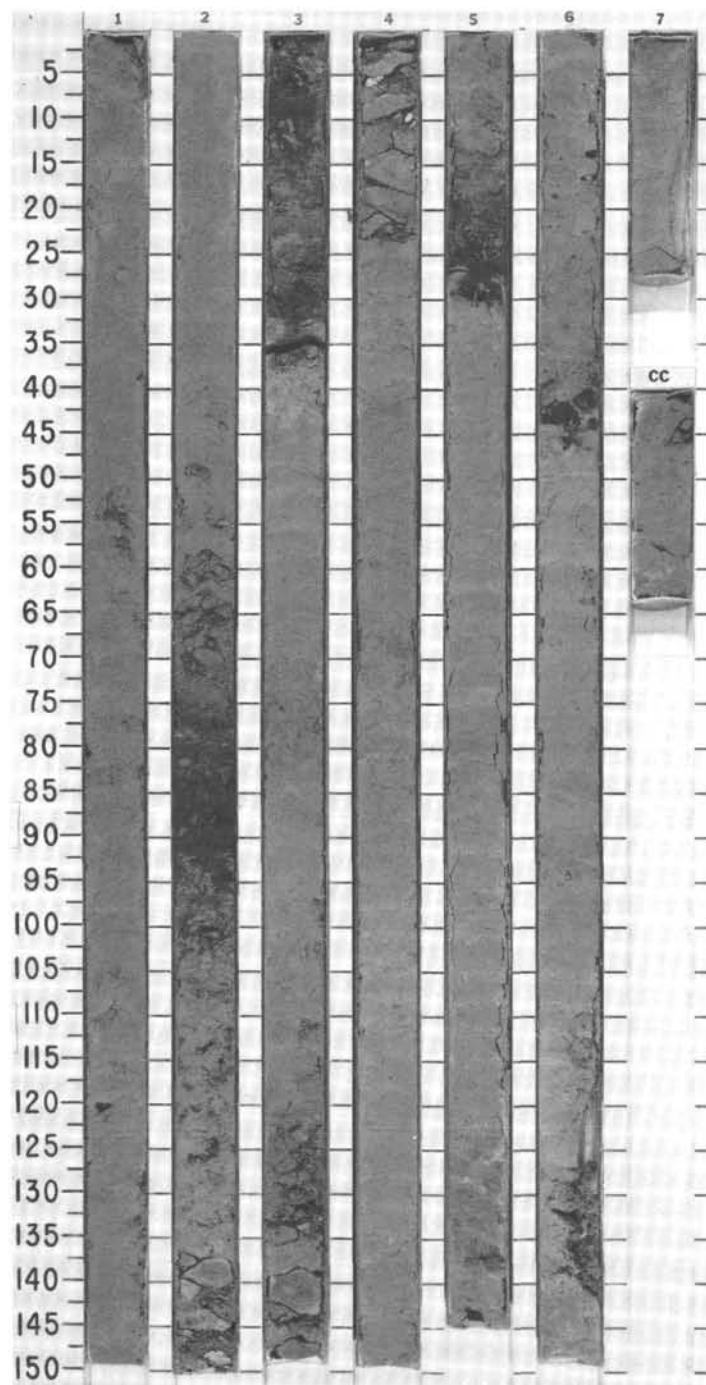


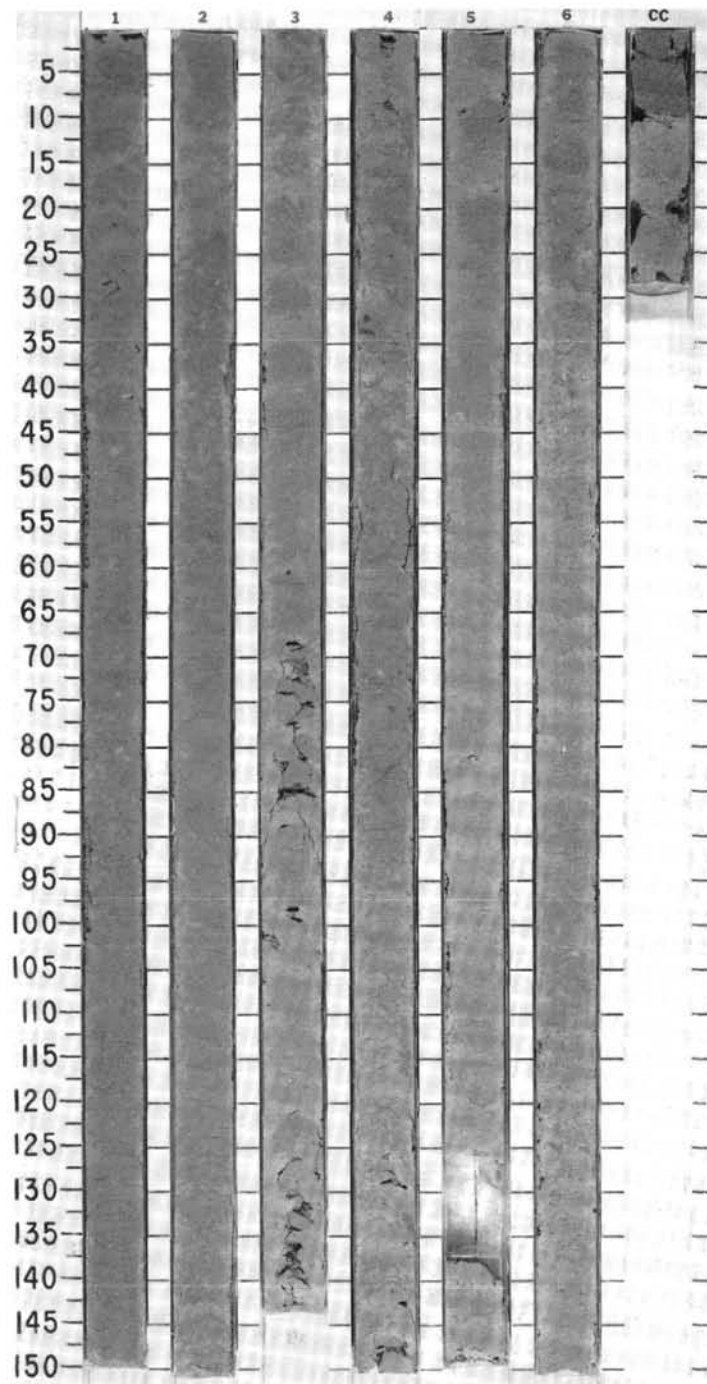
SITE 676 HOLE A CORE 28 X CORED INTERVAL 5312.8-5322.3 mbsl; 253.2-262.7 mbsf

TIME-ROCK UNIT	BIOSTRAT. ZONE/ FOSSIL CHARACTER				PALEOMAGNETICS	PHYS. PROPERTIES	CHEMISTRY	SECTION	METERS	GRAPHIC LITHOLOGY	DRILLING DISTURB.	SED. STRUCTURES	SAMPLES	LITHOLOGIC DESCRIPTION
	FORAMINIFERS	NANNOFOSSILS	RADIOLARIANS	DIATOMS										
?	B	Barren				Y=1.54 ● 0=72.0	● 0.0 %		1					CLAYSTONE and ASHY MUDSTONE
	B	Barren							2					Olive-gray (5Y5/2, 5Y4/2, 10Y4/2) CLAYSTONE and ASHY MUDSTONE; moderately to intensely bioturbated; ashy intervals mottled with dark gray (N4, N5).
	B	Barren							3					Structure: three-dimensional network of scaly shear surfaces, Section 7, 22-30 cm.
									4					SMEAR SLIDE SUMMARY (%):
									5					1, 126 1, 144 4, 16 D D D
									6					TEXTURE:
									7					Sand — 1 —
									CC					Silt 3 24 5
														Clay 97 75 95
														COMPOSITION:
														Quartz — 3 1
														Feldspar 1 5 —
														Clay 97 75 96
														Volcanic glass 1 17 1
														Calcite/dolomite Tr Tr 1
														Accessory minerals — — —
														Opales 1 — 1
														Nannofossils — Tr Tr
														Radiolarians Tr — Tr



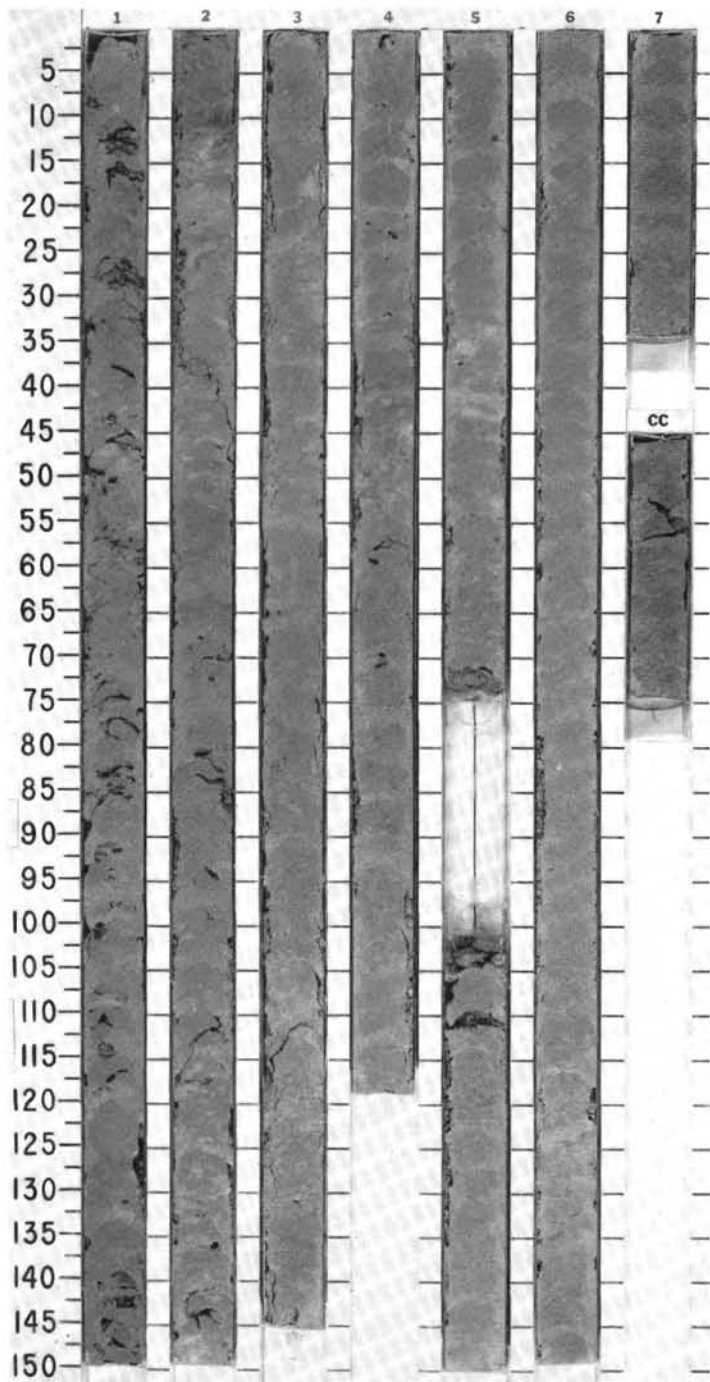
SITE 676

[illegible]

[illegible]

SITE 676 HOLE A CORE 32 X CORED INTERVAL 5350.8-5360.3 mbsl; 291.2-300.7 mbsf

TIME-ROCK UNIT	BIOSTRAT. ZONE/ FOSSIL CHARACTER	PALEOMAGNETICS	PHYS. PROPERTIES	CHEMISTRY	SECTION	METERS	GRAPHIC LITHOLOGY	DRILLING DISTURB.	SED. STRUCTURES	SAMPLES	LITHOLOGIC DESCRIPTION
	FORAMINIFERS										
	NANNOFOSSILS										
	RADIOLARIANS										
	DIAZONES										
LOWER MIOCENE	Barren Barren A/G <i>Stichocorys wolffii</i> Zone		$\gamma = 1.58$ $\delta = 66.5$ • 0.0 %		1	0.5					<p>SILICEOUS MUDSTONE</p> <p>Olive-brown (2.5Y6/2, 2.5Y6/4, 2.5Y5/3) to light yellowish brown (10YR6/4) SILICEOUS MUDSTONE; slightly to intensely bioturbated. Local minor greenish gray (5GY6/1) mottles are probably highly altered ash.</p> <p>Minor lithology: locally common orange-pink mottling in Sections 4 and 5 may be rhodochrosite(?).</p> <p>Structure: sub-vertical (60-90°) spaced "vein structure" is locally developed in Sections 1 and 2.</p> <p>SMEAR SLIDE SUMMARY (%):</p> <p>Silt 2.88 Clay 0</p> <p>TEXTURE:</p> <p>Silt 15 Clay 85</p> <p>COMPOSITION:</p> <p>Quartz — Feldspar 2 Clay 73 Volcanic glass 10 Radiolarians 15 Sponge spicules Tr</p>
						1.0					
						2					
						3					
						4					
						5					
						6					
			$\gamma = 1.64$ $\delta = 64.7$ • 0.0 %		7						
					CC						



SITE 676 HOLE A CORE 33 X CORED INTERVAL 5360.3-5369.8 mbsl; 300.7-310.2 mbsf

TIME-ROCK UNIT

FORAMINIFERS

NANNOFOSSILS

RADIOLARIANS

DIATOMS

BIOSTRAT. ZONE/
FOSSIL CHARACTER

LOWER MIOCENE

Barren

Barren

A/P indet.

A/M *Lychnocanoma elongata* Zone

A/M *Cyrtocapsella tetrapera* Zone

PALEOMAGNETICS

PHYS. PROPERTIES

CHEMISTRY

SECTION

METERS

GRAPHIC LITHOLOGY

DRILLING DISTURB.

SED. STRUCTURES

SAMPLES

LITHOLOGIC DESCRIPTION

CLAYSTONE

Yellowish brown, reddish brown, to olive-yellow (10YR5/8, 2.5YR5/8, 2.5Y6/6) slightly siliceous CLAYSTONE with local whitish spherules (probably zeolite).

Structure: one steeply dipping fault with associated scaly fabric (Section 1, 20-40 cm); steeply dipping vein structure.

SMEAR SLIDE SUMMARY (%):

1, 32

1, 64

5, 74

cc, 22

cc, 35

M

D

D

M

M

TEXTURE:

Sand

Silt

Clay

5

90

5

5

12

83

—

7

93

—

2

98

100

COMPOSITION:

Quartz

Feldspar

Clay

Accessory minerals

Authigenic carbonate (rhodocrosite ?)

Authigenic clay or zeolite

Barite (?)

Mn oxide

Radiolarians

Sponge spicules

—

—

5

—

—

—

—

—

—

—

1

Tr

83

91

—

—

—

—

—

—

—

—

—

—

—

—

—

—

—

—

—

—

—

—

—

—

—

—

—

—

—

—

—

—

—

—

—

—

—

—

—

—

—

—

—

—

—

—

—

—

—

—

—

—

—

—

—

—

—

—

—

—

—

—

—

—

—

—

—

—

—

—

—

—

—

—

—

—

—

—

—

—

—

—

—

—

—

—

—

—

—

—

—

—

—

—

—

—

—

—

—

—

—

—

—

—

—

—

—

—

—

—

—

—

—

—

—

—

—

—

—

—

—

—

—

—

—

—

—

—

—

—

—

—

—

—

—

—

—

—

—

—

—

—

—

—

—

—

—

—

—

—

—

—

—

—

—

—

—

—

—

—

—

—

—

—

—

—

—

—

—

—

—

—

—

—

—

—

—

—

—

—

—

—

—

—

—

—

—

—

—

—

—

—

—

—

—

—

—

—

—

—

—

—

—

—

—

—

—

—

—

—

—

—

—

—

—

—

—

—

—

—

—

—

—

—

—

—

—

—

—

—

—

—

—

—

—

—

—

—

—

—

—

—

—

—

—

—

—

—

—

—

—

—

—

—

—

—

—

—

—

—

—

—

—

—

—

—

—

—

—

—

—

—

—

—

—

—

—

—

—

—

—

—

—

—

—

—

—

—

—

—

—

—

—

—

—

—

—

—

—

—

—

—

—

—

—

—

—

—

—

—

—

—

—

—

—

—

—

—

—

—

—

—

—

—

—

—

—

—

—

—

—

—

—

—

—

—

—

—

—

—

—

—

—

—

—

—

—

—

—

—

—

—

—

—

—

—

—

—

—

—

—

—

—

—

—

—

—

—

—

—

—

—

—

—

—

—

—

—

—

—

—

—

—

—

—

—

—

—

—

—

—

—

—

—

—

—

—

—

—

—

—

—

—

—

—

—

—

—

—

—

—

—

—

—

—

—

—

—

—

—

—

—

—

—

—

—

—

—

—

—

—

—

—

—

—

—

—

—

—

—

—

—

—

—

—

—

—

—

—

—

—

—

—

—

—

—

—

—

—

—

—

—

—

—

—

—

—

—

—

—

—

—

—

—

—

—

—

—

—

—

—

—

—

—

—

—

—

—

—

—

—

—

—

—

—

—

—

—

—

—

—

—

—

—

—

—

—

—

—

—

—

—

—

—

—

—

—

—

—

—

—

—

—

—

—

—

—

—

—

—

—

—

—

—

—

—

—

—

—

—

—

—

—

—

—

—

—

—

—

—

—

—

—

—

—

—

—

—

—

—

—

—

—

—

—

—

—

—

—

—

—

—

—

—

—

—

—

—

—

—

—

—

—

—

—

—

—

—

—

—

—

—

—

—

—

—

—

—

—

—

—

—

—

—

—

—

—

—

—

—

—

—

—

—

—

—

—

—

—

—

—

—

—

—

—

—

—

—

—

—

—

—

—

—

—

—

—

—

—

—

—

—

—

—

—

—

—

—

—

—

—

—

—

—

—

—

—

—

—

—

—

—

—

—

—

—

—

—

—

—

—

—

—

—

—

—

—

—

—

—

—

—

—

—

—

—

—

—

—

—

—

—

—

—

—

—

—

—

—

—

—

—

—

—

—

—

—

—

—

—

—

—

—

—

—

—

—

—

—

—

—

—

—

—

—

—

—

—

—

—

—

—

—

—

—

—

—

—

—

—

—

—

—

—

—

—

—

—

—

—

—

—

—

—

—

—

—

—

—

—

—

—

—

—

—

—

—

—

—

—

—

—

—

—

—

—

—

—

—

—

—

—

—

—

—

—

—

—

—

—

—

—

—

—

—

—

—

—

—

—

—

—

—

—

—

—

—

—

—

—

—

—

—

—

—

—

—

—

—

—

—

—

—

—

—

—

—

—

—

—

—

—

—

—

—

—

—

—

—

—

—

—

—

—

—

—

—

—

—

—

—

—

—

—

—

—

—

—

—

—

—

—

—

—

—

—

—

—

—

—

—

—

—

—

—

—

—

—

—

—

—

—

—

—

